

# Gold Electrode Electrochemistry in Protein Based Solar Cells

by

Bahar Iranpour

B.A.Sc., University of British Columbia, 2009

A THESIS SUBMITTED IN PARTIAL FULFILMENT OF

THE REQUIREMENTS FOR THE DEGREE OF

**MASTER OF APPLIED SCIENCE**

in

The Faculty of Graduate Studies

(Electrical and Computer Engineering)

THE UNIVERSITY OF BRITISH COLUMBIA

(Vancouver)

April, 2012

© Bahar Iranpour, 2012

## **ABSTRACT**

The high quantum efficiency of photosynthetic reaction centers makes them candidates for use in solar energy harvesting devices. A bio-photovoltaic cell can be made by dissolving reaction centers and two mediators, such as quinone and cytochrome c, in the conductive electrolyte of an electrochemical cell. The mediators transfer the photo-generated charges to the electrodes upon illumination. So far such protein-based devices have shown low overall power conversion efficiency. Previously it has been shown that slow charge transfer limits the efficiency of these devices. Moreover, it has been observed that the cell response is dependent on the electrode materials and their interactions with the proteins and the mediators. In this thesis, the importance of the cleanliness of the system, the adsorption of two types of reaction centers: Wild-type and cysteineless, two mediators: quinone and cytochrome c, and detergents (used to make the reaction center water soluble) on a gold electrode are investigated. It is shown that common cleaning methods such as sonication in a mixture of deionized water and ethyl alcohol, sulfuric acid potential cycling, and piranha solution may not be practical and sufficient to remove the reaction centers and mediators from the electrodes and the container. Additionally, it is shown that eliminating oxygen can result in the reduction of unwanted parasitic reactions in the cell, which could lower the generated photocurrent and hence the overall efficiency of the cell. Therefore, new methods for cleaning and a new cell design are proposed and used throughout the experiments. Capacitance measurements, using cyclic voltammetry and AC voltammetry techniques, in the absence and the presence of each of the cell analytes suggest that unmodified reaction centers, detergents, and the mediators bind to the surface of the gold electrode irreversibly. Finally, it is shown that cysteineless reaction centers also adsorb irreversibly on the surface of the gold, demonstrating that cysteine S-Au bonding is not the only irreversible binding mechanism.

# TABLE OF CONTENTS

<b>ABSTRACT .....</b>	<b>ii</b>
<b>TABLE OF CONTENTS.....</b>	<b>iii</b>
<b>LIST OF TABLES .....</b>	<b>vi</b>
<b>LIST OF FIGURES .....</b>	<b>vii</b>
<b>ACKNOWLEDGEMENTS .....</b>	<b>xiv</b>
<b>1 INTRODUCTION.....</b>	<b>1</b>
<b>1.1 Introduction.....</b>	<b>1</b>
<b>1.2 Thesis Goal and Outline .....</b>	<b>4</b>
1.2.1 Thesis Goal.....	4
1.2.2 Thesis Outline .....	4
<b>2 PROTEIN ADSORPTION ON METAL SURFACE .....</b>	<b>5</b>
<b>2.1 Adsorption of Proteins: Introduction.....</b>	<b>5</b>
<b>2.2 Surface Properties.....</b>	<b>6</b>
<b>2.3 Solution Properties.....</b>	<b>7</b>
<b>2.4 Adsorption Strength .....</b>	<b>7</b>
<b>2.5 Structure of Charged Interface.....</b>	<b>8</b>
2.5.1 Double Layer.....	8
2.5.2 Structure of Double Layer with Adsorbed Species .....	9
<b>2.6 Theoretical Approaches for Protein Adsorption.....</b>	<b>10</b>
2.6.1 Langmuir Adsorption Isotherm .....	10
2.6.2 Random Sequential Model.....	11
<b>3 EXPERIMENTAL METHODS, CELL PREPARATION, MATERIALS .....</b>	<b>12</b>
<b>3.1 Experimental Methods .....</b>	<b>12</b>
3.1.1 Cyclic Voltammetry .....	12

3.1.2	AC Voltammetry .....	14
<b>3.2</b>	<b>Cell Preparation .....</b>	<b>15</b>
3.2.1	Electrode Fabrication .....	15
3.2.2	Cleaning Methods: .....	15
<b>3.3</b>	<b>Experimental Setup .....</b>	<b>17</b>
<b>3.4</b>	<b>Materials .....</b>	<b>18</b>
<b>4</b>	<b>RESULTS .....</b>	<b>20</b>
<b>4.1</b>	<b>Electrochemical Characterization of the Gold Electrode .....</b>	<b>20</b>
<b>4.2</b>	<b>Effect of the Preparation of the Gold Electrode .....</b>	<b>20</b>
<b>4.3</b>	<b>Oxygen Elimination .....</b>	<b>23</b>
<b>4.4</b>	<b>Electrolyte .....</b>	<b>24</b>
4.4.1	Organic Buffers .....	24
4.4.2	Potassium Phosphate Buffer .....	26
<b>4.5</b>	<b>Adsorption of Phosphate Buffer on Bare Gold Electrode .....</b>	<b>28</b>
<b>4.6</b>	<b>Cytochrome c .....</b>	<b>30</b>
4.6.1	Adsorption of Cytochrome c on Bare Gold Electrode .....	31
4.6.2	Effect of Exposure Time on Cyt c Adsorption .....	32
4.6.3	Effect of Applied Potential during Electrode Exposure .....	34
4.6.4	Reversibility of the Cytochrome c Adsorption on Gold .....	36
4.6.5	Electrochemical Studies of Cytochrome c on a Bare Gold Electrode .....	36
<b>4.7</b>	<b>Quinone .....</b>	<b>39</b>
4.7.1	Electrochemical Studies of Quinone on Bare Gold Electrode .....	41
4.7.2	Adsorption of Quinone on Bare Gold Electrode .....	46
<b>4.8</b>	<b>Surfactants .....</b>	<b>50</b>
4.8.1	LDAO .....	50
4.8.2	Electrochemical Characterization of LDAO .....	51
4.8.3	Adsorption of LDAO on Bare Gold Electrode .....	53
4.8.4	DDM and $\beta$ -OG .....	55
4.8.5	Electrochemistry of DDM and $\beta$ -OG .....	56

4.8.6	Adsorption of DDM and $\beta$ -OG on Bare Gold Electrode .....	58
<b>4.9</b>	<b>Reaction Center.....</b>	<b>60</b>
4.9.1	Electrochemistry of Rhodobacter sphaeroides RC .....	61
4.9.2	Adsorption of Rhodobacter sphaeroides RC .....	67
<b>4.10</b>	<b>Cysteine-less Reaction Centers .....</b>	<b>70</b>
4.10.1	Electrochemistry of Cysteineless Rhodobacter sphaeroides RC .....	70
4.10.2	Adsorption of Cysteineless Rhodobacter Sphaeroides RC.....	73
<b>5</b>	<b>CONCLUSION .....</b>	<b>77</b>
5.1	Future Work.....	80
<b>6</b>	<b>REFERENCES: .....</b>	<b>82</b>

## LIST OF TABLES

Table 4-1: The oxidation and second reduction peak currents for three different concentrations of quinone. ....	44
Table 4-2: Amount and capacitance measurements for Quinone during cyclic voltammetry tests.....	47
Table 4-3: LDAO amount and capacitance measurements during CV and ACV tests. ....	54
Table 4-4: double layer capacitance changes for different amount of LDAO in phosphate buffer.....	54
Table 4-5: Gold active surface area after RC adsorption in dark and light from a 20 $\mu\text{M}$ RC containing solution. ....	67
Table 4-6: Double layer capacitance ( $\mu\text{F}$ ) and the capacitance changes when bare gold electrode is exposed to phosphate buffer containing RC at various amounts listed. Negative sign is an indication of capacitance reduction. ....	69
Table 4-7: Double layer capacitance ( $\mu\text{F}$ ) and the capacitance changes when bare gold is exposed to phosphate buffer containing cysteineless RC at various amounts listed. Negative sign is an indication of capacitance reduction. ....	75
Table 5-1: Summary of the obtained results.....	80

## LIST OF FIGURES

Figure 1-1: A monolayer of Rhodobacter sphaeroides reaction centers linked to electrode to facilitated electron transfer between $Q_B$ and the electrode. ....	2
Figure 1-2: Schematic of photogalvanic cell composed of dissolved reaction centers and 2 mediators. ....	3
Figure 2-1: A schematic to show globular protein adsorption and its conformational changes during interactions with the metal surface .....	5
Figure 2-2: Schematic of double layer in an electrolyte in contact with a negatively charged metal ....	9
Figure 2-3: A disturbed double layer structure in the presence of proteins at the interface .....	9
Figure 2-4: Schematic for surface adsorption, conformational changes, and desorption of proteins...	11
Figure 3-1: Potential time and current potential plots for an equivalent RC circuit for cyclic voltammetry.....	13
Figure 3-2: Surface coverage calculation from the area underneath the peak obtained in cyclic voltammetry.....	14
Figure 3-3: Potential time and corresponding current potential plots for AC voltammetry.....	14
Figure 3-4: The three electrode experimental setup used in an oxygen free cell to perform electrochemical tests.....	18
Figure 4-1: Cyclic voltammetry results for left: gold slide; right: gold bead (with superimposed slide plot as shown in blue) in 0.1 M Tris-HCl solutions at the scan rate of 20 mV/s.....	21
Figure 4-2: Zoomed in plot for the cyclic voltammetry tests for gold slide and gold bead at 20 mV/s in 0.1 M Tris-HCl solution. ....	22
Figure 4-3: Cyclic voltammetry for 0.1 M potassium phosphate buffer pH 7. Blue: regular cell exposed to air ; red: deoxygenated and sealed cell.....	23
Figure 4-4: Representation of Tris – HCl chemical structure .....	24

Figure 4-5: CV graph for gold bead electrode from -1 to 1 V vs. Ag/AgCl reference in 0.1 M Tris-HCl at a scan rate of 20 mV/s.....	25
Figure 4-6: Chemical structure of : left: HEPES; right: MOPS .....	25
Figure 4-7: CV graph for gold bead electrode: left from -0.8 to 1.2 V vs. Ag/AgCl reference in 0.1 M HEPES; right: from -0.8 to 1 V vs. Ag/AgCl in 0.1 M MOPS both at a scan rate of 20 mV/s.....	26
Figure 4-8: Cyclic voltammogram of clean gold electrode in 0.1 M potassium phosphate buffer at pH 7, right: at scan rates: blue: 20, red: 10, and green: 5 mV/s; left: at scan rates: blue: 10 mV/s and red: 5 mV/s. The solution is deoxygenated with N <sub>2</sub> for 15 minutes and a N <sub>2</sub> blanket kept the solution degassed during the measurements. ....	27
Figure 4-9: Cyclic voltammogram of clean gold electrode in 0.1 M deoxygenated potassium phosphate buffer at pH 7. Scan rate 20 mV/s. Left: the voltage is increased by 0.1 V toward negative; right: the voltage is increased by 0.1 V toward positive values. ....	28
Figure 4-10: Capacitance profile measurements for bare gold electrode exposed to blue: 2.5 ml 50 mM potassium perchlorate solution; red: 2 μl; magenta: 7 μl; green: 20 μl potassium phosphate buffer. Frequency: 25 Hz, amplitude: 5 mV, scan rate: 5 mV/s.....	29
Figure 4-11: Cyclic voltammograms for bare gold electrode exposed to: blue: 2.5 ml of 50 mM potassium perchlorate solution, red: 2 μl, magenta: 7 μl, green: 20 μl 10 mM potassium phosphate buffer added to KClO <sub>4</sub> . Scan rate: 5 mV/s. ....	30
Figure 4-12: Left: Capacitance profile measurements; right: cyclic voltammograms for bare gold electrode exposed to: blue: 2.5 ml of 100 mM potassium phosphate buffer along with red: 2 μl, magenta: 7 μl, green: 20 μl reduced cyt c <sup>2+</sup> added. Frequency: 25 Hz, amplitude: 5 mV, scan rate: 5 mV/s. ....	31
Figure 4-13: Comparison of full scan CVs recorded on a bare gold electrode after adsorption of different amounts of cyt c (blue: 2.5 ml phosphate buffer, red: 2 μl, magenta: 7 μl, and green: 20 μl of cyt c <sup>2+</sup> added to buffer) . CVs are recorded at a scan rate of 5 mV/s. ....	32
Figure 4-14: Comparison of CVs measured on a bare gold electrode after adsorption of cyt c <sup>2+</sup> (20 μM, pH 7) at a scan rate of 20 mV/s. The exposure times are listed as legends in the graph. Potentials are versus Ag/AgCl reference electrode.....	33

Figure 4-15: Capacitive current profile for the bare gold electrode for 20  $\mu\text{M}$  cytochrome c in pH 7. The protein adsorption has happened at open circuit potential. All the CVs are recorded at a scan rate of 20 mV/s ..... 34

Figure 4-16: Capacitive current profile for bare gold electrode exposed to 20  $\mu\text{M}$  of cyt  $\text{c}^{2+}$  at pH 7. The cyclic voltammograms are recorded in 100 mM potassium phosphate buffer after adsorption of cyt  $\text{c}^{2+}$  for various times at different voltages. The applied voltage is indicated in legend of the graphs. The scan rate is 20 mV/s. .... 35

Figure 4-17: Left: cyclic voltammograms used to compare double layers formed on a gold electrode surface immediately (blue) after adsorption of cytochrome c (10.5  $\mu\text{M}$ , pH 7), and then after keeping the electrode in a fresh buffer for 10 hours (red). Right: Comparison of gold redox peaks immediately (blue) after adsorption of cytochrome c (10.5  $\mu\text{M}$ , pH 7) and after keeping the electrode in a fresh buffer for 10 hours (red). All CVs are performed at a scan rate of 5 mV/s. .... 36

Figure 4-18: CV graph for 20  $\mu\text{l}$  cyt c dissolved in 2.5 ml 0.1 M phosphate buffer at a scan rate of 20 mV/s. .... 37

Figure 4-19: Cyclic voltammograms for 20  $\mu\text{M}$  cytochrome c in phosphate buffer on bare gold electrode recorded at the scan rate of 20 mV/s. The measurements are performed in potassium buffer pH 7 with two concentrations: blue) 100 mM, red) 30 mM. .... 38

Figure 4-20: Cyclic voltammetry plot for 20  $\mu\text{M}$  reduced cytochrome c added to 2.5 mL of 30 mM phosphate buffer on bare gold electrode at a scan rate of 20 mV/s ..... 38

Figure 4-21: Diagram of oxidation and reduction states of Quinone. The species in the red rhombuses exist in both primary ( $\text{Q}_\text{A}$ ) and secondary quinone ( $\text{Q}_\text{B}$ ) sites. The species in the dark grey rhombuses are found in secondary quinone. The species in light grey do not exist in RCs and aqueous solution. 40

Figure 4-22: Quinone's: a- two electron reduction at alkaline pH; b – Single step two electron two proton reduction at acidic pH; c-Two-electron one-proton reduction at neutral pH. .... 41

Figure 4-23: Cyclic voltammetry of 60  $\mu\text{M}$  quinone in 0.1 M phosphate buffer at pH 7 at a scan rate of 5 mV/s ..... 42

Figure 4-24: Two superimposed cyclic voltammograms for 70  $\mu\text{M}$  quinone in 0.1 M potassium phosphate buffer at pH 7 on gold electrode performed in two separate cells. The solution is

deoxygenated with N <sub>2</sub> gas for 15 minutes and is kept degassed by flowing N <sub>2</sub> on top of the surface of the solution. Scan rate: 5 mV/s.....	43
Figure 4-25: Cyclic voltammograms for 70 μM quinone in 0.1 M potassium phosphate buffer at pH 7 on gold electrode when the voltage is increased gradually toward the positive values. The solution is deoxygenated with N <sub>2</sub> gas for 15 minutes and is kept degassed by flowing N <sub>2</sub> on top of the surface of the solution. Scan rate: 5 mV/s.....	43
Figure 4-26: Cyclic voltammograms of 10 (blue), 20 (red), and 30 (green) μM Quinone in 0.1 M phosphate buffer at pH 7. Scan rate: 5 mV/s.....	44
Figure 4-27: Peak current (blue: reversible peak, red: irreversible reduction peak) vs. $v^{1/2}$ for 10 μM quinone solution in 0.1 M phosphate buffer at 10, 20, and 30 mV/s scan rate .....	45
Figure 4-28: Cyclic voltammetry plots for 10 μM quinone in 0.1 M phosphate buffer at pH 7 recorded at 20, 10, and 5 mV/s.....	46
Figure 4-29: Cyclic voltammetry tests for blue: 2, red: 6.5, magenta: 20, and green: 70 μl Quinone in 2.5 ml potassium phosphate buffer (100 mM, pH 7) on bare gold electrode (Scan rate = 5 mV/s, 45 minutes after electrode immersion). .....	48
Figure 4-30: AC voltammetry tests for blue: 2, red: 6.5, magenta: 20, and green: 70 μl Quinone in 2.5 ml potassium phosphate buffer (100 mM, pH 7) on bare gold electrode (Scan rate = 5 mV/s).....	48
Figure 4-31: Cyclic voltammetry plots for 20 μl quinone in 2.5 ml potassium phosphate buffer at pH 7 while increasing the negative voltage range. Scan rate: 20 mV/s. ....	49
Figure 4-32: Left: superimposed cyclic voltammetry records for 20 μl quinone in 2.5 ml phosphate buffer at pH 7 (scan rate 20 mV/s); right: zoomed in section to show the quinone redox peak changes from -0.4 to 0.8 V. Scan rate: 20 mV/s. ....	49
Figure 4-33: Lauryldimethylamine-oxide (LDAO) chemical structure .....	51
Figure 4-34: Cyclic voltammetry tests for 0.1% LDAO v/v in 2.5 ml 0.1 M potassium phosphate buffer left: at scan rate blue: 20, red: 10, and green: 5 mV/s; right: scan rate of blue: 10 and red: 5 mV/s. The voltages are presented vs. Ag/AgCl reference.....	51

Figure 4-35: Cyclic voltammetry results for 0.1% v/v LDAO in 2.5 ml potassium phosphate buffer (100 mM, pH7) left: when the voltage is increasing toward the negative values right: the voltage is increased toward the positive values at scan rate of 20 mV/s. .... 52

Figure 4-36: Left: Cyclic voltammetry; right: AC voltammetry tests for 2, 7, and 20  $\mu$ l for LDAO dissolved in 2.5 ml 50 mM KClO<sub>4</sub> pH 7 (Frequency: 25 Hz, amplitude: 5 mV, scan rate: 5 mV/s). The solution is deoxygenated with N<sub>2</sub> gas for 15 minutes and is kept degassed by flowing N<sub>2</sub> on top of the surface of the solution. The voltages are presented vs. Ag/AgCl reference. .... 53

Figure 4-37: Left: Cyclic voltammetry; Right: AC voltammetry tests for 2, 7, and 20  $\mu$ l for LDAO dissolved in 2.5 ml 100 mM phosphate buffer pH 7 (Frequency: 25 Hz, amplitude: 5 mV, scan rate: 5 mV/s). The solution is deoxygenated with N<sub>2</sub> gas for 15 minutes and is kept degassed by flowing N<sub>2</sub> on top of the surface of the solution. The voltages are presented vs. Ag/AgCl reference. .... 53

Figure 4-38: Chemical structure of left: n-Dodecyl- $\beta$ -D-Maltoside (DDM) and right: n-Octyl- $\beta$ -D-Glucopyranoside ( $\beta$ -OG) ..... 55

Figure 4-39: Left: double layer; Right: full scan CVs of DDM detergent (~ 2.5  $\mu$ l) in potassium phosphate buffer (100 mM buffer, pH 7, voltage range: -0.3 to 0.1 V vs. Ag/AgCl). Scan rates blue: 20, red: 10, green: 5 mV/s for double layer region CVs; scan rates blue: 10 and red: 5 mV/s for full scans (Voltage range: -0.3 to 0.1 V vs. Ag/AgCl) ..... 56

Figure 4-40: Left: Cyclic voltammetry at double layer region between -0.3 to 0.1 V vs. Ag/AgCl at three scan rates: 20, 10, and 5 mV/s; right: full scan between -0.8 to 1.2 V vs. Ag/AgCl at two scan rates: 10 and 5 mV/s CV of  $\beta$ -OG detergent (~ 2.5  $\mu$ l) in potassium phosphate buffer (100 mM buffer, pH 7) ..... 57

Figure 4-41: Cyclic voltammograms of bare gold electrode at 20 mV/s for 0.1% v/v DDM detergent in 100 mM potassium phosphate buffer pH 7 while increasing the voltage toward the left: negative values; right: positive values. .... 58

Figure 4-42: Cyclic voltammograms of bare gold electrode at 20 mV/s for 0.1% v/v  $\beta$ -OG detergent in 100 mM potassium phosphate buffer pH 7 while increasing the voltage toward the left: negative values; right: positive values. .... 58

Figure 4-43: Capacitance profile measurements for bare gold electrode exposed left: (50 mM KClO<sub>4</sub>) right : 100 mM Potassium phosphate buffer. blue: 2.5 ml buffer 2- red: 2  $\mu$ l 3- magenta: 7  $\mu$ l 4- green:

20  $\mu\text{l}$  5- purple: 80  $\mu\text{l}$  DDM detergent diluted in 2.5 ml buffer. The ACVs are recorded at scan rate: 5 mV/s, amplitude 5mV/s, and frequency: 25 Hz. .... 59

Figure 4-44: Capacitance profile measurements for bare gold electrode exposed left: (50 mM  $\text{KClO}_4$ ) right : 100 mM Potassium phosphate buffer. blue: 2.5 ml buffer 2- red: 2  $\mu\text{l}$  3- magenta: 7  $\mu\text{l}$  4- green: 20  $\mu\text{l}$  5- purple: 80  $\mu\text{l}$   $\beta$ -OG detergent diluted in 2.5 ml buffer. The ACVs are recorded at scan rate: 5 mV/s, amplitude 5mV/s, and frequency: 25 Hz. .... 59

Figure 4-45: Left: schematic view of photosynthetic RC of Rhodobacter sphaeroides. L, M, and H represent the protein subunits. The photosynthetic electron transfer between the cofactors, indicated by arrows, is one sided along the L subunit. The corresponding time constants are shown for each electron transfer process. Right: photochemistry energy diagram for electron transfer process in reaction center. The potential is reported vs. NHE..... 60

Figure 4-46: CVs of 20  $\mu\text{M}$  Rhodobacter sphaeroides RCs on bare gold electrode in potassium phosphate buffer ( 100 mM, pH 7) with 0.1% v/v red: LDAO, green: DDM, blue:  $\beta$ -OG..... 62

Figure 4-47: Full scan CVs of 20  $\mu\text{M}$  Rhodobacter sphaeroides RCs on bare gold electrode in potassium phosphate buffer (100 mM, pH 7) with 0.1% v/v red: LDAO, green: DDM, blue:  $\beta$ -OG. The final sweep for each sample is recorded 1 hour after the last scan and its graph is superimposed on the plots. .... 63

Figure 4-48: CVs of 20  $\mu\text{M}$  illuminated Rhodobacter sphaeroides RCs on bare gold electrode in potassium phosphate buffer ( 100 mM, pH 7) with 0.1% v/v red: LDAO, green: DDM, blue:  $\beta$ -OG. 64

Figure 4-49: Full scan CVs of 20  $\mu\text{M}$  illuminated Rhodobacter sphaeroides RCs on bare gold electrode in potassium phosphate buffer ( 100 mM, pH 7) with 0.1% v/v red: LDAO, green: DDM, blue:  $\beta$ -OG..... 64

Figure 4-50: Cyclic voltammograms of blue: 20  $\mu\text{M}$ , red: 40  $\mu\text{M}$  RC with  $\beta$ -OG in potassium phosphate buffer (100 mM, pH7) when illuminated at 5 mV/s..... 65

Figure 4-51: Cyclic voltammogram of 40  $\mu\text{M}$  RC with  $\beta$ -OG in potassium phosphate buffer (100 mM, pH7) when illuminated at 5 mV/s..... 66

Figure 4-52: Left: in dark; right: during illumination - Capacitance profile measurements for bare gold electrode exposed to blue: 2.5 ml 100 mM potassium phosphate buffer; red: 2  $\mu\text{l}$ ; green: 7  $\mu\text{l}$ ;

magenta: 20  $\mu$ l RC with 0.1% v/v LDAO detergent diluted in 2.5 ml phosphate buffer. The ACVs are recorded at scan rate: 5 mV/s, amplitude: 5 mV, and frequency: 25 Hz. .... 67

Figure 4-53: Left: In dark; right: during illumination - Capacitance profile measurements for bare gold electrode exposed to blue: 2.5 ml 100 mM potassium phosphate buffer; red: 2  $\mu$ l; green: 7  $\mu$ l; magenta: 20  $\mu$ l RC in 0.1% v/v DDm detergent diluted in 2.5 ml phosphate buffer. The ACVs are recorded at scan rate: 5 mV/s, amplitude: 5 mV, and frequency: 25 Hz. .... 68

Figure 4-54: Left: In dark-right: during illumination - Capacitance profile measurements for bare gold electrode exposed to blue: 2.5 ml 100 mM potassium phosphate buffer; red: 2  $\mu$ l; green: 7  $\mu$ l; magenta: 20  $\mu$ l RC in 0.1% v/v  $\beta$ -OG detergent diluted in 2.5 ml phosphate buffer. The ACVs are recorded at scan rate: 5 mV/s, amplitude: 5 mV, and frequency: 25 Hz. .... 68

Figure 4-55: Two cyclic voltammograms (blue – small voltage range to probe the double layer, red – large voltage range) of 40  $\mu$ M cysteineless *Rhodobacter sphaeroides* RCs on bare gold electrode in potassium phosphate buffer ( 100 mM, pH 7) with 0.1% v/v LDAO in Dark. .... 71

Figure 4-56: Two cyclic voltammograms of 40  $\mu$ M cysteineless *Rhodobacter sphaeroides* RCs on bare gold electrode under illumination in potassium phosphate buffer (100 mM, pH 7) with 0.1% v/v LDAO. The blue curve covers the capacitive region of the response. .... 71

Figure 4-57: Cyclic voltammograms for 40  $\mu$ M cysteineless RC in 0.1 M potassium phosphate buffer at pH 7 on gold electrode before (blue) and after (red) exposure to light. Scan rate: 5 mV/s ..... 72

Figure 4-58: Full cyclic voltammograms for 40  $\mu$ M cysteineless RC in 0.1 M potassium phosphate buffer at pH 7 on gold electrode before (blue) and after (red) exposure to light. Scan rate: 5mV/s .... 73

Figure 4-59: In dark - Capacitance profile measurements for bare gold electrode exposed to: blue: 2.5 ml 100 mM potassium phosphate buffer; red: 2  $\mu$ l 3- magenta: 7  $\mu$ l, green: 20  $\mu$ l cysteineless RC with 0.1% v/v LDAO detergent diluted in 2.5 ml ..... 74

Figure 4-60: During illumination - Capacitance profile measurements for bare gold electrode exposed to 1- Blue: 2.5 ml 100 mM Potassium Phosphate buffer 2- Red: 2  $\mu$ l 3- magenta: 7  $\mu$ l 4- green: 20  $\mu$ l cysteineless RC with 0.1% v/v LDAO detergent diluted ..... 74

## **ACKNOWLEDGEMENTS**

First and foremost I owe my deepest appreciation to my supervisor Dr. John Madden and my Co-Supervisors Dr. Dan Bizzotto and Dr. Tom Beatty, for providing ongoing advise, support, and encouragement throughout my research. It is difficult to overstate my gratitude to Dr. Madden and Dr. Bizzotto whose inspiration and great efforts to explain concepts clearly made electrochemistry fun for me. I would have been lost without their exceptional teaching skills, ideas, and company. I am also deeply indebted to my colleague and friend Ali Mahmoudzadeh whose help and patience contributed significantly to this work. I would also like to express my gratitude to Dr. Arash Takshi, my colleagues and friends Seyed Mohammad Mirvakili, Eddie Fok, Ashwin Usgaocar, and Joanna Slota for their invaluable feedback and discussions during my studies.

I am particularly thankful to Dr. Beatty's group members, Daniel Jun and Rafael Saer, who prepared and provided the proteins and buffers used in this research.

I wish to thank my cousin Shaghayegh Akhtari, and my best friends Zahra Sadat and Elham Hosseini Beheshti for helping me get through difficult times, and for all the support they provided.

Lastly, and most importantly, I would like to thank my family, particularly my father Ali, my mother Soudabeh, and my sister Nahal, for their continual love, support, and understanding throughout my studies. To them I dedicate this thesis.

# 1 INTRODUCTION

## 1.1 Introduction

Solar energy, known as the most abundant renewable energy source, has the potential to provide a large portion of the electricity requirements of the world [1]. In addition, this clean energy could play a very important role in solving environmental issues [2]. However, the high cost of energy conversion and energy storage in the conventional solid-state junction photovoltaic devices has impeded the extensive commercial use of solar energy. Some emerging developments in solar have been taking place in the past few decades to improve the situation. Organic solid state devices, such as conducting polymer films, are the second generation of solar cells that offer low cost manufacturing and tuneable properties. Dye-sensitized solar cells (DSSCs), introduced by Micheal Gratzel and his team in 1991, are the third generation of solar devices in which an electrolyte has replaced the semiconductor contacting phase. These devices are closest in operation to the cells presented here.

The operational principle of DSSCs is based on charge absorption and electron-hole separation in photon-absorbing dyes linked to wide band gap nanocrystalline semiconductors such as  $\text{TiO}_2$ . Upon absorbing a photon, an electron is elevated to an excited state. In a fraction of a second, this electron is transferred to the conduction band of the titanium dioxide and then it diffuses to an external electrode. The oxidized dye is then reduced by an anion such as  $\text{I}^-$  in the solution phase. The efficiency in dye sensitized solar cells depends on several factors such as dye absorption spectrum, the dye/anion and dye/semiconductor interface behaviour, the ion transport at the solution interface and the charge transfer and transport at the semiconductor. Also, in practice, efficiently separating the electron-hole pair before they recombine is a major factor that can limit the performance of these cells.

A recent and not well understood generation of photovoltaic devices are those which incorporate biological systems, such as bacterial photosynthetic reaction centers (RC), to capture the photons [3]. A number of protein membranes are responsible for converting the light into chemical energy in photosynthesis. Soluble cytochrome c (cyt c) reduces the oxidized bacteriochlorophyll dimer in bacterial reaction centers [3]. In protein-based solar devices the dipole formed due to excited an electron in the RC is neutralized by the charge from the mediators that alternate their oxidation states and carry the excess charge to the suitable electrode. In the absence of recombination of the excited

state, the ultimate theoretical power conversion efficiency in such device is calculated to be 27% [4]. One commonly used electrode material, especially if the RCs are intended to be immobilized on the surface of the electrode in a specific orientation, is the gold [5–8]. Two basic device architectures are being investigated. The principle operation of the first involves the use of RCs immobilized on an electrode (similar to DSSCs) and the second is a novel approach introduced by our group that has similarities to photogalvanic cells [9].

In the first approach, as in DSSCs, a monolayer of oriented RCs can be coated on the surface of one electrode. Upon illumination and photo-excitation, charge separation takes place rapidly in RCs. In order to efficiently transfer the photo-generated charges by tunnelling, the RCs have to be attached to the electrode surface with the minimum possible distance between the positively charged P site or negatively charged  $Q_B$  (see Figure 1-1; refer to chapter 4, section 4.9, page 60 for detailed structure of RC). The opposite charges are carried to the second electrode by the diffusion of charge-carrying mediators. The side close to the electrode may exhibit direct electron transfer [8], or still rely on mediator transport [10]. Interestingly the rates of such transport suggest extremely slow diffusion of mediators. The work presented in this thesis suggests a likely reason – that the surface of the electrode is coated with proteins, surfactants and mediators that may all impeded transport.

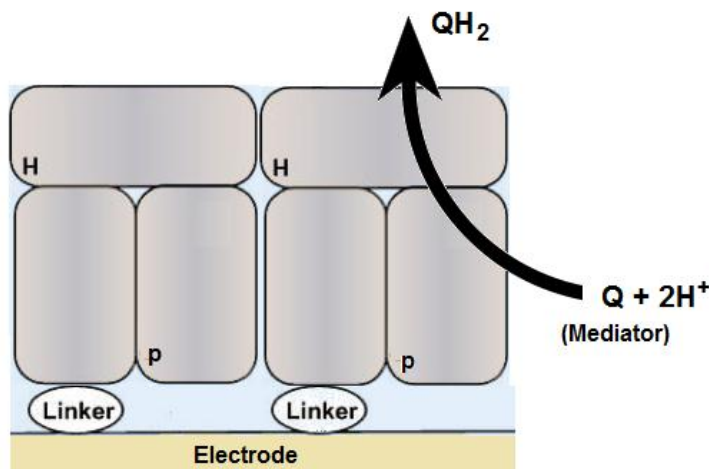


**Figure 1-1: A monolayer of Rhodospirillum rubrum reaction centers linked to electrode to facilitate electron transfer between  $Q_B$  and the electrode.**

Alternatively, it has been reported that if RCs and mediators are dissolved or suspended in an electrolyte, indirect charge transfer can result in photo-current generation [11]. In this approach the RCs are simply dissolved in an electrolyte. The charge transfer to the electrodes takes place using two mediators which are compatible with either the P or Q site of the reaction center. As shown in Figure

1-2, upon photon adsorption, one mediator ( $m_1$ ) donates an electron to the positively charged P site of the reaction center.  $Q_B$  on the other side of the reaction center is oxidized by the second mediator ( $m_2$ ).

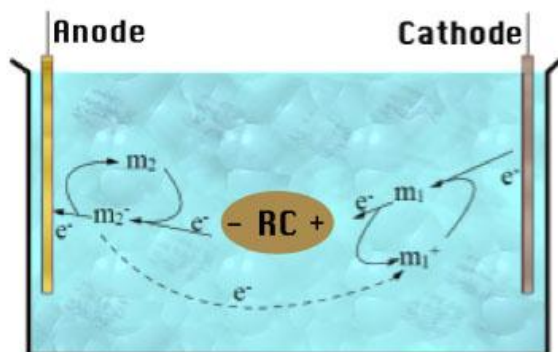


**Figure 1-2: Schematic of photogalvanic cell composed of dissolved reaction centers and two mediators.**

The advantage of the photogalvanic cell approach over immobilizing RCs on the electrode surface is that the current can be increased by increasing the concentration of the reaction centers in solution rather than by having to create a transparent porous electrode coated with RCs [11]. However, the practical efficiency of such system is so far well below the calculated efficiency.

Several factors can influence the efficiency of protein-based solar cells, of which two are investigated in this work. It is found that using an ultra-clean and deoxygenated system results in the reduction of unwanted side reactions on the surface of the gold electrode. To obtain test results with minimum back reactions: 1. new methods for cleaning the cell and the electrodes 2. a new cell design is proposed and used throughout the measurements. Properly removing contaminations from the cell components can result in the elimination of potential parasitic reactions that are generated due to these impurities. Moreover, it can be ensured that the reactants can access the whole surface of the electrodes if the surface is cleaned properly.

In addition, it has been observed that the proteins and other species adsorb irreversibly on the surface of the gold electrode almost spontaneously and thus modifying the electrochemical response of the surface of the electrode. Cyclic voltammetry and AC voltammetry are used to observe double layer capacitance changes when particles such as proteins diffuse into the Helmholtz layer, replace the water molecules, and result in dielectric constant changes and thickness changes between the parallel plates of the capacitor. The electrode surface blockage due to the adsorption of cell

components hinders the charge transfer through the electrode and hence reduces the overall photocurrent.

The experimental protocol presented in this work can provide guidance for electrochemical analysis of new potential electrodes that are to be used in protein-based solar cells in the future.

## **1.2 Thesis Goal and Outline**

### **1.2.1 Thesis Goal**

In this work, the importance of the cleanliness of the system and parasitic reactions is investigated. In addition, the adsorption of the RCs, the dissolving detergents, and the mediators is studied, since the adsorption of these analytes can greatly affect the photocurrent generation in the system. The adsorption of the cell components on the surface of the gold electrode is investigated by detecting the double layer capacitance changes on the working electrode surface using cyclic voltammetry and AC voltammetry.

In addition, it is shown that by keeping the electrode at specific potentials, the adsorption process for cytochrome c can be accelerated or decelerated. Moreover, the electrode surface coverage is estimated for the reaction centers.

### **1.2.2 Thesis Outline**

The thesis is organized as follows:

1. Chapter 2 describes the protein adsorption process and factors affecting the adsorption and desorption of the proteins.
2. Chapter 3 contains the experimental methods, the cell setup used to perform the tests on the cell and the specification of the materials used.
3. Chapter 4 introduces the functions of each species in the system plus the final results obtained for different solutions, detergents, reaction center and the two mediators.
4. Chapter 5 contains the concluding remarks and the suggested future work.

## 2 PROTEIN ADSORPTION ON METAL SURFACE

This chapter provides an overview of protein adsorption driving forces, the environmental factors that can influence the adsorption process, and the strength of the adsorption on a solid surface. Since the protein adsorption is mainly observed through double layer capacitance changes during this work, the double layer structure in the absence and the presence of the proteins is discussed to provide a more clear insight about the experimental results presented in the following chapter.

### 2.1 Adsorption of Proteins: Introduction

Proteins are complex, three-dimensional structures with both hydrophobic and hydrophilic regions, which can undergo conformational changes when adsorbed on a surface [12]. Polar amino acid side chains of proteins tend to strongly interact with metal surfaces regardless of the net charge of the protein or the surface [12]. The charge distribution and net charge of the protein are effective factors in electrostatic interactions between the proteins and the surface [13]. The adsorption behaviour of some proteins is more affected by hydrophobicity. This group, known as “soft proteins”, tend to denature upon adsorption and are usually irreversibly adsorbed on the surface [14], [13]. The second group which resembles a colloidal system to some extent, known as “hard proteins”, is more affected by the electrostatic interactions between the proteins and the solid surface [13]. Moreover, the hydrophobic chains of the adsorbed proteins can be exposed to the solution. This may cause the adsorption of a second layer of proteins that result in the reduction of the free surface energy [12].

Previous work reports that if the amount of the adsorbed proteins on the surface is high, less conformational change is observed due to the lack of space for the proteins to spread out [13]. Hence, conformational changes are reported to be higher when the surface coverage is low since other molecules can affect the protein to change shape [13].

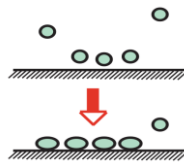


**Figure 2-1: A schematic to show globular protein adsorption and its conformational changes during interactions with the metal surface.**

Nakanishi *et al.* states that hydrophobic and electrostatic interactions between the metal surface and the proteins are major forces governing the adsorption [14]. The electrostatic repulsions can be overcome by entropy gain caused by conformational changes and thus the adsorption can happen [13], [14]. The largest gain in entropy can probably result from the large number of mobile small molecules, such as water molecules that gain many degrees of freedom, displaced from the electrode surface by the protein. In the case of small conformational changes however, the proteins are reported to remain bioactive after adsorption. Nevertheless, soft proteins and hard proteins that undergo major structural changes after adsorption are generally less functional on the metal surface [13].

Depending on the surface hydrophobicity or hydrophilicity and the protein properties the adsorption process can be reversible or irreversible. Proteins may desorb from the metal surface if the pH or the ionic strength of the solution is changed [13]. This usually applies to the adsorption of hard proteins on a hydrophilic surface in which the proteins undergo minor conformational changes. Soft protein adsorption, however, is reported to be irreversible in almost all cases [13], [14].

Nakanishi *et al* also report that it is possible for proteins to refold to their native shapes after desorption. Converting back to the native conformation is stated to be dependent on the protein stability and concentration, and electrostatic charges and the hydrophobicity of the metal surface [14]. At low concentration, proteins spread more on the surface and have more space for conformational changes. If the proteins are spreading for a long time on the surface, they tend to denature strongly which results in smaller chances for refolding to their original conformation [13], [14].

If there are different types of proteins added to a solution, the proteins with higher molecular weight tend to replace the lighter ones on the solid surface. However, there is currently little work done on how the competitive adsorption is evaluated for different types of proteins exposed to one surface at the same time [13–15].

## **2.2 Surface Properties**

It is generally less favourable for proteins to adsorb to a hydrophilic surface rather than to a hydrophobic surface [16]. In a study performed by Yoon *et al.* the adsorption of bovine serum albumin (BSA) on Microspheres of polystyrene/poly (methylmethacrylate) is investigated. They state that hydrophobic interactions and hydrogen bonding are the main reasons of the protein adsorption in their tests. Van der Waals interactions and ionic interactions, however, are reported to be less considerable.

The surface topography effects of a modified surface of evaporated titanium on the adsorption of F- actin protein are studied by Galli *et al.* Two different structures with surface roughness (heights) of 3 to 4 nm and 1 to 2 nm are examined. It is reported that less adsorption is observed on the surface with greater height than on the surface with less height. In addition, the proteins adsorbed on the surface with less height showed more specific orientation during adsorption [17]. Galli *et al.* describe the phenomenon by explaining that the proteins tend to adsorb on the surfaces with features that are similar in size to their size.

### **2.3 Solution Properties**

Several solution conditions, of which two are described in this subsection, can affect the adsorption of proteins. In a study made by Malmsten *et al.* it is reported that in a pH at which the protein net charge is zero, the isoelectric point, maximum adsorption occurs on the metal surface [18]. At the isoelectric point, the interactions between the proteins are favorable and the interaction between the proteins and solution are less important. The pH at which the experiments are performed in this work is 7 since they are known to be stable at this pH.

Hook *et al.* have studied the globular protein hemoglobin (Hb) adsorption on a gold surface covered by a monolayer of hydrophobic methyl-terminated thiol. At high ionic strength, negligible adsorption dependency on pH is reported at pH ranges between 6.5 and 7.5 [18]. The amount of the adsorption is measured using a quartz crystal microbalance (QCM) method, observing frequency changes due to the change of adsorbed mass [18]. The tests performed near the isoelectric point at 200 mM KCl salt concentration show high protein stability. Moreover, protein electrostatic interactions are stated to be lower at such high concentration compared to low ionic strengths. Hence, one monolayer is expected to form on the electrode surface at high ionic strength [18]. Stevens *et al.* have tested the response of an immobilized protein monolayer formed on a gold electrode surface using QCM and surface plasmon resonance (SPR) technique at a pH range between 4.5 and 11.2. They suggest that a rigid protein layer is formed at low pH. This layer can change to a fluidic layer as the pH increases. This fluidic layer then can permit the flow of water into and out of the immobilized layer and assists the protein deformation [19].

### **2.4 Adsorption Strength**

Adsorption strength and the amount of the proteins adsorbed on the surface are two key factors for characterizing the adsorbed layer. The orientation, conformational changes, and denaturation of the

proteins are influenced by how closely the proteins are packed on the surface. It is shown that with the increase in the amount of the adsorbed protein, the conformational changes of the adsorbed layer decrease due to less available space for the proteins to spread out [13]. According to Malmsten *et al.*, the jamming limit, defined as maximum space filled on the surface, is usually about 50 to 60% for colloidal particles. However, only hard proteins may behave close to colloidal particles. During and after adsorption the proteins can undergo conformational changes to reach lower energy. Even though the adsorption and initial conformational changes may occur within microseconds, the major conformational changes and relaxation may take place over a very long time in the order of hours to days [13], [16].

In general, proteins are known to change their orientation to allow more protein adsorption on the solid surface. In other words, the orientation changes will increase the amount of the proteins adsorbed on the surface. More importantly, because of higher surface coverage, the orientation changes reduce the chemical activities of the solid surface that is exposed to protein containing solution [13], [18].

## **2.5 Structure of Charged Interface**

An ideal polarizable electrode (IPE) is defined as a metallic electrode that does not allow charge transfer across the electrode/solution boundary regardless of the voltage applied from an external source. Thus, an IPE behaves as a capacitor. However, in practice, metallic electrodes behave as an IPE only in a limited voltage range [20]. In the IPE region, the only Faradaic currents expected to be observed are caused by impurities such as oxygen, organic species, and extra metal ions. Such currents can be reduced if the system is properly cleaned and sealed. Moreover, adsorption of external particles such as proteins can cause capacitance changes at IPE region as is explained in the following two subsections.

### **2.5.1 Double Layer**

An electrical double layer is formed on the surface of a metal electrode when it is placed in an ionic solution. The double layer capacitance (DLC), typically measured in the range of 10 to 40  $\frac{\mu F}{cm^2}$ , can be characterized when a certain potential is applied to the electrode [20]. The double layer on the solution side is made up of three layers: Inner Helmholtz, outer Helmholtz, and diffuse layer (Figure 2-2). The Inner Helmholtz layer is the first layer that contains the solution molecules and specifically adsorbed ions. The Outer Helmholtz layer is composed of non-specifically adsorbed solvated ions

that interact with the metal only through long electrostatic forces. The distribution of non-specifically adsorbed ions from the outer Helmholtz layer to the bulk of the solution in three dimensional regions forms the diffuse layer [20].

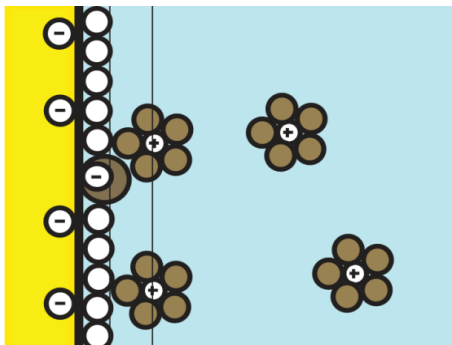


**Figure 2-2: Schematic of double layer in an electrolyte in contact with a negatively charged metal. White dots represent the inner Helmholtz layer, the outer Helmholtz layer is shown between two thin black lines, and the diffused layer is the bulk section containing free ions.**

The strong fields in the inner Helmholtz layer align polar solvent molecules such that they form an ice-like layer with lower dielectric constant than the bulk. As can be seen in Figure 2-2, an Ice-like layer mostly containing water molecules is formed on the metal surface in the absence of proteins. This layer acts as an isolating layer which prevents the propagation of impurities.

### 2.5.2 Structure of Double Layer with Adsorbed Species

Several models have been suggested to represent a charged interface with adsorbed organic species on the solid surface [20]. One commonly used model for a double layer formed in the presence of proteins is shown in Figure 2-3.

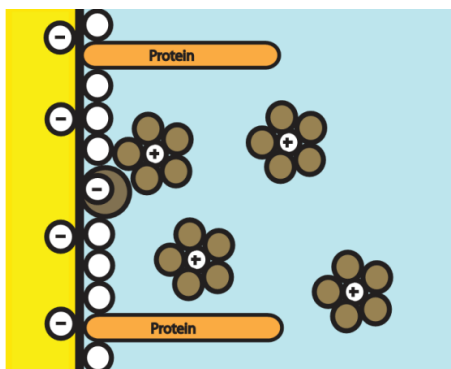


**Figure 2-3: A disturbed double layer structure in the presence of proteins at the interface.**

In this model, the initial inner layer breaks down: the proteins overcome the hydration forces and replace some of the water molecules in this layer. The proteins first migrate from the bulk solution by convection or diffusion and then mostly by diffusion toward the surface. Due to hydrophobic and electrostatic interactions the proteins displace the water molecules on the surface of the electrode. According to Young *et al*, the adsorption rate is a function of the surface coverage as the proteins fill in the surface and thus it is lower than the initial diffusion rate [22]. The reduction in the adsorption rate may be caused by electrostatic repulsions which can form an energy barrier against protein deposition [22], [23].

It is worth emphasizing that the proteins will later reorient themselves on the surface if their reorientation reduces the surface energy.

## 2.6 Theoretical Approaches for Protein Adsorption

Two commonly used methods to analyze the adsorption rate are introduced. These models have not been used in this work, however, they may be useful for further analysis and future work done on the adsorption of proteins on the surface of the electrodes.

### 2.6.1 Langmuir Adsorption Isotherm

The Langmuir isotherm is the most frequently used approach to quantify the amount of adsorption of a species onto a solid surface. The basic assumptions of this model are [24]:

- 1- Only a monolayer is adsorbed on a perfectly homogenous surface
- 2- The adsorbing sites the surface are separate and equally active
- 3- The neighbouring occupied sites do not affect the ability of the adsorption on another site

The final form of the kinetic equation becomes:

$$\frac{\partial \rho}{\partial t} = K_a C \left(1 - \frac{\rho}{\rho_{ml}}\right) - K_d \rho,$$

where  $K_a$  is the adsorption constant,  $K_d$  is the desorption constant,  $C$  represents the adsorbing species concentration at the surface ( $\frac{\mu g}{ml}$ ),  $\rho$  and  $\rho_{ml}$  are concentration of adsorbed species on the surface and the complete monolayer concentration on the surface respectively ( $\frac{\mu g}{cm^2}$ ) [24].

## 2.6.2 Random Sequential Model

Conformational and orientation changes of the proteins on the surface are considered in the proposed model [25]. As shown in Figure 2-4, the proteins adsorb on the surface in a random and sequential manner. Note that most of the proteins go through conformational changes and do not desorb from the metal surface which is shown as red protein. However, some hard proteins do not go through major shape changes and they may desorb from the metal surface after adsorption. Desorption of hard proteins is shown as yellow protein in the second step in Figure 2-4. The proteins then either go through conformational changes if there is enough space on the surface or desorb from the surface [24], [26]. The equations for this model are:

$$\frac{\partial \rho_{\alpha}}{\partial t} = K_a C \varphi_{\alpha} - K_d \rho_{\alpha} - K_s \rho_{\alpha} \varphi_{\alpha\beta},$$

$$\frac{\partial \rho_{\beta}}{\partial t} = K_s \rho_{\alpha} \varphi_{\alpha\beta},$$

where the adsorbed protein density in the un-spread and spread state is represented by  $\rho_{\alpha}$  and  $\rho_{\beta}$ ,  $K_a$ ,  $K_d$ ,  $K_s$  are the adsorption, desorption, and spreading rates,  $C$  is the bulk concentration of the proteins, and  $\varphi_{\alpha}$  and  $\varphi_{\alpha\beta}$  are the adsorption and spreading probability of molecules respectively [25], [27].

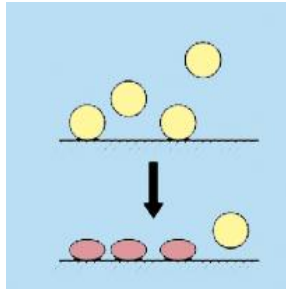


Figure 2-4: Schematic for surface adsorption, conformational changes, and desorption of proteins.

### **3 EXPERIMENTAL METHODS, CELL PREPARATION, MATERIALS**

This chapter introduces two experimental methods that are used to perform the tests during this work: cyclic voltammetry (CV) and AC voltammetry (ACV). Additionally, electrode fabrication and various cleaning methods considered and used are presented. The cell setup is then introduced. Finally, the specifications for the counter and reference electrode, salts, organics, proteins and surfactants are presented in the last section.

#### **3.1 Experimental Methods**

Various methods can be used to detect and measure protein adsorption on a solid surface. Some of these methods are based on electrochemical principles, for instance, cyclic voltammetry, AC voltammetry, and electrochemical impedance spectroscopy. Other non-electrochemical methods such as quartz crystal microbalance, which operates based on weight change detection, and techniques based on optical principals such as ellipsometry, internal reflection fluorescence, radio-labelling also exist [28], [29]. In this work cyclic voltammetry and AC voltammetry are used to observe protein adsorption and obtain measurements for adsorption based on double layer capacitance changes. These methods are briefly described in this section.

##### **3.1.1 Cyclic Voltammetry**

In cyclic voltammetry (CV) a voltage, applied between the working and reference electrodes, is scanned back and forth at a sweep rate  $\frac{dV}{dt} = \pm v$  between two desired voltage limits and the corresponding current flow in the system is measured vs. voltage (See Figure 3-1).

In the absence of electrochemical reactions, the current starts from zero and reaches a steady value (when the capacitor is fully charged) during each sweep. The rise time for the potential difference across the capacitor plates, until it reaches similar level of the applied potential, is shown in Figure 3-1 IE curve.

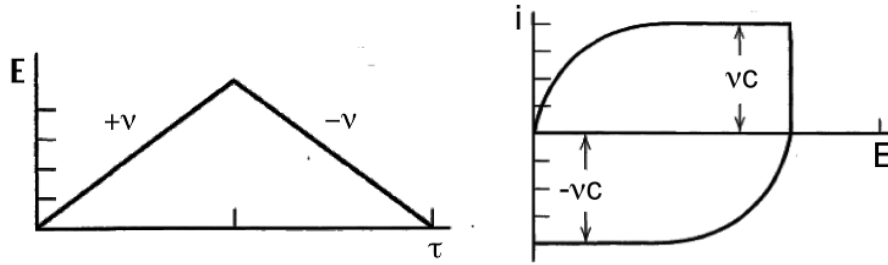


**Figure 3-1: Potential time and current potential plots for an equivalent RC circuit for cyclic voltammetry.**

For a purely capacitive behaviour, the double layer capacitance at the steady state can be defined as follows [20]:

$$i = C_d \frac{dV}{dt} = \pm v C_d \rightarrow C_d = \frac{i}{|v|}.$$

In the presence of electrochemical reactions, oxidation and reduction peaks are expected to be observed in the voltammogram plots. The start of such a reaction is expected to add a slope to the horizontal current plot, which can be modeled by adding a non-linear leakage resistor in parallel with the double layer capacitor. The leakage resistor can represent some unwanted charge flow in the system that can be in the opposite direction to the photocurrent in the photovoltaic cell. This unwanted charge flow is a result of an oxidation or reduction of a reactant in the system. The oxidative current is observed as a positive current rise by increasing voltage and the reductive current is generated during negative voltage application and hence is negative. The sign difference between the currents is an indication of opposite current flow across the interface. Such parasitic current can affect higher photo-current in the photo-voltaic system.

In addition, cyclic voltammetry can be used to evaluate the surface coverage due to adsorbed particles. During adsorption or desorption of reactants in a sequential CV, a gradual change in the anodic and cathodic peak can be observed. The reduction in the peak height can be an indication of progressive particle accumulation on the working electrode surface. The amount of charge consumed during the adsorption of species can help determine the surface coverage (see Figure 3-2) [29]. The equation for surface coverage, if the number of the electrons (n) is known, is:

$$Q = nFA\Gamma,$$

when  $Q$ , calculated from integrating the area under each peak, represents the charge.  $F$  and  $A$  represent Faraday's constant and the electrode surface area, respectively and the surface coverage in moles of adsorbed molecules per area is shown by  $\Gamma$ .

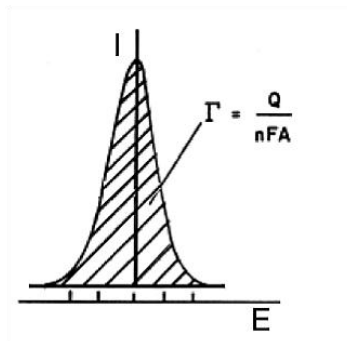


**Figure 3-2: Surface coverage calculation from the area underneath the peak obtained in cyclic voltammetry**

Gold surface coverage as a result of Cytochrome, Quinone, and reaction center adsorption is calculated by integrating the area under the gold oxidation peak and subtracting the result from the original area under the peak in the absence of the species.

### 3.1.2 AC Voltammetry

AC voltammetry (ACV) is the same as cyclic voltammetry with an additional superimposed high frequency, sinusoidally oscillating voltage. The frequency dispersion is then considered in impedance data analysis at a given potential. ACV is generally useful in systems where the dominant mode of transport is diffusion [20]. Figure 3-3 is a plot of an AC signal superimposed on a cyclic voltammetric signal. Note that the amplitude of the AC signal is exaggerated in the figure to show the variations of the current.

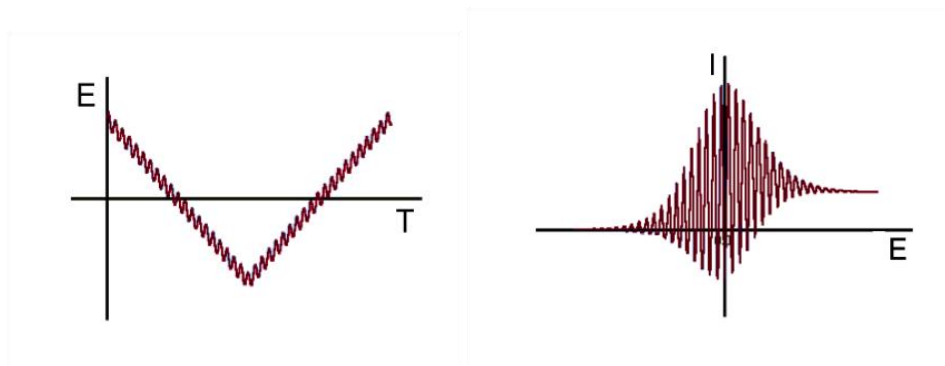


**Figure 3-3: Potential time and corresponding current potential plots for AC voltammetry.**

As can be seen in Figure 3-3, the magnitude of the AC sinusoid, usually an amplitude equal or less than 5 mV, is negligible in comparison to the overall potential change occurring during the scans. The small oscillation will result in negligible concentration changes in the proximity of the working electrode surface. This ensures analysis can be done in accordance to the assumption of linear effects of the electrode kinetics when in reality the electrode kinetics are exponentially dependent on the voltage. The major assumptions in ACV analysis are: 1. it is possible to uncouple the AC and DC components of the current, 2. due to the long DC time scale, the DC response follows Nernstian behaviour [20]. The advantage of this method is that the solution resistance and the double layer capacitance are evaluated more easily and more precisely during the electrode process.

The capacitance admittance is derived from

$$i = C_{dl} \cdot v,$$

from which,

$$Y_{dl} = i\omega C_{dl},$$

when  $\omega$  represents the angular frequency.

## 3.2 Cell Preparation

The fabrication and cleaning techniques for the working electrode and the glassware are discussed in this section.

### 3.2.1 Electrode Fabrication

The initial electrodes examined in the photovoltaic system, are 800 nm thick vapor deposited gold films on a glass surface with a 100 nm titanium adhesive layer between the gold and the glass substrate. The gold slide is then replaced with a 1.78 mm in diameter polycrystalline gold bead made from 24 carat gold wire due to ease of fabrication, cleaning method, and reducing the risk of exposed-titanium reactions at the edges of the electrode.

### 3.2.2 Cleaning Methods:

As mentioned in the introductory chapter, properly cleaning the electrodes and container is essential to ensure reactants access the total electrode surface and to reduce unintended parasitic reactions. It is of significant importance to emphasize that suitable techniques should be used to

ensure the removal of proteins and other organics from the surface of the electrodes and the container after each test.

Three cleaning methods are used to clean the gold slide surfaces. The first method is used in our lab as the primary cleaning technique for gold slides. The other two are the common methods used to clean the gold substrate [31].

#### **3.2.2.1 Sonication**

Prior to being transferred into the cell, the gold slides are kept in DI water for 8 hours, and then they are sonicated in 70% ethanol and DI water for 45 minutes. Finally, the electrodes are rinsed with DI water for several times.

#### **3.2.2.2 Hydrogen Peroxide and Sulfuric Acid**

The gold slides are treated with a solution of mild piranha clean containing 50 mM Sulfuric acid ( $\text{H}_2\text{SO}_4$ ) and 25% hydrogen peroxide ( $\text{H}_2\text{O}_2$ ) in pure, deionized water for 20 minutes at cleanroom. The slides are then rinsed with DI water.

#### **3.2.2.3 Sulfuric Acid Potential Cycling**

A common electrochemical cleaning method for gold is potential cycling of the electrode in sulfuric acid solution [31]. The gold potential is cycled at a rate of 100 mV/s from -0.5 to 1.4 v (vs. Ag/AgCl) in 50 mM sulfuric acid ( $\text{H}_2\text{SO}_4$ ) until a stable cyclic voltammetry is observed.

#### **3.2.2.4 Flaming**

The gold beads are flamed and heated just to redness three times and are washed with DI water each time. Since the gold can melt during the flaming, extra care should be taken not to heat the gold beyond the first signs of redness.

#### **3.2.2.5 Glassware Cleaning**

Sodium hydroxide (NaOH) is widely used for cleaning glassware containing proteins. This cleaning agent dissolves proteins by saponifying the fat. The ethanol washed glass cell is placed in a 0.5 M NaOH and ethanol for 5 hours at room temperature and then it is washed with DI water for several times.

### 3.2.2.6 Reference Electrode Cleaning

The Ag/AgCl reference electrode used in this work is made of PEEK (polyetheretherketone). This material is highly resistant toward most of the organic solvents. The electrode is completely leakless which prohibits chloride or silver ion contamination into the solution. The producer suggests letting the electrode rest in water or KCl solution after usage. To remove the adsorbed materials, the electrode is washed by immersing in NaOH saturated solution or strong acids such as 6 mol/L H<sub>2</sub>SO<sub>4</sub> for half an hour and then sonicating in DI water.

## 3.3 Experimental Setup

For both cyclic voltammetry and AC voltammetry tests to detect the adsorption and evaluate the double layer capacitance changes, a three-electrode setup is used. The cell setup is illustrated in Figure 3-4. To ensure working with a deoxygenated system, first the solution is poured into the cell and the electrodes are placed into their proper position as is illustrated. However, the working and the counter electrode are kept outside the solution in the wider space on the top of the container during deoxygenating process. Nitrogen gas is then injected into the solution from a narrow glass tube. At the same time Nitrogen flows from an air inlet to form a nitrogen blanket on top of the solution. The excess gas flows out of the air outlet to maintain proper pressure inside the cell. Every solution is bubbled for at least 15 minutes before performing any tests. The airflow into the solution needs to be stopped during the tests since it can introduce a lot of noise in such a small container, while the nitrogen on top of the solution flows constantly while the experiments are running. Extra attention should be paid when degassing the solutions containing any amount of detergent since foam is created on the surface of the solution during bubbling and fills out the overall container. The Gold Working Electrode (WE), Platinum Counter Electrode (CE), and Ag/AgCl Reference Electrode (RE) are connected to the potentiostat.

In all the tests presented, the applied voltage to the working electrode with respect to the reference electrode voltage is swept between -0.1 V vs. Ag/AgCl to 0.1 V vs. Ag/AgCl and at 5, 10, and 20 mV/s. The negative and positive voltage limit is then increased in several steps separately, each time by 0.1 V, up to -0.8 V vs. Ag/AgCl toward negative value and 1.2 V vs. Ag/AgCl toward positive value and the tests are repeated. The reason for increasing the voltage by a small value each time is to determine up to what voltage range the system is behaving capacitively. Moreover, by incrementing the voltage gradually at slow scan rates, it is possible to detect the redox peaks that may not be

observable during sweeps in larger voltage ranges if the peaks are hidden due to the start of a new reaction.

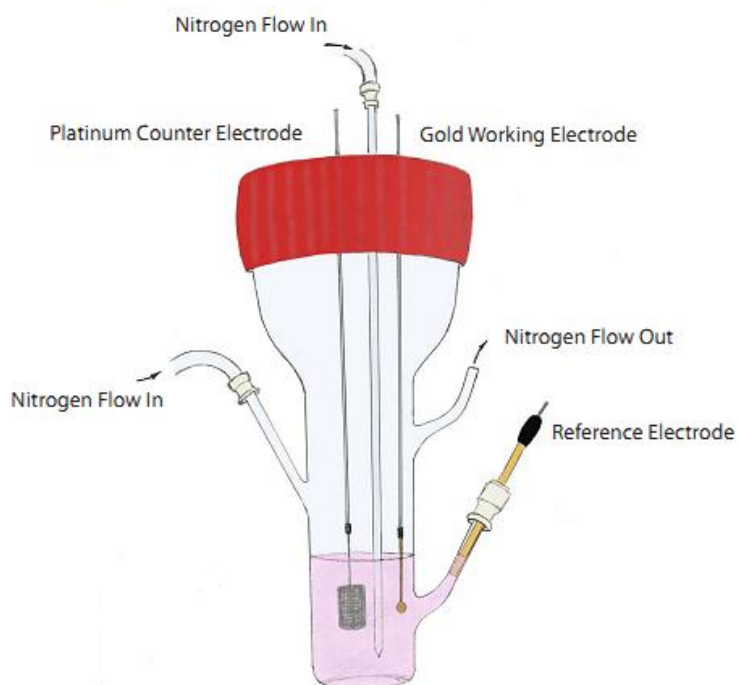


**Figure 3-4: The three electrode experimental setup used in an oxygen free cell to perform electrochemical tests.**

The adsorption behaviour of cytochrome c, Quinone, Reaction center, and three different surfactants on the surface of gold electrode is verified by means of cyclic voltammetry and AC voltammetry using the cell setup discussed in this section.

### 3.4 Materials

In this work, a 2.5 cm x 2.5 cm folded platinum mesh is used as the counter electrode and a leakless Ag/AgCl electrode from eDAQ is used as the reference electrode. The 99.9% pure platinum gauze made from 100 mesh woven from 0.0726 mm diameter (product number: 10282) is purchased from Alfa Aesar located in Massachusetts, USA. The miniature leakage free reference electrode (model ET072) is purchased from eDAQ Inc. located in Colorado, USA. A gold bead electrode made from 24 carat gold available in our lab is used as the working electrode.

The reaction centers used in the cyclic voltammetry and AC voltammetry tests are from the purple bacterium, *Rhodobacter sphaeroides* 2.4.1. The wild-type reaction center (conc:0.52 mM),

cysteineless RC (conc: 0.48 mM), cytochrome c, and detergent batches are provided from Dr. J. Thomas Beatty's lab, Department of Microbiology and Immunology, at the University of British Columbia. The reaction centers are dissolved in 0.1% v/v LDAO (purity  $\geq$  99%) to make them soluble in water based electrolytes. The proteins are kept in sealed Teflon plastic containers at  $-30^{\circ}$  C. It is suggested to keep the proteins and carry out the experiments in Teflon vials since other containers may release residues to the containing solution and also proteins show high affinity to plastic and glass substrates.

Cytochrome is reduced to cyt  $c^{2+}$  by adding  $\text{Na}_2\text{S}_2\text{O}_4$  to 70 mg of dissolved protein in 6 mL of 0.1 M Tris-HCl buffer at pH 7. The protein sample is then eluted with Tris-HCl buffer in a Sephadex G-50 column to remove the excess  $\text{Na}_2\text{S}_2\text{O}_4$ . The red/ orange portion of the solution is collected to be analyzed using UV-Vis spectroscopy. The reduced cyt c concentration used in this work is calculated to be 1.305  $\mu\text{M}$ .

Ubiquinone - 2 (Q) (purity  $\geq$  90%, conc: 15.7 mM) and Tris (purity  $\geq$  99.8%) are purchased from Sigma Aldrich. Monopotassium phosphate and Dipotassium phosphate (purity  $\geq$  99%), originally purchased from Sigma Aldrich, are provided from Dr. Beatty's lab.

pH 7 Tris-HCl and Phosphate buffers are made using the salts mentioned dissolved in deionized water with a pH of 5.5 to 6 at room temperature.

## **4 RESULTS**

In this chapter the experiment specifications, particular setups for each test, and the test results are presented. Sections 4.1 to 4.5 introduce the gold electrode characterization in the presence of different possible buffers. The electrochemical characterization of the gold electrode when it is exposed to cytochrome c, quinone, surfactants, wild reaction center, and cysteineless reaction center is presented in sections 4.6, 4.7, 4.8, 4.9, and 4.10, respectively.

### **4.1 Electrochemical Characterization of the Gold Electrode**

During oxidation or reduction, charge transfer occurs across the metal-solution interface. According to Faraday's law of electrolysis, the amount of the charge passed is proportional to the extent of the chemical reactions that result from current [20]. Thus such reactions are known as Faradaic processes.

To obtain the maximum photocurrent, the unwanted Faradaic reactions should be eliminated. This includes eliminating the possible unwanted reactants that can migrate to and react on the surface of the working electrode to produce side reactions and thus reduce the generated photo-current. To reach this goal several steps have been taken which are explained in this chapter.

A Solatron SI 1287 potentiostat is used to perform the cyclic voltammetry and AC voltammetry tests. Initially, the electrolyte solution consisted of 0.1 M Tris-HCl buffer at pH 7 in DI water was used, however as is explained in section 4.4, this buffer is replaced by potassium phosphate buffer to carry out the remaining tests. Leakage free Ag/AgCl and platinum mesh are used as the reference and counter electrodes respectively. All electrochemical measurements are performed in the custom made glass cell with 2.5 mL deoxygenated buffer as illustrated in Figure 3-4 in the previous chapter. It is worth mentioning that fresh solution and freshly cleaned cell components are used to perform each individual test.

### **4.2 Effect of the Preparation of the Gold Electrode**

Initially, gold films vapour-deposited on chromium or titanium adhesive layers, on glass slides were used during the bio-photovoltaic experiments. The major issue with using the gold films was adequate sealing of the edges to prevent the leakage and chemical reaction of chromium or titanium in the electrolyte. Also the electrodes and the containers were often cleaned using sonication methods

which are found to be not adequate to clean the components that are exposed to proteins. Cleaning the gold slide using piranha or other acids is also a challenging task as the cleaning should take place in the clean room. It should be mentioned that little amount of protein is enough to poison the acid solution, thus new solution should be made for each cleaning session. In contrast, gold bead electrode is easy and fast to fabricate and can be cleaned sufficiently in the lab environment. Cyclic voltammetry is used to compare the currents and redox peaks of the gold electrode for both gold and gold bead. The aim of these tests is to determine whether using an ultra-clean system can affect the photocurrent generation in our cell.

The cyclic voltammograms for two sample gold electrodes at a scan rate of 20 mV/s are shown in Figure 4-1. Sample 1, shown in the left plot, is a 800 nm thick gold film with an area of 38.5 mm<sup>2</sup> thermally evaporated on a glass substrate with a 200 nm thick titanium as an adhesive layer using the Evaporator 2000 system with automated vacuum process control system at UBC's clean room. This sample is cleaned using piranha solution in the clean room. However, the electrode is kept in the lab environment for a day in a closed container before performing the tests. The second sample is a pure gold bead with an area of 9.95 mm<sup>2</sup> which is flamed and washed three times before the experiments. Its voltammogram is shown on the right in Figure 4-1.

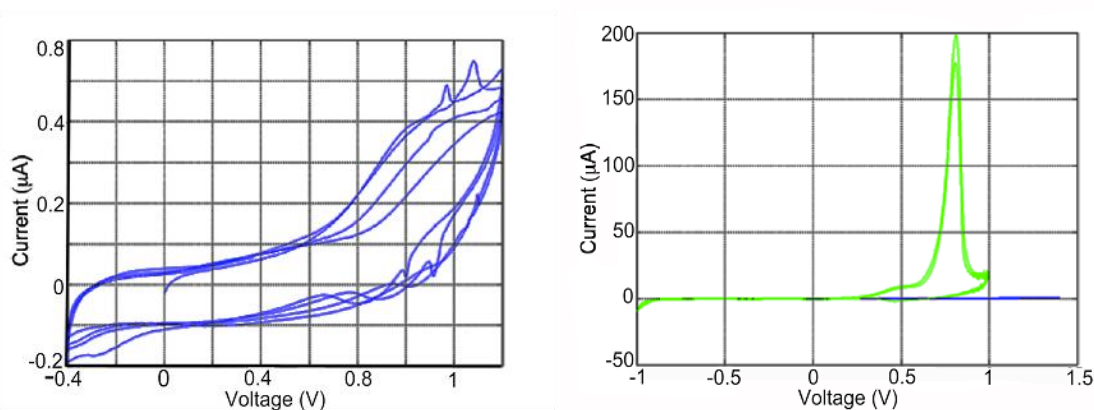


**Figure 4-1: Cyclic voltammetry results for left: gold slide; right: gold bead (with superimposed slide plot as shown in blue) in 0.1 M Tris-HCl solutions at the scan rate of 20 mV/s.**

Figure 4-2 is an illustration of the zoomed in superimposed CVs for the gold slide and the gold bead. As it is evident from Figure 4-1 and Figure 4-2, the capacitive current and the redox peaks for the gold bead are clearly larger than the resultant currents for the gold slide. The small currents, distorted gold oxidation peak, and no signs of reduction for the gold in the left plot indicates that only a small fraction of the total gold surface is exposed to the solution and the rest of the surface is covered with contamination.

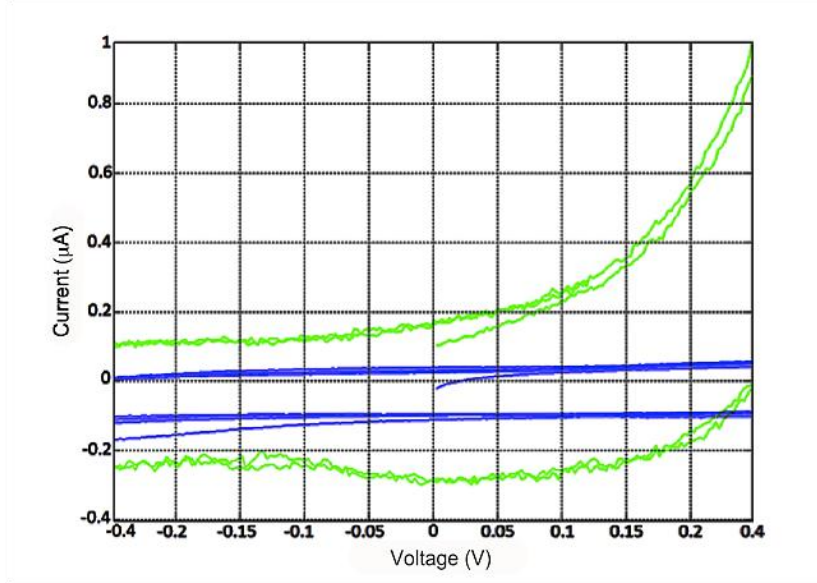


**Figure 4-2: Zoomed in plot for the cyclic voltammetry tests for gold slide and gold bead at 20 mV/s in 0.1 M Tris-HCl solution.**

The currents at -0.2 V, where the behaviour of the system is almost capacitive, for the gold slide and the gold bead are measured as 0.0284 and 0.114 µA respectively. The current density for each electrode is calculated as:

$$\rho_s = \frac{I_s}{A_s} = \frac{0.0284}{38.5} \approx 0.0007 \left( \frac{\mu A}{mm^2} \right),$$

$$\rho_b = \frac{I_b}{A_b} = \frac{0.114}{9.95} \approx 0.011 \left( \frac{\mu A}{mm^2} \right),$$

$$\rightarrow \frac{\rho_b}{\rho_s} \approx 16.$$

Thus, the current density during the CV test for the gold bead is 16 times larger than the current per unit area generated during the tests performed on the gold slide electrode.

Given these results, it is concluded that the reactants in the protein based solar cell have only had access to a small fraction of the original active area of the gold electrode. Therefore, generated photocurrents were smaller than the expected photocurrents.

### 4.3 Oxygen Elimination

If the solution is not deoxygenated, a large reduction response current is generally observed near the lower potential limit due to the reduction of dissolved oxygen in the solution. In addition to a significant cathodic current that is observed in the cell containing only buffer solution and the clean bare gold electrode, a reversible couple peak is also observed with a mid-point potential located at around 0 V vs. Ag/AgCl due to the dissolved oxygen. The recorded CVs show that the redox couple vanishes and the reduction response is significantly reduced when the system is deoxygenated (Figure 4-3). This suggests that oxygen may be facilitating the oxidation and reduction of an unknown species in the cell. To deoxygenate the solution, pure nitrogen is used which is known as a chemically inert gas. If the buffer is not bubbled with nitrogen for a sufficient time and then sealed, the response of some residual oxygen is still observable. Therefore, for every measurement made in this work, nitrogen gas flows into and over the solution to eliminate the oxygen from the cell.

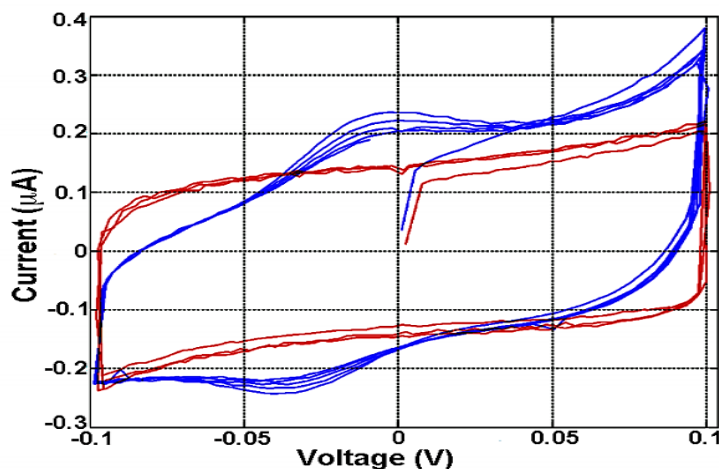


Figure 4-3: Cyclic voltammetry for 0.1 M potassium phosphate buffer pH 7. Blue: regular cell exposed to air ; red: deoxygenated and sealed cell.

As stated before, parasitic reactions taking place on the surface of the electrode reduce the available area for the solar cell species reactions and can act in the opposite direction of the photocurrent, again reducing cell current. Therefore, the generated photocurrent is expected to be reduced in the presence of such unwanted back reactions.

## 4.4 Electrolyte

To our knowledge, no electrochemical study related to the redox behaviour of possible organic buffers on the surface of gold and oxidation of gold has been reported. This is important to know in our system, since it provides valuable information about the possible faradaic reactions on the surface of the electrode that take place due to buffer reactants. These reactions can occur at voltage regions where the key components of the cell are expected to react on the electrode surface. Therefore, these reactions are considered as back reactions in protein based solar cells, which reduce the photocurrent and thus the efficiency of the system.

### 4.4.1 Organic Buffers

Most studies on the redox behaviour of proteins and bio-photovoltaic cells are conducted in Tris-HCl buffer at pH 6.5 to 8 since the proteins show a stable behaviour in this buffer and the stated pH range [5]. Figure 4-4 shows the chemical structure of Tris-HCl. In general, using appropriate buffer solution is important since buffer tends to stabilize the native structure of the protein as well as preventing protein attachment to surfaces such as plastic and glass. 1 M Tris-HCl buffer is prepared by dissolving 121.1 grams of Tris base in 800 mL DI water. The pH is adjusted to 7 by adding concentrated HCl. Then DI water is added to the solution to bring the volume to 1000 mL.

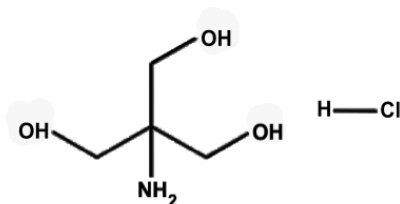


**Figure 4-4: Representation of Tris – HCl chemical structure.**

The cyclic voltammogram for the gold electrode in 0.1 M Tris-HCl pH 7 is shown in Figure 4-5. It can be observed that an oxidation current starts at 0.2 V vs. Ag/AgCl within the double layer region and a current peak appears at about 0.78 V during the positive sweep and another oxidation peak appears at about 0.4 V negative scan at a scan rate of 20 mV/s. Generally it is expected to observe a clear reduction peak which corresponds to the oxide being removed from the surface of the electrode. However, during the negative sweep, a much smaller reduction peak is observed, indicating that under our experimental conditions oxidation of Tris on the surface of gold is an almost irreversible reaction (irreversible charge transfer process). As soon as the gold reduces, the Tris oxidizes itself on

the surface again causing a bell shape CV implying that the oxidation of Tris could be happening on the surface of the electrode. Due to the unclear behaviour of the Tris-HCl, three other possible buffers, MOPS, HEPES, and Potassium phosphate, are examined as potential replacements for this buffer.

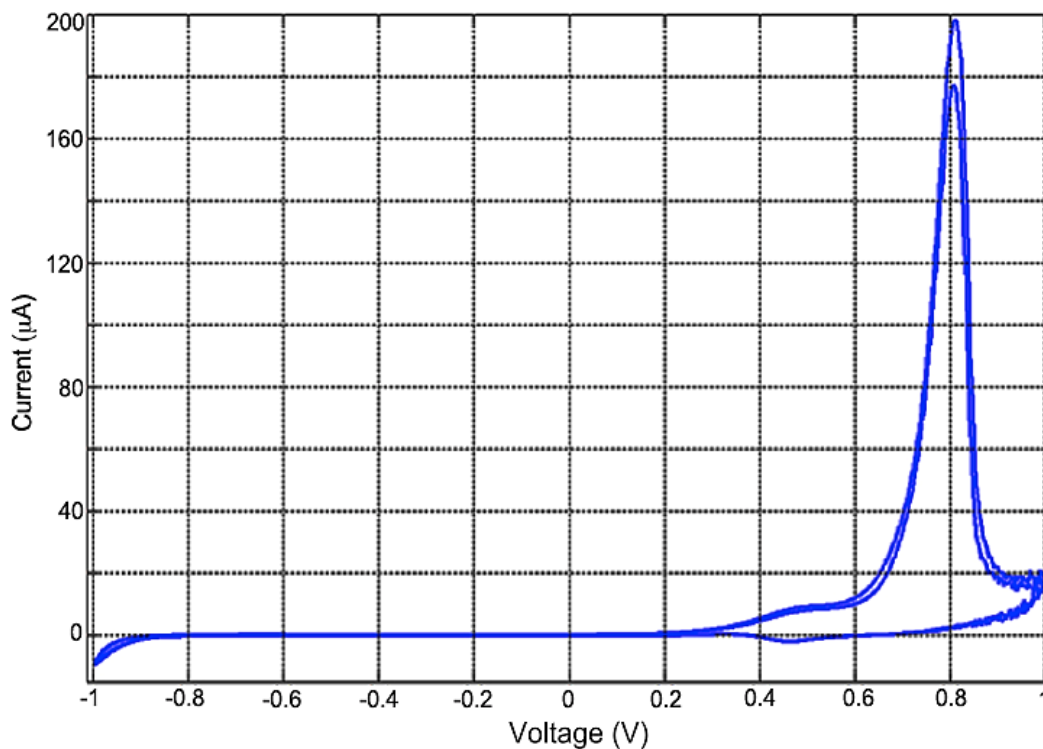


**Figure 4-5:** CV graph for gold bead electrode from -1 to 1 V vs. Ag/AgCl reference in 0.1 M Tris-HCl at a scan rate of 20 mV/s.

HEPES and MOPS, illustrated in Figure 4-6, are two other buffers that are used with biological experiments. The cyclic voltammeteries of both buffers, 0.1 M at pH 7 at 20 mV/s also show an electro-oxidation behaviour in the presence of gold electrode. Figure 4-7 shows the full scan voltammogram of the gold electrode in the presence of HEPES and MOPS buffers.



**Figure 4-6:** Chemical structure of : left: HEPES; right: MOPS.

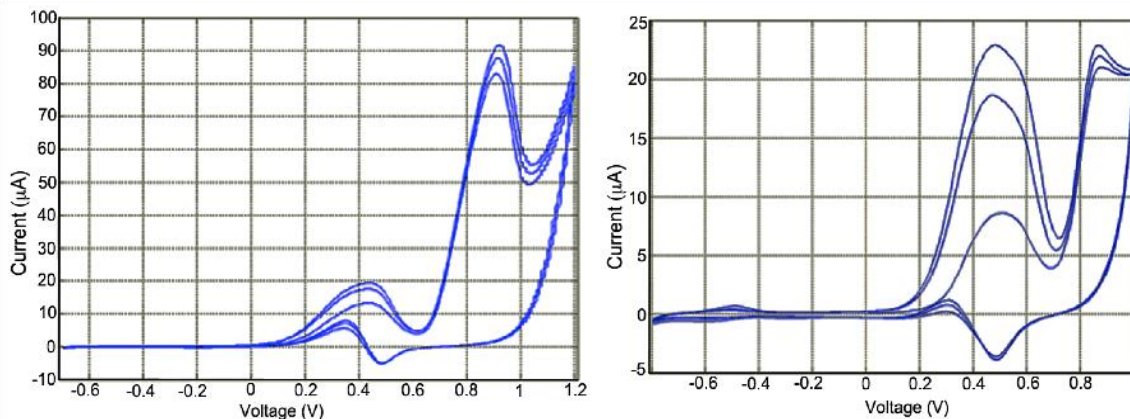


**Figure 4-7: CV graph for gold bead electrode: left from -0.8 to 1.2 V vs. Ag/AgCl reference in 0.1 M HEPES; right: from -0.8 to 1 V vs. Ag/AgCl in 0.1 M MOPS both at a scan rate of 20 mV/s.**

The large oxidation current detected in the oxidation of these three organic buffers, especially HEPES and MOPS, on the gold surface may be the result of some discharged species that generate strong oxidation mediators on the surface of the electrode and act as catalysts that significantly speed up the oxidation reaction [32].

The oxidation potential of Tris, HEPES, and MOPS has been found to be at about +0.5 V vs. Ag/AgCl reference on gold electrode. As detected in the CV results from the peaks from the far right, gold oxidizes at around 0.8 V vs. Ag/AgCl in the presence of Tris-HCl. However, its oxidation potential is shifted to the right in the presence of MOPS and HEPES. The oxidation potential of the gold in the presence of MOPS and HEPES is observed to be around 0.9 V vs. Ag/AgCl.

#### 4.4.2 Potassium Phosphate Buffer

100 ml of 1 M Potassium phosphate buffer at pH 7 is prepared by mixing off 61.5 ml of 1M Monopotassium phosphate ( $\text{KH}_2\text{PO}_4$ ) and 38.5 ml of 1M Dipotassium phosphate ( $\text{K}_2\text{HPO}_4$ ). pH 7 is chosen because most of the biological proteins are usually kept and are stable at this pH.

Gold electrode cyclic voltammetry in Phosphate Buffer solution is performed in the absence of oxygen at three different scan rates 20, 10, and 5 mV/s (See Figure 4-8 - right). Full scans from -0.8 to 1.2 V vs. Ag/AgCl are performed at 10 and 5 mV/s (See Figure 4-8 - left). The plots for the full scans show some fine features in the double layer region of the phosphate buffer between -0.5 to 0 V vs. Ag/AgCl. These features may be associated with the formation of partially discharged  $(\text{OH})^{(1-x)-}$  of the buffer or reorientation of water molecules on the surface of the electrode.

The voltammetric response of gold in phosphate buffer solution has two distinct peaks, shown in Figure 4-8 corresponding to oxide formation on the gold surface during the positive sweep, and removal of the oxide layer when reversing the scan direction.

The buffer has an oxidation peak at + 0.35 V vs. Ag/AgCl distinct from the oxidation peak of gold which occurs at 0.85 V vs. Ag/AgCl. A sharp increase in current is observed at potentials less than - 800 mV vs. Ag/AgCl which is due to hydrogen evolution.

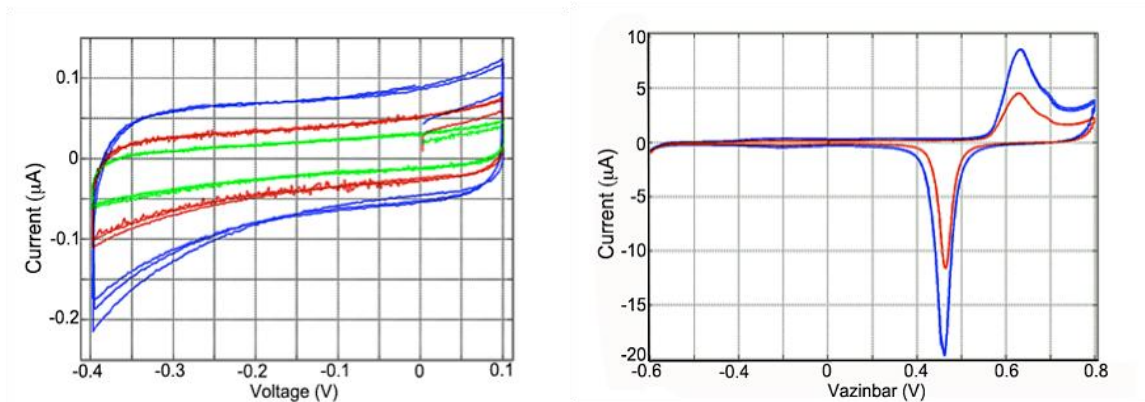


**Figure 4-8: Cyclic voltammogram of clean gold electrode in 0.1 M potassium phosphate buffer at pH 7, right: at scan rates: blue: 20, red: 10, and green: 5 mV/s; left: at scan rates: blue: 10 mV/s and red: 5 mV/s. The solution is deoxygenated with N<sub>2</sub> for 15 minutes and a N<sub>2</sub> blanket kept the solution degassed during the measurements.**

Figure 4-9 - left demonstrates 7 superimposed CVs of gold at 20 mV/s while the voltage is increased by 0.1 V toward the negative voltage range and Figure 4-9 - right shows the CVs of gold in phosphate buffer as the voltage is increased toward more positive voltages.

As can be seen, the positive capacitive current and hence the double layer capacitance is increasing by scanning toward more negative voltages. We suspect that this may indicate that phosphate adsorbs on the gold surface at the positive voltage and it is being increasingly desorbed as the voltage is swept in negative ranges.

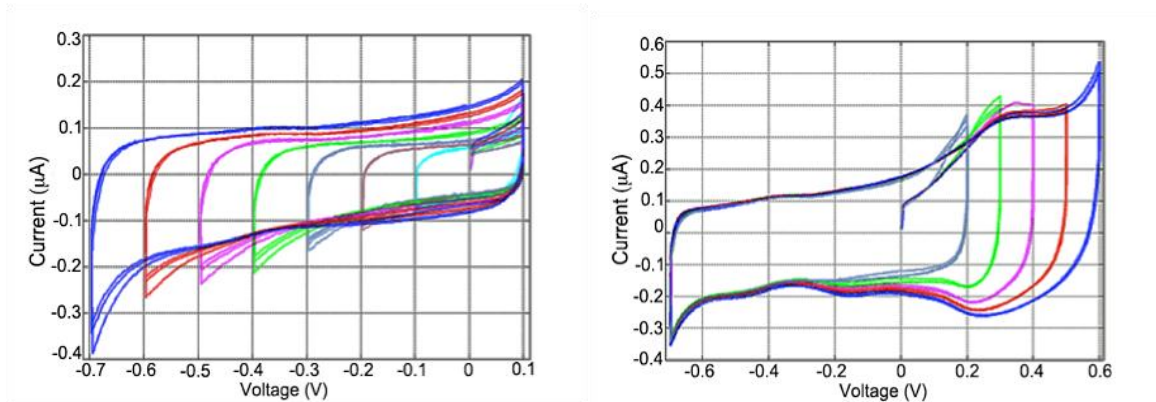


**Figure 4-9:** Cyclic voltammogram of clean gold electrode in 0.1 M deoxygenated potassium phosphate buffer at pH 7. Scan rate 20 mV/s. Left: the voltage is increased by 0.1 V toward negative; right: the voltage is increased by 0.1 V toward positive values.

It should be noted that such increase in the current as shown in the above plots in the left can also be a sign of pH changes near the surface of the electrode. A change in the current is expected if the surface protonation is changed due to gold oxidation.

After comparing the results from all four buffers, phosphate buffer is chosen as the electrolyte for carrying out the rest of the tests on the mediators, surfactants, and the reaction centers. Phosphate does not seem to adsorb on the surface of the electrode so strongly. Moreover, the gold redox peaks measured in phosphate buffer indicate that the gold oxidation and reduction occur in a reversible manner, whereas in the case of the organic buffers, adsorption on the surface hindered the electron transfer significantly. Therefore, the use of Tris-HCl, MOPS, and HEPES pose the risk of having buffer reagents competing with the solar cell mediators for reactions on the surface of the electrode.

#### 4.5 Adsorption of Phosphate Buffer on Bare Gold Electrode

To test the adsorption of phosphate on the gold surface, ACVs are recorded while sequentially spiking 2, 7, 20, and 75  $\mu\text{l}$  of 100 mM phosphate buffer into 2.5 ml solution of 50 mM potassium perchlorate ( $\text{KClO}_4$ ). Potassium perchlorate is used as the main electrolyte since its components do not adsorb on the surface of the gold, and also the electrochemistry of gold has been well characterized in this solution.

Upon the addition of phosphate to  $\text{KClO}_4$ , any change in capacitance would be expected to be due to the replacement of water molecules with phosphate ions. The results are shown in Figure 4-10. The blue dots represent the double layer capacitance in the absence of phosphate. As the concentration is increased, the capacitance decreases. The surface seems to get saturated after the addition of 20  $\mu\text{l}$ ,

since adding more (75  $\mu\text{l}$ ) phosphate buffer does not result in further changes in the capacitance. Note that the capacitance profile for 75  $\mu\text{l}$  phosphate buffer in 2.5 ml of  $\text{KClO}_4$  is not shown since it is identical to the green plot belonging to 20  $\mu\text{l}$  phosphate buffer spiked in the perchlorate solution demonstrated in Figure 4-10.

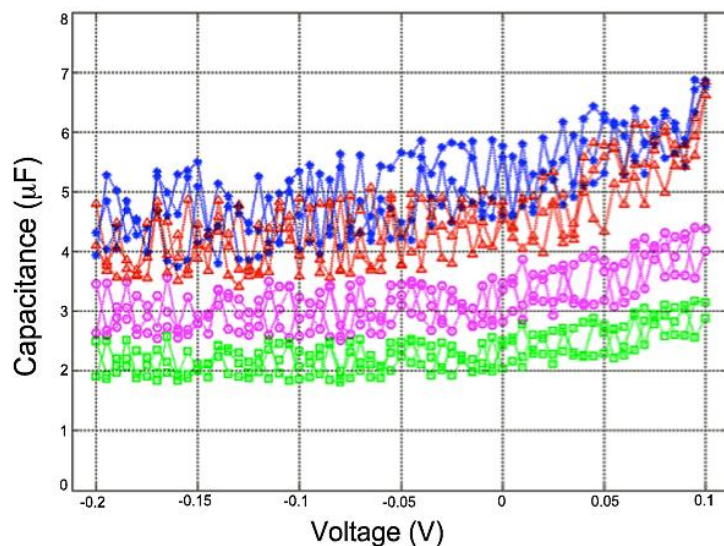


**Figure 4-10: Capacitance profile measurements for bare gold electrode exposed to blue: 2.5 ml 50 mM potassium perchlorate solution; red: 2  $\mu\text{l}$ ; magenta: 7  $\mu\text{l}$ ; green: 20  $\mu\text{l}$  potassium phosphate buffer. Frequency: 25 Hz, amplitude: 5 mV, scan rate: 5 mV/s.**

The addition of phosphate buffer might be expected to produce an increase in the double layer capacitance since phosphate ions are very polarizable and they are expected to increase the dielectric constant [32]. However, we suspect that due to higher molarity of the phosphate buffer, the concentration of phosphate ions in the double layer has increased significantly. At high molarity, lower capacitance is expected since more ions replace the water molecules in the double layer and cause a thickness increase in this region [20].

To verify the capacitance changes, CVs are recorded after each recording of the ACVs for each concentration, see Figure 4-11. The trend is the same as is observed by ACV.

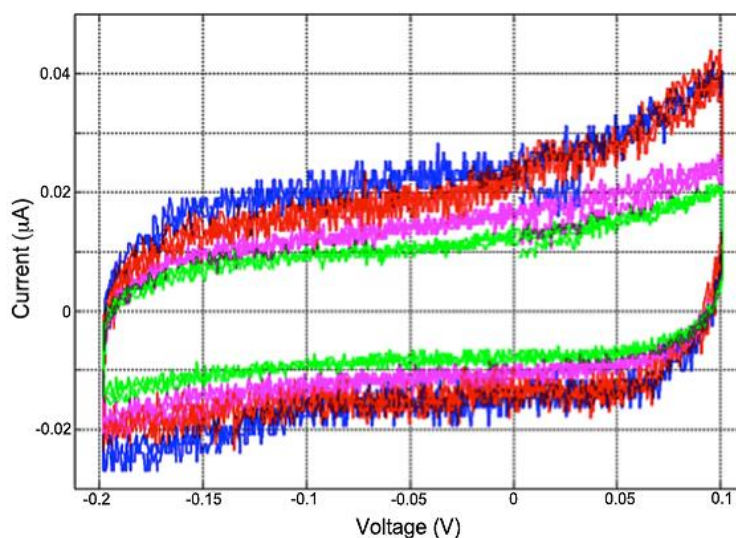


**Figure 4-11:** Cyclic voltammograms for bare gold electrode exposed to: blue: 2.5 ml of 50 mM potassium perchlorate solution, red: 2  $\mu$ l, magenta: 7  $\mu$ l, green: 20  $\mu$ l 10 mM potassium phosphate buffer added to  $\text{KClO}_4$ . Scan rate: 5 mV/s.

The CV and ACV tests indicate that potassium phosphate buffer may be a preferable choice over the other three buffers. According to the results presented in this section, the use of Tris-HCl, MOPS, and HEPES suppresses the activity of the gold. However, phosphate does not block the electrode surface activity even though some adsorption is detected when gold is immersed in the phosphate buffer.

## 4.6 Cytochrome c

Cytochrome c is a water soluble, commonly distributed protein among living organisms which transfers the charge in mitochondrial respiratory chains and is also used in purple bacteria to reduce the RC [3],[12], [33]. Cytochrome c is used as one of the charge mediators in the bio-photovoltaic device, thus its electrochemical characterization and adsorption on the surface of electrode is of great interest. Cyclic voltammetry and AC voltammetry are used to study the redox and adsorption behaviour of this protein.

It is observed that at pH 7 potassium phosphate buffer the voltammetric response of cytochrome c is quite poor at bare unmodified gold electrodes, most likely due to protein aggregation and denaturation at the metal electrode surface which passivates the gold surface and leads to extremely slow electron-transfer kinetics. Evidence of this aggregation is presented in this section.

#### 4.6.1 Adsorption of Cytochrome c on Bare Gold Electrode

Figure 4-12 – right plot shows cyclic voltammograms recorded at the scan rate of 5 mV/s for 2.5 ml of the pure phosphate buffer when 2, 6.5, 20, and 70  $\mu\text{L}$  of reduced cyt c (cyt  $c^{2+}$ ) is added sequentially to the solution. It can be observed that the capacitive currents drop by increasing the concentration of the proteins. In order to track down the capacitance changes more accurately, ACV is recorded for the mentioned amounts of the cyt  $c^{2+}$ . The effect of varying the concentration of the protein in the solution during the adsorption is shown in Figure 4-12 – left.

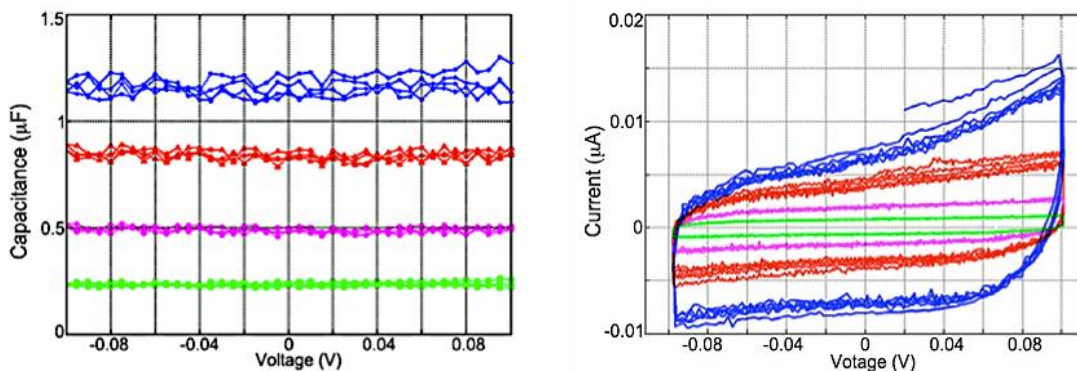


**Figure 4-12:** Left: Capacitance profile measurements; right: cyclic voltammograms for bare gold electrode exposed to: blue: 2.5 ml of 100 mM potassium phosphate buffer along with red: 2  $\mu\text{L}$ , magenta: 7  $\mu\text{L}$ , green: 20  $\mu\text{L}$  reduced cyt  $c^{2+}$  added. Frequency: 25 Hz, amplitude: 5 mV, scan rate: 5 mV/s.

The ACV recorded for reduced cytochrome c when the concentration is increased in a logarithmic trend shows a linear decrease in the capacitance until the surface reaches saturation at 70  $\mu\text{L}$  reduced cyt c in 2.5 mL phosphate buffer. Note that capacitance profile for the 70  $\mu\text{L}$  is eliminated from the graph since it is similar to the profile for 20  $\mu\text{L}$  cyt  $c^{2+}$  added to phosphate buffer.

Figure 4-13 is an illustration of full scan CVs recorded at 5 mV/s. According to this plot the redox peaks of the gold are reduced as the concentration of cyt c is increased. This indicates that adsorption of cyt c at the surface of the electrode can block the oxidation/ reduction of gold and lower the peak currents depending on coverage. The protein coverage on the surface for each concentration can be determined by calculating the charge underneath the oxidation and reduction peak of gold. The peak heights are lowest after adding 20  $\mu\text{L}$  of reduced cytochrome c. Adding 70 more of cyt c does not reflect in the capacitance of the double layer or the gold redox peaks, thus it is concluded that a 11  $\mu\text{M}$  solution of protein in phosphate buffer can saturate the surface of the gold electrode used in our experiments. Assuming that the diameter of the cyt c is around 3.2 nm [33], [34], then we expect that

each molecule occupies an area of around  $10 \text{ nm}^2$ . From the last peak charge and surface coverage, the adsorbed amount seems to cover about 85% of the surface.

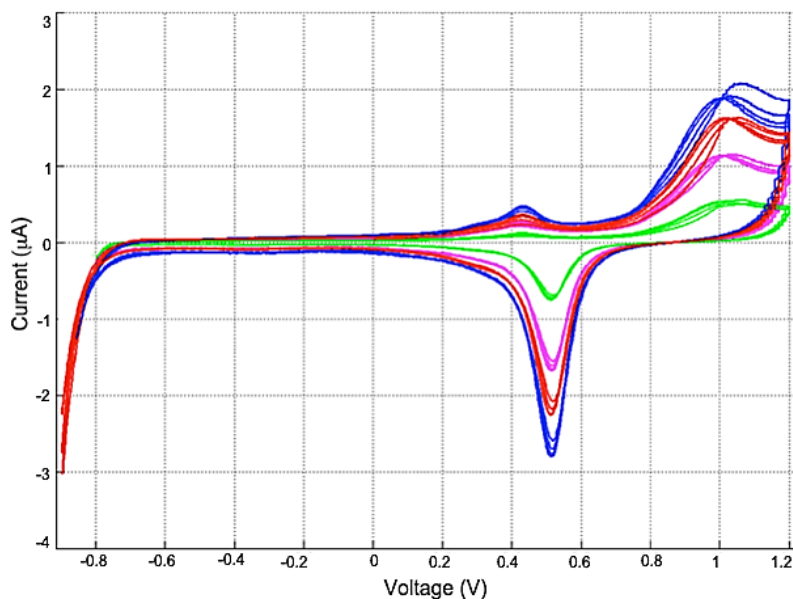


**Figure 4-13: Comparison of full scan CVs recorded on a bare gold electrode after adsorption of different amounts of cyt c (blue: 2.5 ml phosphate buffer, red: 2  $\mu\text{l}$ , magenta: 7  $\mu\text{l}$ , and green: 20  $\mu\text{l}$  of cyt  $c^{2+}$  added to buffer). CVs are recorded at a scan rate of 5 mV/s.**

According to the CVs in Figure 4-13, when sweeping the voltages more negative than  $-0.2 \text{ V}$  vs. Ag/AgCl, the current in the double layer region starts to increase compared to the currents read in Figure 4-12 - left. The more negative the voltage is, the larger the capacitance becomes. However, neither the capacitance nor the peak currents for gold redox reaction recover to the original value measured in the absence of protein. This indicates that the protein layer formed on the surface of the electrode may consist of both specifically and non-specifically adsorbed proteins depending on the binding orientation of the cytochrome. We hypothesize that the specifically bound cytochromes will not be desorbed from the surface but the loosely bound proteins are desorbed from the substrate upon applying negative voltages due to reduction of electrostatic attraction or increase of electrostatic repulsion.

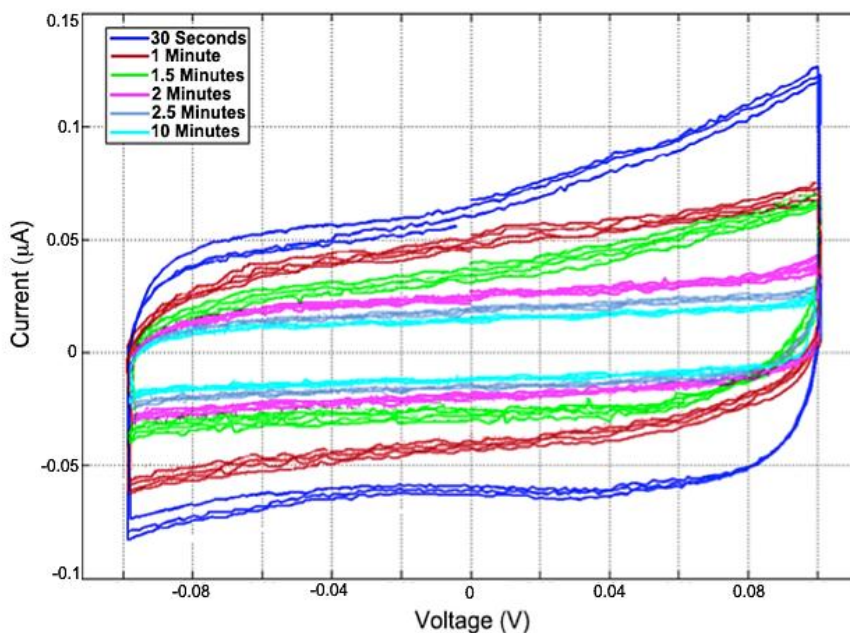
#### 4.6.2 Effect of Exposure Time on Cyt c Adsorption

In order to evaluate the cytochrome c specific adsorption time course, the gold electrode is immersed in a  $20 \mu\text{M}$  reduced cyt c prepared in  $100 \text{ mM}$  phosphate buffer for 30 seconds. The electrode is then washed with potassium phosphate buffer solution and is placed in a cell containing

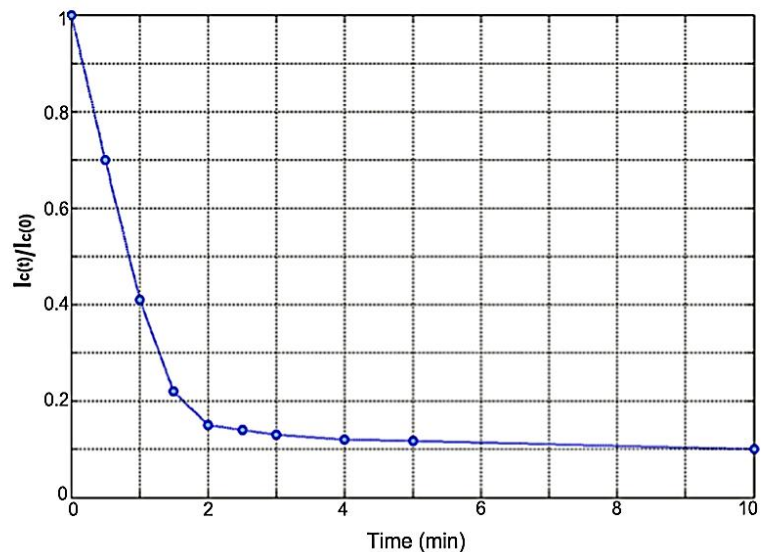
fresh phosphate buffer. The solution is deoxygenated and cyclic voltammetry of the exposed electrode to reduced cytochrome c is recorded at a scan rate of 20 mV/s. The process is repeated for further reduced cyt c exposure times of 1, 1.5, 2, and 2.5 minutes. For each test a fresh degassed buffer solution and a clean bare gold electrode is used. Thus, before each test, a blank CV is measured in 100 mM phosphate buffer to ensure the same test conditions. In every case, the recorded CVs for fresh solution vary negligibly, indicating that any change after exposure to cyt c is due to protein adsorption.

Figure 4-14 shows successive cyclic voltammetry records in potassium phosphate buffer before and after immersion in reduced cyt c - containing solution. As can be seen, the magnitude of the capacitive current decreases as the immersion time is increased.

The ratio of the capacitive currents at time  $t$ ,  $I_{c(t)}$  to the initial capacitive current,  $I_{C(0)}$  at 0V vs. Ag/AgCl are plotted as a function of time in Figure 4-15. The current is reduced to 25% of its original value after 10 minutes immersion. This test indicates that cyt  $c^{2+}$  considerably adsorbs on the surface of the gold even from a dilute solution.



**Figure 4-14:** Comparison of CVs measured on a bare gold electrode after adsorption of cyt  $c^{2+}$  (20  $\mu$ M, pH 7) at a scan rate of 20 mV/s. The exposure times are listed as legends in the graph. Potentials are versus Ag/AgCl reference electrode.



**Figure 4-15: Capacitive current profile for the bare gold electrode for 20  $\mu\text{M}$  cytochrome c in pH 7. The protein adsorption has happened at open circuit potential. All the CVs are recorded at a scan rate of 20 mV/s**

### 4.6.3 Effect of Applied Potential during Electrode Exposure

To observe the effect of voltage on the speed of adsorption, similar tests as explained in previous subsection are repeated 4 more times while applying -0.1, -0.3, 0.1, and 0.3 V respectively when the electrode is immersed in the 20  $\mu\text{M}$  protein contained solution for various time. Significant decelerated adsorption is observed when -0.3 V vs. Ag/AgCl is applied. Moreover, the application of positive voltage to the gold electrode accelerates the process.

The capacitive current profiles presented in Figure 4-16 demonstrate the effect of applying various potentials during electrode exposure to the protein solution. This plot shows that surface blockage due to cytochrome adsorption varies as a function of voltage and exposure time.

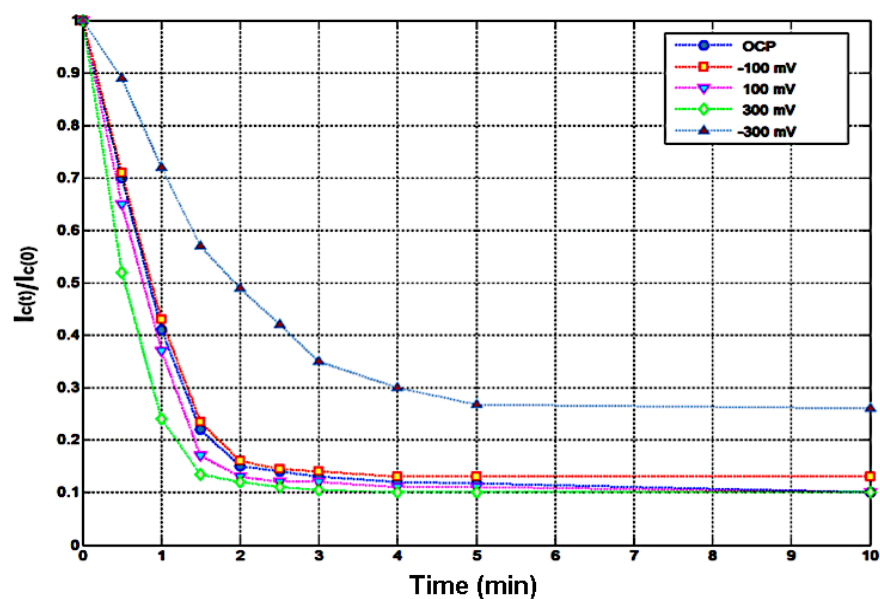


**Figure 4-16:** Capacitive current profile for bare gold electrode exposed to 20  $\mu\text{M}$  of cyt  $c^{2+}$  at pH 7. The cyclic voltammograms are recorded in 100 mM potassium phosphate buffer after adsorption of cyt  $c^{2+}$  for various times at different voltages. The applied voltage is indicated in legend of the graphs. The scan rate is 20 mV/s.

The result for -300 mV shows that after 10 minutes the current dropped to 30% of its original value, suggesting less gold surface blockage. The results for 100 and 300 mV show faster adsorption reaching the maximum surface coverage. Considering electrostatic influences on the adsorption of cytochrome c, it can be concluded that adsorption at positive voltage is favourable and facilitated over adsorption in negative voltage which suggests that cyt c carries a net negative charge. However, both cyt c and the cyt  $c^{2+}$  carry net positive charge especially around their heme group which is responsible for most of this protein's interactions with electrode surface or other redox species [6]. Thus it can be hypothesized that cytochrome is adsorbed on the surface of the gold from a side that has more of localized negative charge domains and hence applying the negative voltage desorbs the non-specifically adsorbed proteins from the gold surface.

In all cases it is observed that the surface blockage reaches its maximum after about 5 minutes. This suggests that at times greater than 5 minutes electron transfer process is not influenced even if surface coverage by the proteins is continued. However, for cyt c the amount of electron transfer blocking at both -100 mV and OCP after 10 minutes is the same, while at -300 mV it is less.

#### 4.6.4 Reversibility of the Cytochrome c Adsorption on Gold

To evaluate the reversibility of the cyt c adsorption on the gold electrode, the gold electrode is exposed to a 10.5  $\mu\text{M}$  cytochrome c solution for 30 minutes, the electrode is rinsed with the buffer and it is immersed in the phosphate buffer alone for 10 hours. The electrode is then rinsed with a fresh phosphate buffer and CVs at 5 mV/s are recorded in a fresh solution of 100 mM phosphate buffer at pH 7. The result is shown in Figure 4-17.

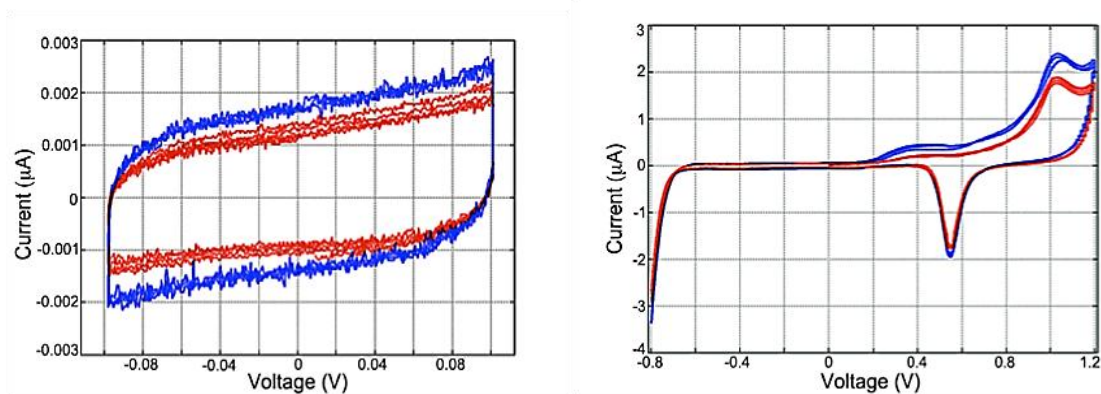


**Figure 4-17:** Left: cyclic voltammograms used to compare double layers formed on a gold electrode surface immediately (blue) after adsorption of cytochrome c (10.5  $\mu\text{M}$ , pH 7), and then after keeping the electrode in a fresh buffer for 10 hours (red). Right: Comparison of gold redox peaks immediately (blue) after adsorption of cytochrome c (10.5  $\mu\text{M}$ , pH 7) and after keeping the electrode in a fresh buffer for 10 hours (red). All CVs are performed at a scan rate of 5 mV/s.

The double layer capacitance is smaller at long times and the peak currents are decreased. This suggests that adsorption of the reduced cyt c on the surface is not reversible meaning that proteins cannot be removed from the surface simply by rinsing and they do not appear to desorb significantly over time. In addition, the reduction in the capacitance and the peak currents may suggest that the gold surface has induced reduced cyt c conformational changes or denaturation. The globular shape of the cyt c may change to an unfolded shape on the surface, which can increase the coverage on the surface and leave less active areas on the gold surface to react. Also slight changes in the capacitance suggest that conformational changes or reorientation of the adsorbed proteins may result in thickening of the layer formed on the surface compared to the globular proteins. Thus the double layer thickness may have increased after the protein is unfolded.

#### 4.6.5 Electrochemical Studies of Cytochrome c on a Bare Gold Electrode

Figure 4-18 displays a CV of a 20  $\mu\text{M}$  cytochrome c in phosphate buffer on a gold electrode produced using a scan rate of 20 mV/s. A very short lived weakly defined irreversible cyt c reaction is

sometimes observed during the tests. The reversibility of the reaction has shown a time and voltage dependent behaviour. It is realized that the shoulder like oxidation peak for the cyt c is more readily observed at fast scan rates. Moreover, as can be seen in Figure 4-18, if the voltage range is increased toward positive values, the peak disappears probably due to an adsorbed layer of protein which blocks further electron transfer.

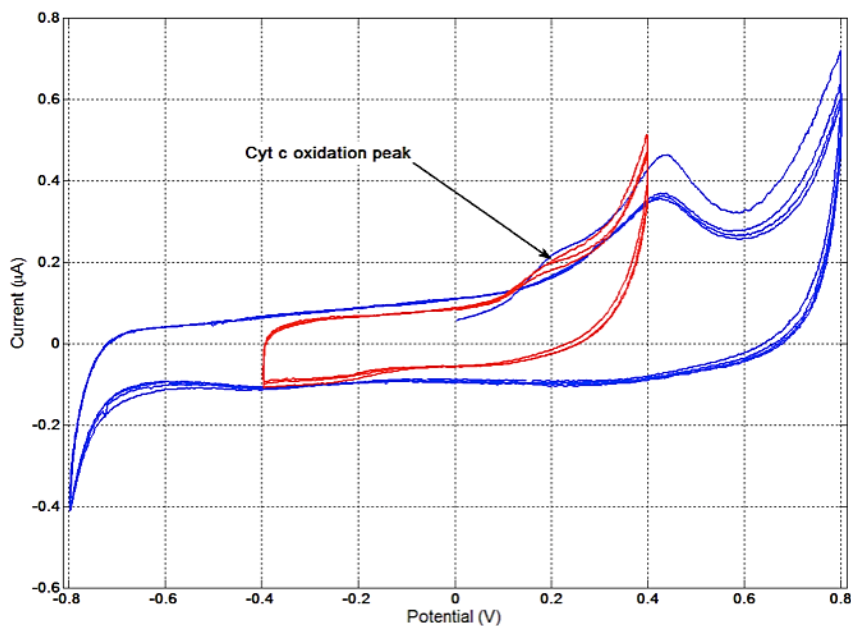


**Figure 4-18:** CV graph for 20 µl cyt c dissolved in 2.5 ml 0.1 M phosphate buffer at a scan rate of 20 mV/s.

If the gold surface is not thoroughly cleaned, or if it is flamed but exposed to lab atmosphere for a long time, no reduced cytochrome c Faradaic response is observable. Other than electrode cleaning, it is also realized that stability and reversibility of the cyt c redox behaviour can be dependent on the concentration of the buffer solution. Cyt c shows a quasi-reversible redox behaviour in a phosphate buffer of 30 mM concentration after around three hours as illustrated in Figure 4-19 and Figure 4-20.

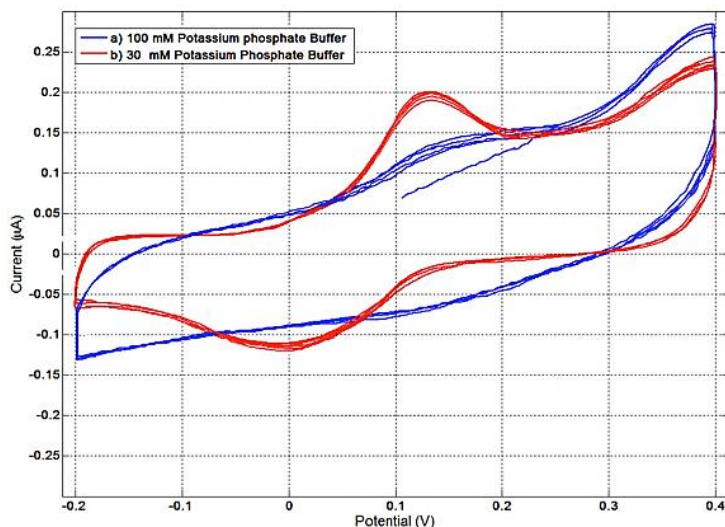


**Figure 4-19:** Cyclic voltammograms for 20  $\mu\text{M}$  cytochrome c in phosphate buffer on bare gold electrode recorded at the scan rate of 20 mV/s. The measurements are performed in potassium buffer pH 7 with two concentrations: blue) 100 mM, red) 30 mM.

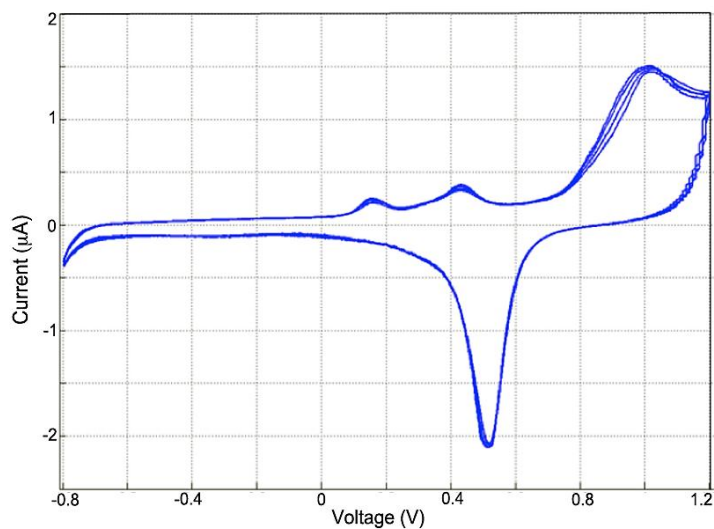


**Figure 4-20:** Cyclic voltammetry plot for 20  $\mu\text{M}$  reduced cytochrome c added to 2.5 mL of 30 mM phosphate buffer on bare gold electrode at a scan rate of 20 mV/s.

Typically no or very weak broad peaks with no well-defined positions are observed if CVs are recorded immediately after immersing the gold into the buffer solution containing reduced cytochrome c. However, if the protein is kept in the buffer solution for a few hours before starting the test, then the electrochemical response of cyt c is observable. If the solution is bubbled with  $\text{N}_2$  again in case of observing unwanted cathodic currents as a result of oxygen entering the system, no good

reduced cyt c response is detected shortly afterwards. The solution then needs to rest for a few hours to show the original response again. Considering that it takes around 3 hours for the open circuit potential to become relatively stable, it can be said that cyt c requires a long time to reach the equilibrium state in the buffer solution. This may be due to testing less pure cyt c, containing some aggregated molecules. If the solution contains aggregated proteins, the linked proteins may need time to disaggregate to individual proteins and to be responsive. Bubbling may cause the formation of aggregated proteins again; thus, after bubbling the proteins do not show any Faradaic response unless the solution is left to rest for a few more hours. However, it can be also hypothesized that since at least 85% of the surface is well covered with cytochrome c after a few hours of rest, the response of the cytochrome is caused by adsorbed and possibly deformed protein on the gold surface.

It is also observed that if the solution is bubbled for a long time the response can vanish completely. Thus the system seems to be very sensitive to mechanical impacts.

From the results in this section we conclude that cytochrome response in the protein based solar cell seems to be dependent on the concentration of the buffer solution and time of the exposure to the electrode. This means that for the solar cell also, the molarity of the buffer should be suitable for the cytochrome c when optimized performance of such proteins is expected. Also we have shown that cytochrome c adsorbs irreversibly and probably goes through conformational changes on the gold electrode. This surface coverage can result in less active area being exposed to the solution in a cell containing dissolved RC. Moreover, the high affinity of cytochrome c toward gold electrodes may result in adsorption competition between reaction centers and this protein when only the RC is required to bond to the surface of the gold electrode. In both scenarios, adsorption of reduced cytochrome c on the gold surface can lower the photo generated current in the system.

## 4.7 Quinone

Quinones are the main mobile electron carriers in the membrane of bacterial cells and chloroplasts [35]. The reactions involving oxidation and reduction of quinones are observed in photosynthetic charge transfer process of type 1 and type 2 reaction centers. In type 1 reaction center quinone is reduced to semiquinone. In type 2 center and in the purple bacteria reaction center, quinone undergoes a double reduction process, is converted to hydroquinone, and is released from the reaction center [36]. The two electron, two proton electrochemistry of quinone can have 9 redox states. Except for quinone and hydroquinone, the remaining 7 states are unstable in the cell membrane or water [36], [37]. In reaction centers, the reduction of primary quinone ( $Q_A$ ) to anionic semiquinone ( $Q_A^-$ ) reduces

the oxidized secondary quinone,  $Q_B$ , to semiquinone  $Q_{B.(H)}$ . The H is the indication of protonation of semiquinone in some cases [36].  $Q_{B.(H)}$  is reduced again after the primary quinone ( $Q_A$ ) is re-reduced. Hence, the primary quinone is expected to be a strong reductant capable of reducing both secondary quinone and  $Q_{(H)}$ . In addition,  $Q_{B.(H)}$  should have a long lifetime to allow the protein to undergo the second reduction of primary quinone [35]. The chemical reaction sequence in the primary and secondary quinones in the purple bacteria *Rhodobacter sphaeroides* reaction centers is described in this section. A diagram of the oxidation and reduction of quinone in different states is shown in Figure 4-21 [38].

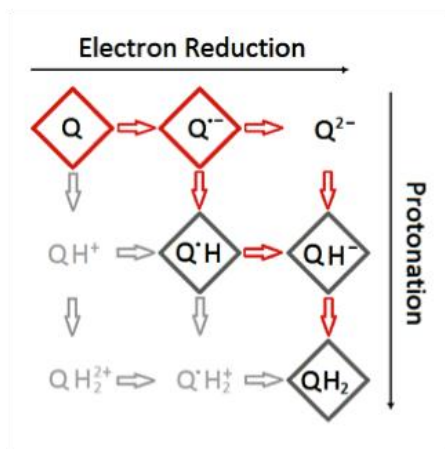


**Figure 4-21: Diagram of oxidation and reduction states of Quinone. The species in the red rhombuses exist in both primary ( $Q_A$ ) and secondary quinone ( $Q_B$ ) sites. The species in the dark grey rhombuses are found in secondary quinone. The species in light grey do not exist in RCs and aqueous solution.**

The electrochemical behaviour of Quinone-Hydroquinone pair is a common example of organic redox systems and has been a subject of interest for many decades [38]. Evaluation of reaction mechanisms, redox standard potentials, and adsorption of quinone on the surface of the working electrode at an aqueous buffer are essential to realize quinone's mode of action in the photovoltaic system. Cyclic voltammetry and AC voltammetry have been used to investigate the redox behaviour of quinone-hydroquinone couple and quinone adsorption on the surface of gold electrode in protein based solar cell. The objective in this section is to realize whether quinone existence in the cell can also be a limiting factor for the electron transport.

As illustrated in Figure 4-22, the reduction of quinone in acidic solutions can involve very fast two-electron two-proton reduction, whereas in alkaline solution the reduction involves only two-electrons with no protons. The reduction of quinone can involve two-electron one proton or only two-electrons with no protonation in neutral pH [38], [39].

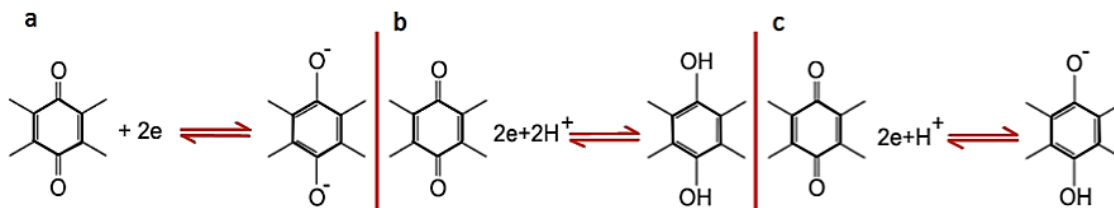


**Figure 4-22: Quinone's: a- two electron reduction at alkaline pH (dianion); b – Single step two electron two proton reduction at acidic pH (hydroquinone) ; c-Two-electron one-proton reduction at neutral pH (semiquinone).**

The redox potential varies with the pH as described by the Nernst equation. It is also known that in neutral aprotic solutions, semiquinone and the quinonedianion are generated in two successive one electron steps which results in two separate reduction peaks. The first peak is reversible and the second peak is quasi-reversible at different scan rates [38].

#### 4.7.1 Electrochemical Studies of Quinone on Bare Gold Electrode

A wealth of information is available about general properties of quinone and its response on carbon based electrodes and modified gold electrodes, however, we were unable to find sufficient information about the redox behaviour of quinone on bare gold electrodes. In this subsection 1,4-Benzoquinone (C<sub>6</sub>H<sub>4</sub>O<sub>2</sub>) is tested using cyclic voltammetry in order to observe quinone's redox peaks in the presence of unmodified gold electrode.

According to the CV tests results for a 60 μM 1,4 - Benzoquinone (C<sub>6</sub>H<sub>4</sub>O<sub>2</sub>) solution in 0.1 M phosphate buffer at pH 7 recorded at 5 mV/s, a redox couple with an oxidation peak at around -75 mV and a corresponding reduction peak at approximately -110mV vs. Ag/ AgCl is detected. The result for 60 μM quinone is shown in Figure 4-23. The peak separation is estimated to be 35 mV. The peak separation for a reversible system is given by [20]:

$$\Delta E_p = E_{pa} - E_{pc} = \frac{60}{n} mV,$$

where n represents the number of electrons transferred. Therefore, the peak separation for a fast one-electron process should be around 60 mV and the peak separation for a two electron transfer process is around 30 mV. Therefore, the final peak separation represents a reversible two electron transfer process.

It is noticed that if the CV is recorded a few minutes after immersing the gold electrode in the solution, the peak separation of around 125 mV is typically measured. However, if the cell goes

through several cycles for several minutes, it is observed that the oxidation peak slightly shifts to the left and the reduction peak shifts to the right. In addition, the peak current decreases after each cycle until it become constant after several cycles.

Figure 4-23 shows two super imposed cyclic voltammograms recorded immediately after the electrode exposure to the solution and 30 minutes after the electrode exposure to the solution containing quinone. As can be seen, the peaks are significantly shifted and reduced in height from their original positions until the oxidation and reduction voltages become fixed at around -75 mV and -110 mV respectively. Reduction in the peak height and the voltage shift in the peaks maybe a sign of quinone surface adsorption since adsorption of organic species can change the electrode surface potential and hence the open circuit potential. After observing this effect and the rest of results presented in this subsection, AC voltammetry is performed (refer to subsection 4.7.2) to determine the adsorption of quinone on the bare gold surface.

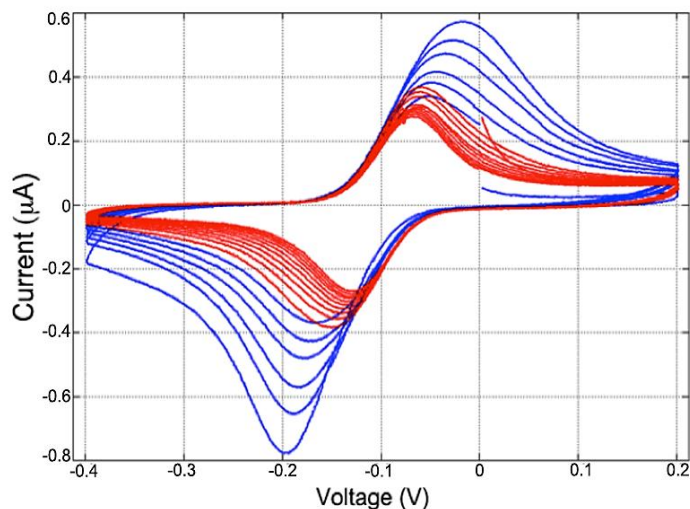


**Figure 4-23: Cyclic voltammetry of 60  $\mu\text{M}$  quinone in 0.1 M phosphate buffer at pH 7 at a scan rate of 5 mV/s. The Graph in blue is recorded immediately after gold electrode exposure and red graph is recorded half an hour after gold exposure to quinone containing the solution.**

In addition to the redox peaks, an irreversible reduction peak with no suggestion of any oxidation is seen in the blue graph shown in Figure 4-24 at -550 mV vs. Ag/AgCl. As is apparent from Figure 4-25 the irreversible peak becomes visible when the positive voltage limit is increased. It is of significant importance to mention that the plot in Figure 4-24 is composed of two superimposed plots of two separate sets of experiments with cleaned setup and freshly made solution. However, the plots

shown in Figure 4-25 are recorded in a sequential manner from a cell as the voltage is increased, thus the gradual decrease in the quinone redox peaks is visible in this figure.

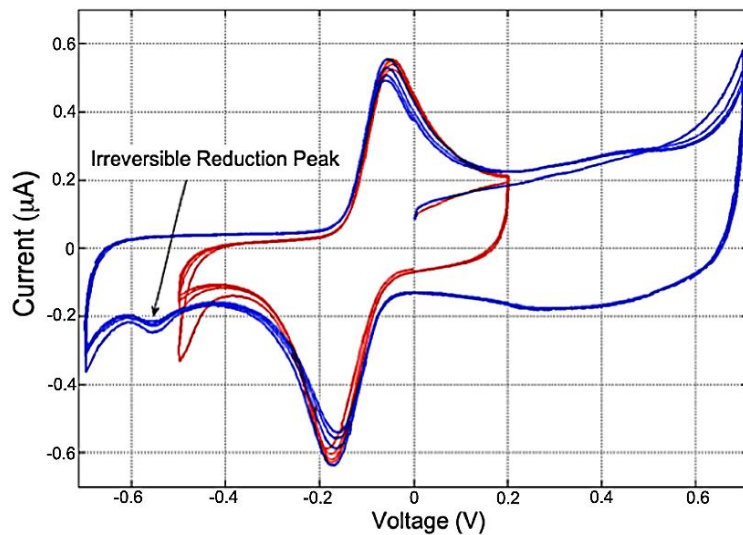


**Figure 4-24:** Two superimposed cyclic voltammograms for 70  $\mu\text{M}$  quinone in 0.1 M potassium phosphate buffer at pH 7 on gold electrode performed in two separate cells. The solution is deoxygenated with  $\text{N}_2$  gas for 15 minutes and is kept degassed by flowing  $\text{N}_2$  on top of the surface of the solution. Scan rate: 5 mV/s.

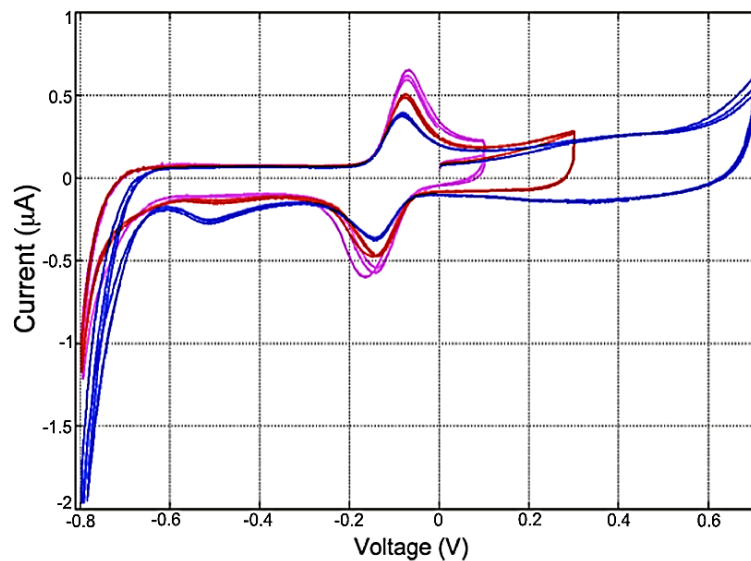


**Figure 4-25:** Cyclic voltammograms for 70  $\mu\text{M}$  quinone in 0.1 M potassium phosphate buffer at pH 7 on gold electrode when the voltage is increased gradually toward the positive values. The solution is deoxygenated with  $\text{N}_2$  gas for 15 minutes and is kept degassed by flowing  $\text{N}_2$  on top of the surface of the solution. Scan rate: 5 mV/s.

To ensure that the second reduction peak belongs to quinone, the changes in this peak are tracked with changing concentration of the quinone by carrying out sequential cyclic voltammetry tests with a scan rate of 20 mV/s from -0.8 to 1.2 V vs. Ag/AgCl (see Figure 4-26). The three concentrations and the peak currents are listed in Table 4-1.

**Table 4-1: The oxidation and second reduction peak currents for three different concentrations of quinone.**

Quinone Concentration ( $\mu\text{M}$ )	10	20	30
Oxidation Peak Current (nA)	270	510	790
Second Reduction peak current ( $\mu\text{A}$ )	0.32	5.3	8

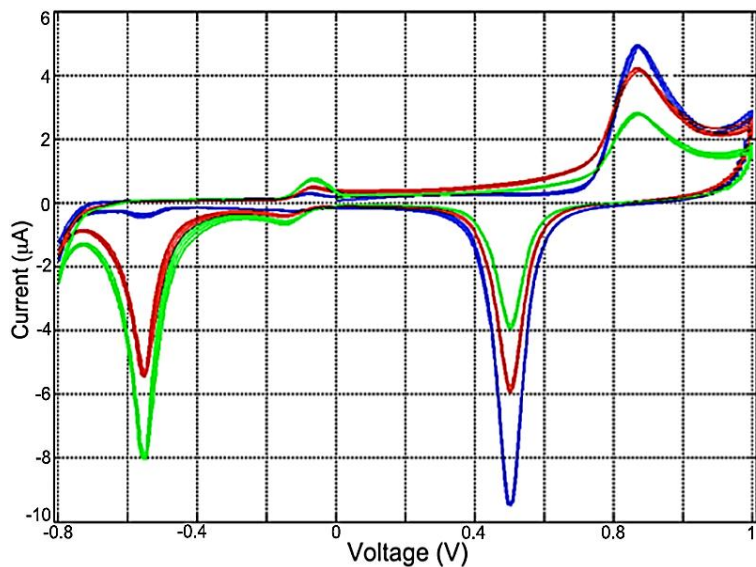


**Figure 4-26: Cyclic voltammograms of 10 (blue), 20 (red), and 30 (green)  $\mu\text{M}$  Quinone in 0.1 M phosphate buffer at pH 7. Scan rate: 5 mV/s.**

As can be seen both peaks belonging to quinone are increased by increasing the concentration of the quinone while the peaks assigned to gold oxidation and reduction are decreased as the concentration of the quinone is increased. According to equation (1), the peak for a diffusion limited current to the electrode substrate is proportional to the concentration of the species [20].

$$i_p = 2.69 \times 10^5 n^{3/2} A D_0^{1/2} C_0^* \nu^{1/2} \quad (1)$$

In this equation  $n$  represents the number of electrons,  $A$  is the electrode surface area in  $\text{cm}^2$ ,  $D_0$  is the diffusion coefficient in  $\text{cm}^2/\text{s}$ ,  $C_0^*$  is the concentration in  $\text{mol}/\text{cm}^3$  and  $\nu$  is the scan rate in  $\text{V}/\text{s}$ .

The peak currents for the reversible peak of quinone seem to follow the trend in the equation (1) if the electrode is exposed to the solution for a few hours and the voltage is not swept toward the negative limits. However, the irreversible reduction peak does not follow a linear trend and increases significantly for concentrations above  $20 \mu\text{M}$ .

In accordance with equation (1), the peak currents at three different scan rates of 20, 10, and 5  $\text{mV}/\text{s}$  for a  $10 \mu\text{M}$  quinone solution are proportional to the square root of the scan rate (See Figure 4-27). However, as shown in this plot, the irreversible reduction peak current is not proportional to the square root of the sweep rate.

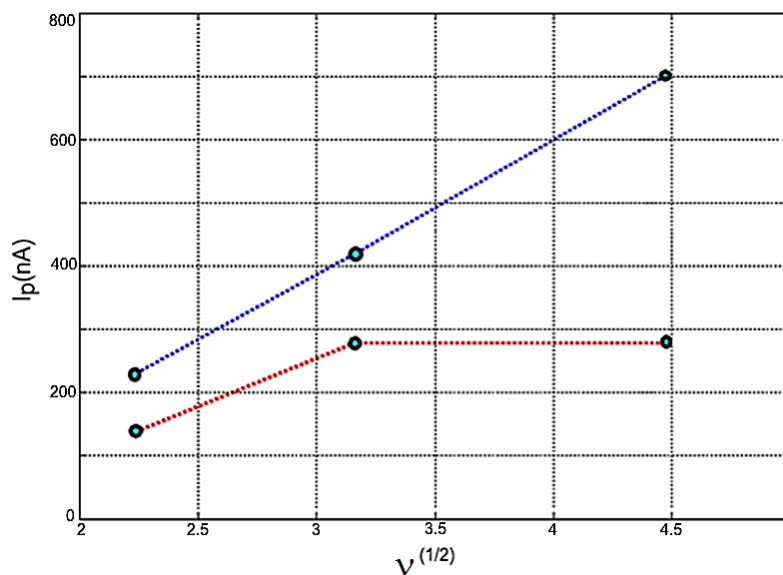


**Figure 4-27: Peak current (blue: reversible peak, red: irreversible reduction peak) vs.  $\nu^{1/2}$  for  $10 \mu\text{M}$  quinone solution in  $0.1 \text{ M}$  phosphate buffer at 10, 20, and 30  $\text{mV}/\text{s}$  scan rate.**

Moreover, it is evident from Figure 4-28, that the  $E_p$  assigned to the second peak varies with the sweep rate by shifting toward more negative values as the scan rate increases.

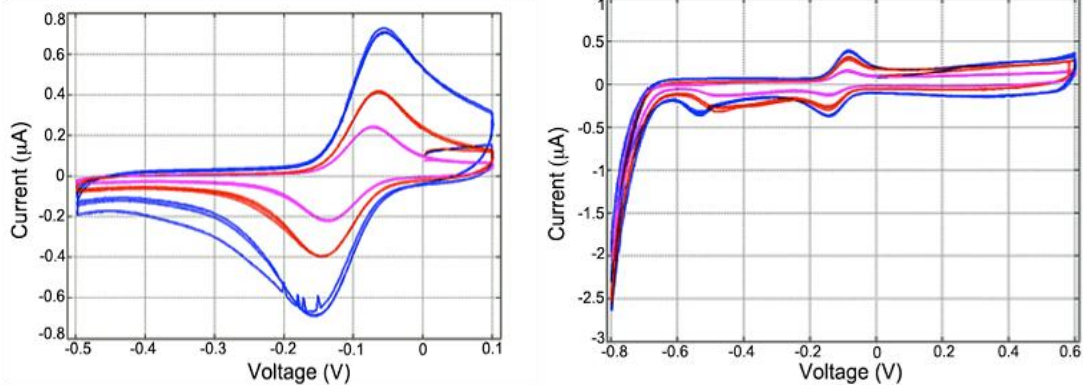


**Figure 4-28: Cyclic voltammety plots for 10  $\mu\text{M}$  quinone in 0.1 M phosphate buffer at pH 7 recorded at 20, 10, and 5 mV/s.**

Observing an irreversible peak for quinone is unexpected and it is unclear what the origin of this peak might be. Irreversible reduction peaks at negative potentials have been reported by other groups who have studied the electrochemistry of Anthracyclines, hydroxy-9, and 10-anthraquinone [38]. The irreversible reduction of the carbonyl side chain adjacent to the nucleus of anthraquinones been suggested as the source of this peak.

A similar reduction peak has also been observed in quinizarin and sodium quinizarin-2-sulphonate. This peak has been assigned to catalyzed hydrogen evolution by hydroxyl groups that are adjacent to quinone's benzene rings [38].

1,4 - Benzoquinone, does not possess any carbonyl side chain. Moreover, S.I. Bailey *et al.* reports that CVs for pure 1,4 - Benzoquinone show only one oxidation and its corresponding reduction peak with strong pH dependency [39]. Hence, we suspect that the available quinone may contain a small amount of analogous compounds to quinone.

#### **4.7.2 Adsorption of Quinone on Bare Gold Electrode**

During all of the electrochemical tests, it is noticed that the redox peak currents for quinone drop until they reach a steady state after several minutes. In addition, it is observed that the redox peaks of the gold decrease when adding the quinone. One last observation regarding quinone is that the hydrophilic surface of clean gold electrodes seems to become hydrophobic after being exposed to quinone containing solution. This is evident by the wettability of the surface before and after exposure to the solution containing quinone. Therefore, we suspect that the strong affinity of gold toward quinone makes its surface hydrophobic, similar to what is seen in protein adsorption. It is

suspected that this may be why the first few sweeps show higher redox currents and smaller currents are observed in the later sweeps for both quinone and gold.

In order to evaluate the adsorption of the quinone on the gold substrate, similar to cytc c, CV and ACV measurements at a scan rate of 5 mV/s are performed for 4 different concentrations of quinone, with results presented in Table 4-2, in 2.5 ml of 0.1 M potassium phosphate buffer.

Since it is noticed that the redox peak for the quinone reduces gradually, the ACV measurements were performed twice, the first measurement a few minutes after adding the quinone to the buffer and another measurement after 45 minutes. The capacitances recorded for the electrode that had prolonged exposure to the quinone solution are smaller than those measured soon after immersion.

The results for the CVs and the ACV tests are shown in Figure 4-29 and Figure 4-30 respectively. In both graphs, it is clear that by increasing the concentration, the capacitance of the double layer is reduced until the surface is saturated by quinone at concentration of 0.125 mM (20  $\mu$ l of quinone dissolved in 2.5 ml phosphate buffer).

**Table 4-2: Amount and capacitance measurements for Quinone during cyclic voltammetry tests.**

Amount of Quinone ( $\mu$ l)	2	6.5	20	70
Capacitance - Immediate ( $\mu$ F)	0.95	0.55	0.3	0.3
Capacitance - after 45mins ( $\mu$ F)	0.63	0.3	0.3	0.3

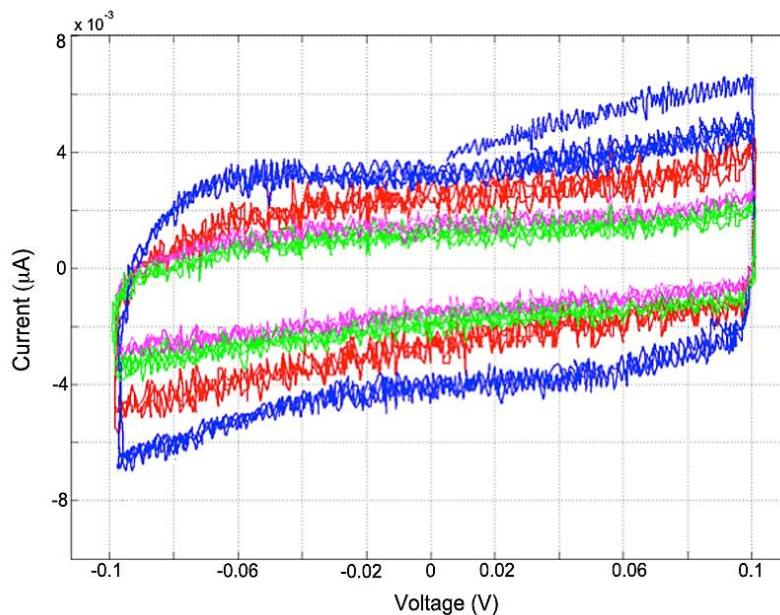


Figure 4-29: Cyclic voltammetry tests for blue: 2, red: 6.5, magenta: 20, and green: 70  $\mu\text{l}$  Quinone in 2.5 ml potassium phosphate buffer (100 mM, pH 7) on bare gold electrode (Scan rate = 5 mV/s, 45 minutes after electrode immersion).

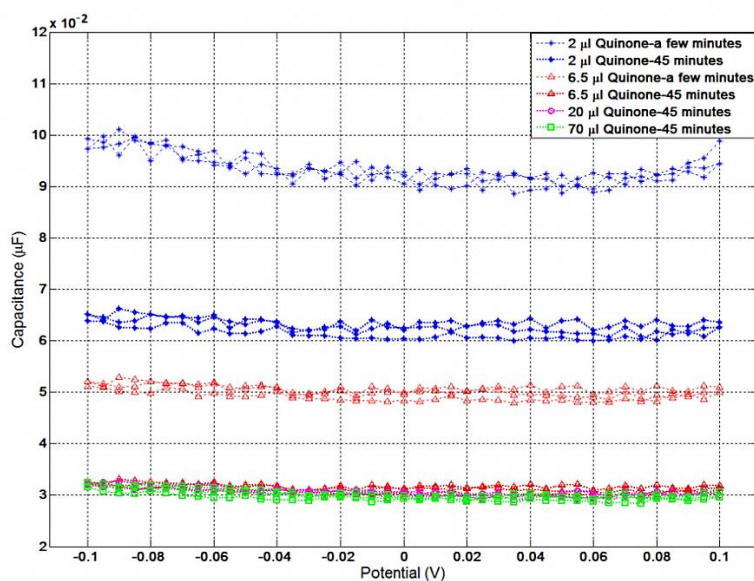
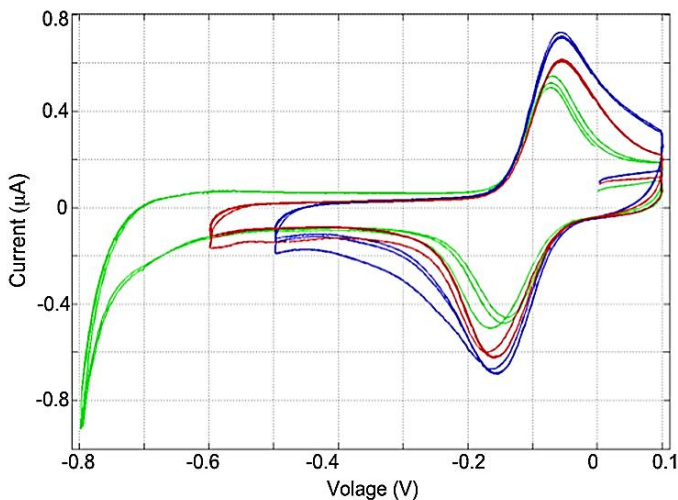


Figure 4-30: AC voltammetry tests for blue: 2, red: 6.5, magenta: 20, and green: 70  $\mu\text{l}$  Quinone in 2.5 ml potassium phosphate buffer (100 mM, pH 7) on bare gold electrode (Scan rate = 5 mV/s).

The adsorption of the 20  $\mu\text{l}$  of quinone is characterized by cycling the gold electrode from -0.8 to 0.1 V vs. Ag/AgCl and from -0.8 to 1.2 V vs. Ag/AgCl for 10 cycles in 2.5 ml deoxygenated 100 mM

phosphate buffer at pH 7 at a scan rate of 20 mV/s. The peak currents during the cycles between -0.8 to 1 V vs. Ag/AgCl are decreased when the voltage range is increased. As shown in Figure 4-31, sweeping in negative voltage ranges, up to the hydrogen evolution, causes further adsorption of the quinone on the surface of the electrode as suggested by the reduced height of the redox peaks.



**Figure 4-31:** Cyclic voltammetry plots for 20  $\mu\text{l}$  quinone in 2.5 ml potassium phosphate buffer at pH 7 while increasing the negative voltage range. Scan rate: 20 mV/s.

According to Figure 4-32, the redox peak currents for the quinone further drop when sweeping the voltage in positive voltage ranges indicating that applying positive voltages facilitates the adsorption.

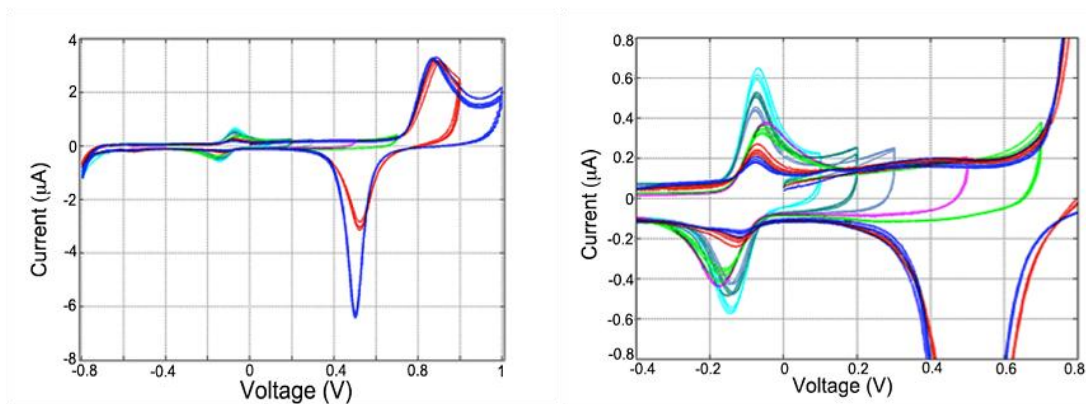


**Figure 4-32:** Left: superimposed cyclic voltammetry records for 20  $\mu\text{l}$  quinone in 2.5 ml phosphate buffer at pH 7 (scan rate 20 mV/s); right: zoomed in section to show the quinone redox peak changes from -0.4 to 0.8 V. Scan rate: 20 mV/s.

Additionally, some preliminary CVs are done for 0.1 M phosphate buffer lacking quinone on a gold electrode rinsed with buffer after being exposed to 70  $\mu\text{M}$  quinone for an hour. The full scan CVs show no considerable change in the redox peaks of gold and quinone, suggesting that quinone adsorbs very strongly on the surface of the gold. The results for those tests are not shown in this work since the results were not reproduced due to time constraints.

Overall, it is observed that the quinone peaks reduce even when the gold surface is being oxidized and reduced. Gold's oxidation and reduction currents are smaller than the original redox peaks recorded for clean bare gold immersed in 100 mM phosphate buffer. The smaller peak currents for gold and peak reduction for quinone indicate that it adsorbs on the surface of gold strongly and does not desorb from the substrate due to either attractive or repulsive electrostatic forces when sweeping the voltage between -0.8 to 1.2 V vs. Ag/AgCl.

## 4.8 Surfactants

Surfactants are water-soluble detergents usually including a long alkyl chain linked to their hydrophilic functional groups. Surfactants lower the surface tension when mixed in water in small amounts, and enable fats to be emulsified. In biochemistry and biomedical tests, surfactants are usually used for multiple purposes such as solubilizing agents for membrane protein, crystallization agents to prevent protein membrane aggregation, and obstructive agents to stop proteins from nonspecific adsorption on some electrodes [40]. In the bio-photovoltaic cell, surfactants are required to make the RCs soluble in the buffers.

Detergents are essential parameters in the protein based solar cell. Therefore, investigating their influence on reaction centers' activity is of significant importance. In this section the electrochemistry and adsorption of three available surfactants: LDAO, DDM, and  $\beta$ -OG are investigated. In addition to providing information about the electrochemistry of the detergents, the experiments are useful to determine whether using any of the surfactants is advantageous over the other two.

### 4.8.1 LDAO

A very frequently used detergent in biochemistry is Lauryldimethylamine-oxide (LDAO,  $\text{C}_{14}\text{H}_{31}\text{NO}$ ). LDAO is an amine oxide surfactant which contains a  $R^3N^+ \rightarrow O^-$  functional group. LDAO exhibits excellent water solubility but usually poor organic solvent solubility [41]. The chemical structure of LDAO is shown in Figure 4-33.

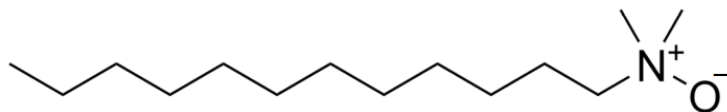


**Figure 4-33: Lauryldimethylamine-oxide (LDAO) chemical structure.**

As demonstrated, the LDAO molecule consists of a long hydrophobic alkyl chain, attached to its water soluble functional group. Also it can be seen that LDAO carries a net charge of zero, however, it carries positive charge at the nitrogen atom and negative charge at its oxygen atom in water. Thus, LDAO is considered as a highly polar molecule.

#### 4.8.2 Electrochemical Characterization of LDAO

A series of initial cyclic voltammograms, recorded to study the electrochemical behaviour of RCs in the presence of a gold electrode, show that LDAO, at a concentration of 0.1% v/v likely interacts with the gold surface. The surfactant interactions with the electrode can result in unwanted background signals that can affect the interactions of RCs, cyt c and quinone with the surface and thus lowering the photocurrent. Therefore, the electrochemical behaviour of LDAO is investigated using the cyclic voltammetry technique.

CVs are recorded at 20, 10, and 5 mV/s in 2.5 ml potassium phosphate buffer solution at pH 7 containing 1% (v/v) for short ‘double layer’ scans (-0.2 V to 0.1 V vs. Ag/AgCl, away from Faradaic reactions), and at scan rates of 10 and 5 mV/s during full scans. The results for the double layer and full scan CV measurements are shown in Figure 4-34.

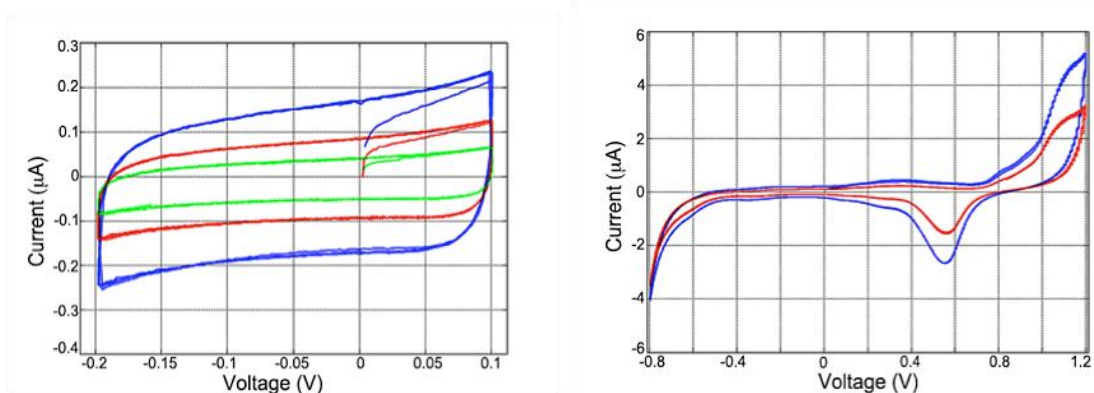


**Figure 4-34: Cyclic voltammetry tests for 0.1% LDAO v/v in 2.5 ml 0.1 M potassium phosphate buffer left: at scan rate blue: 20, red: 10, and green: 5 mV/s; right: scan rate of blue: 10 and red: 5 mV/s. The voltages are presented vs. Ag/AgCl reference.**

According to Figure 4-34, the capacitive currents when LDAO is added to the system are larger than the capacitive currents detected in the case of pure phosphate buffer (See Figure 4-8-left- refer to blue curve, page 27 which shows a current amplitude of  $\sim 0.1$  A during the positive scan, and  $-0.05$  in the negative scan direction at  $0$  V vs. Ag/AgCl). Also from the full scan graph, it is obvious that the gold redox peaks have significantly reduced and broadened compared to the original redox peak for the gold in pure buffer solution. The drop in the gold oxidation peaks suggests a protective but porous or incomplete covering. Both observations combined suggest that LDAO adsorbs on the surface of gold.

Figure 4-35 is a demonstration of superimposed CVs for  $0.1\%$  LDAO v/v in potassium phosphate buffer recorded at the scan rate of  $20$  mV/s when left) the bottom end of the voltage range is increased by  $0.1$  V for each test; right) the voltage range is increased in  $0.1$  V increments toward in the positive direction. LDAO seems to stay on the surface during the application of both positive and negative voltage, as is evident from similarity between the currents of superimposed plots in Figure 4-35. Moreover, the hydrogen evolution (with onset normally at approximately  $-0.8$  vs. Ag/AgCl, as seen in Figure 4-8 page 27), is visibly shifted to the right when LDAO is added to the buffer. No obvious peak associated to LDAO Faradaic reaction is observed. This indicates that either LDAO is not reactive in the voltage ranges between  $-0.8$  to  $1.2$  V vs. Ag/AgCl or the surfactant is strongly adsorbed on the surface and it is possible that electron transfer is either blocked or severely hindered.

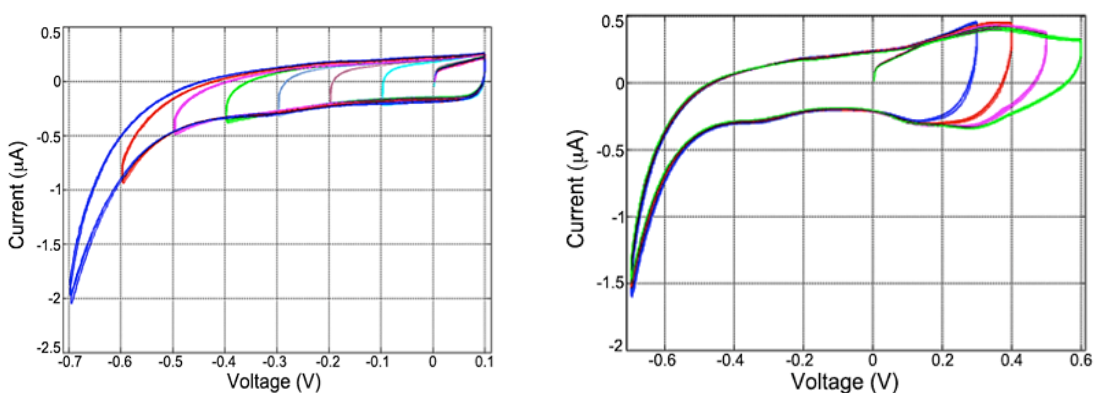


**Figure 4-35: Cyclic voltammetry results for  $0.1\%$  v/v LDAO in  $2.5$  ml potassium phosphate buffer ( $100$  mM, pH7) left: when the voltage is increasing toward the negative values right: the voltage is increased toward the positive values at scan rate of  $20$  mV/s.**

### 4.8.3 Adsorption of LDAO on Bare Gold Electrode

Two sets of cyclic voltammetry and AC voltammetry are recorded for different amounts of LDAO dissolved in 50 mM Potassium perchlorate and 100 mM potassium phosphate buffer both at pH 7. Figure 4-36 and Figure 4-37 represent the CV and ACV results for perchlorate and phosphate buffer containing LDAO respectively. The amounts and the double layer capacitances corresponding to each concentration are listed in Table 4-3. As it is evident in these plots, the double layer capacitance is increased upon addition of the detergents into the buffer solution.

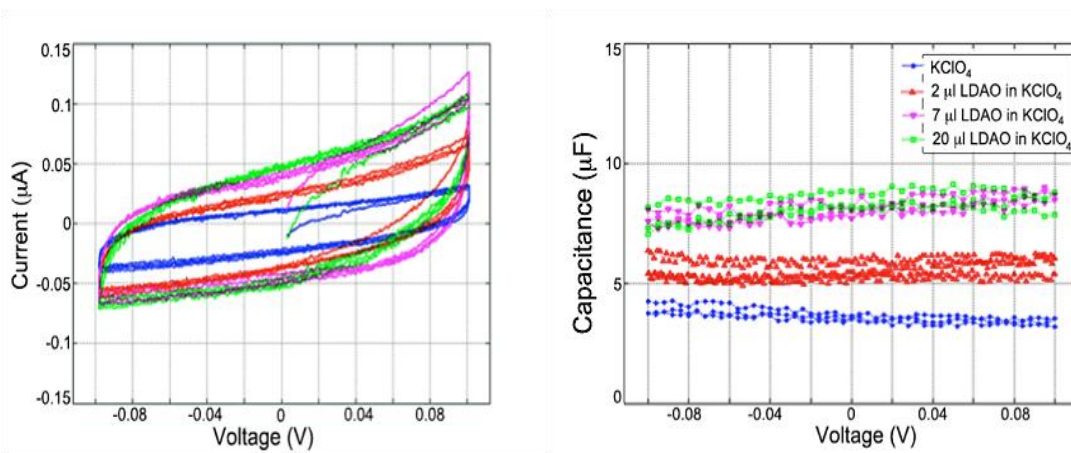


Figure 4-36: Left: Cyclic voltammetry; right: AC voltammetry tests for 2, 7, and 20 μl for LDAO dissolved in 2.5 ml 50 mM KClO<sub>4</sub> pH 7 (Frequency: 25 Hz, amplitude: 5 mV, scan rate: 5 mV/s). The solution is deoxygenated with N<sub>2</sub> gas for 15 minutes and is kept degassed by flowing N<sub>2</sub> on top of the surface of the solution. The voltages are presented vs. Ag/AgCl reference.

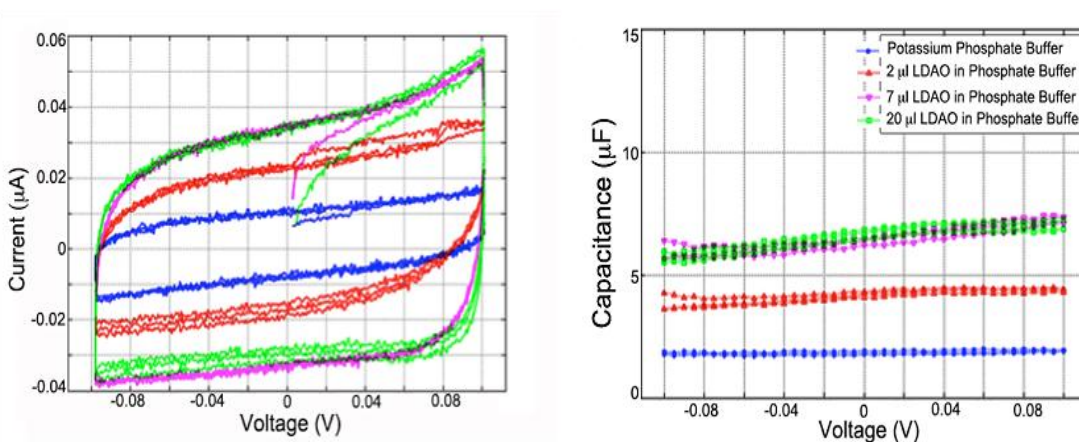


Figure 4-37: Left: Cyclic voltammetry; Right: AC voltammetry tests for 2, 7, and 20 μl for LDAO dissolved in 2.5 ml 100 mM phosphate buffer pH 7 (Frequency: 25 Hz, amplitude: 5 mV, scan rate: 5 mV/s). The solution is deoxygenated with N<sub>2</sub> gas for 15 minutes and is kept degassed by flowing N<sub>2</sub> on top of the surface of the solution. The voltages are presented vs. Ag/AgCl reference.

**Table 4-3: LDAO amount and capacitance measurements during CV and ACV tests.**

LDAO Amount ( $\mu\text{l}$ )	2	7	20	70
Capacitance in Potassium perchlorate ( $\mu\text{F}$ )	5.5	8	8.1	8.1
Capacitance in Phosphate buffer ( $\mu\text{F}$ )	4	6.5	6.5	6.5

The double layer capacitance per unit area ( $9.95 \text{ mm}^2$ ) when gold electrode is exposed to Phosphate buffer is:

$$C_a = \frac{2 \mu\text{F}}{9.95 \times 10^{-2} \text{ cm}^2} = 20 \mu\text{F} \cdot \text{cm}^{-2},$$

and  $C_a$  increases to  $60 \mu\text{F} \cdot \text{cm}^{-2}$  when the gold surface is exposed to  $7 \mu\text{l}$  LDAO and buffer.  $2 \mu\text{l}$  LDAO dissolved in  $2.5 \text{ ml}$   $0.1 \text{ M}$  phosphate buffer results in  $C_a$  of  $40 \mu\text{F} \cdot \text{cm}^{-2}$ , suggesting that even very small amount of dissolved LDAO adsorbs on the electrode surface aggressively and hence, affects the double layer capacitance drastically.

The double layer capacitance changes ( $\Delta\%$  capacitance) are calculated according to:

$$\Delta C = \frac{C_{\text{Exposure}} - C_{\text{initial}}}{C_{\text{initial}}},$$

and the results are summarized in Table 4-4.

**Table 4-4: double layer capacitance changes for different amount of LDAO in phosphate buffer.**

LDAO Amount ( $\mu\text{l}$ )	2	7	20
$\Delta C$ % relative to potassium perchlorate	37.5	100	100
$\Delta C$ % relative to phosphate buffer	60	160	160

As can be seen after adding 7  $\mu\text{l}$  of LDAO to 2.5 ml solutions, the surface becomes covered with monolayers of LDAO surfactant which increases the capacitance to more than twice its original value. The capacitance changes when the LDAO is added to the phosphate buffer are more significant, however, the final capacitance in case of LDAO and phosphate buffer is smaller than the LDAO and  $\text{KClO}_4$ . This may be due to the fact that phosphate itself adsorbs on the surface, however, since it is a weak adsorber, most of the phosphate molecules are replaced by the LDAO molecules in the double layer. Whereas, the double layer formed in case of LDAO and  $\text{KClO}_4$  is probably formed due to water molecule replacement by LDAO molecules. Since LDAO is highly polarizable, the dielectric constant of the double layer capacitance is expected to increase highly and dominate the increase of the thickness of the capacitor.

Although it may be the most commonly used surfactant to make the reaction centers water soluble, the above experiments show that LDAO adsorbs considerably on the surface of the bare gold electrode even at the low concentrations (0.1% v/v) normally used in protein based solar cells. The reduction in the gold redox peaks and the change in the double layer is considerable meaning a large area of the electrode is blocked due to LDAO adsorption, which can hinder the analytes' reactivity on the electrode surface. Therefore, the use of two other possible surfactants is investigated.

#### 4.8.4 DDM and $\beta$ -OG

n-Dodecyl- $\beta$ -D-Maltoside (DDM,  $\text{C}_{24}\text{H}_{46}\text{O}_{11}$ ) and n-Octyl- $\beta$ -D-Glucopyranoside ( $\beta$ -OG,  $\text{C}_{14}\text{H}_{28}\text{O}_6$ ) are two non-ionic water soluble biological detergents that are used to solubilize and stabilize integral membrane protein [42]. DDM is known to better preserve protein membrane activity compared to most of the detergents [43]. In addition, high purity DDM has a very low UV absorption coefficient [43]. Refer to Figure 4-38 for chemical structure of a) DDM and b)  $\beta$ -OG.

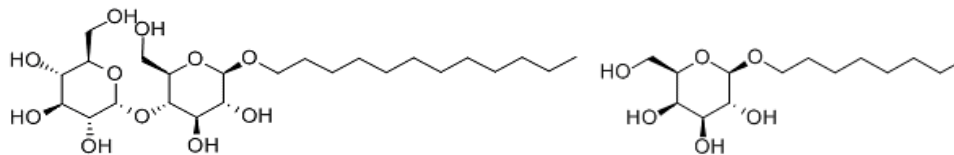
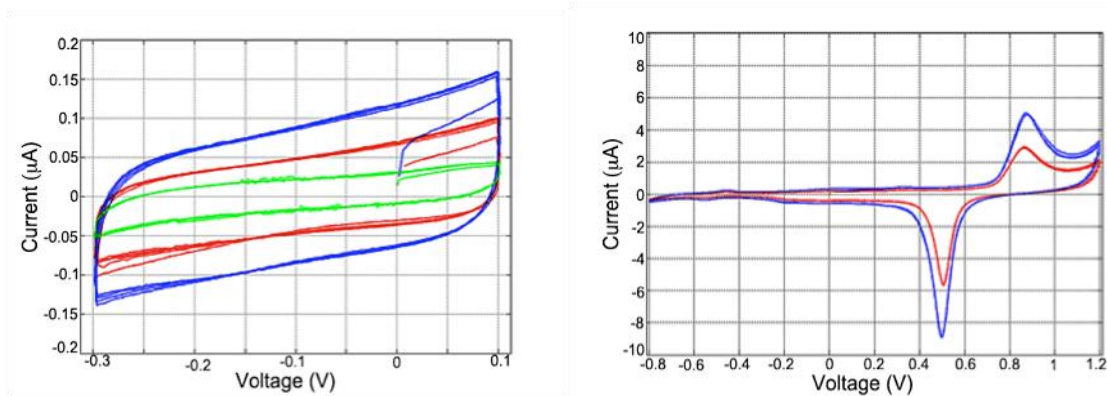


**Figure 4-38: Chemical structure of left: n-Dodecyl- $\beta$ -D-Maltoside (DDM) and right: n-Octyl- $\beta$ -D-Glucopyranoside ( $\beta$ -OG)**

The electrochemical properties and absorption of the new detergents are tested using cyclic voltammetry and ACV respectively.

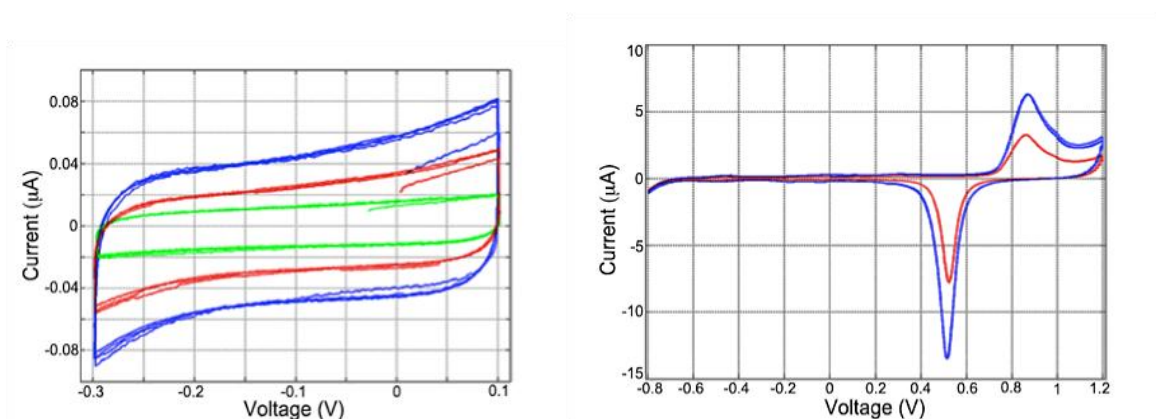
#### 4.8.5 Electrochemistry of DDM and $\beta$ -OG

Figure 4-39-left demonstrates the CVs recorded in the double layer region of the 2.5 ml of 100 mM phosphate buffer at pH 7 and with 0.1% v/v DDM detergent. It is noticed that in the presence of DDM the capacitive currents are higher than the original currents recorded for the pure buffer. However, according to the full scan plots the redox peaks corresponding to gold oxidation/ reduction are reduced in the presence of DDM in solution.



**Figure 4-39: Left: double layer; Right: full scan CVs of DDM detergent (~ 2.5  $\mu$ l) in potassium phosphate buffer (100 mM buffer, pH 7, voltage range: -0.3 to 0.1 V vs. Ag/AgCl). Scan rates blue: 20, red: 10, green: 5 mV/s for double layer region CVs; scan rates blue: 10 and red: 5 mV/s for full scans (Voltage range: -0.3 to 0.1 V vs. Ag/AgCl).**

Double layer region current reduction and gold redox peak reduction are observed when CVs are recorded for 0.1% v/v  $\beta$ -OG detergent solved in 2.5 ml 100 mM phosphate buffer. The results are shown in Figure 4-40. In this case the capacitive currents are lower and gold redox peak heights are reduced in the presence of the surfactant, suggesting adsorption on the gold surface. Furthermore, the slope of current in the DDM CV in the double layer region indicates that larger background signals (start of a faradaic reaction) are present in the system compared to  $\beta$ -OG. A broad oxidation like peak and a corresponding reduction peak is observed at around -0.45 V vs. Ag/AgCl in both DDM and  $\beta$ -OG solutions. The origin of this broad peak is unknown. Usually such peak can be generated by reversible reactions due to the detergent at the negative voltages; however, it can also be due to the molecular reorientations in the double layer at certain voltages.



**Figure 4-40:** Left: Cyclic voltammetry at double layer region between -0.3 to 0.1 V vs. Ag/AgCl at three scan rates: 20, 10, and 5 mV/s; right: full scan between -0.8 to 1.2 V vs. Ag/AgCl at two scan rates: 10 and 5 mV/s CV of  $\beta$ -OG detergent ( $\sim 2.5 \mu\text{l}$ ) in potassium phosphate buffer (100 mM buffer, pH 7).

To determine the other possible reactions of detergents, several cyclic voltammograms are recorded for both DDM and  $\beta$ -OG when the voltage is changed stepwise toward negative and positive values as shown in Figure 4-41 and Figure 4-42 respectively.

According to Figure 4-41, in the presence of DDM, the currents are increasing when voltage is increased toward more negative values beyond -0.4 V vs. Ag/AgCl. The voltage sweep towards positive values shows an increase in anodic current values for voltages above 0.2 V vs. Ag/AgCl. The significant current changes while applying different voltages, plus the obvious reduction in the gold redox peaks shown in the full scan plot suggests that DDM is adsorbing on the surface. The capacitance changes and the surface coverage calculations are shown in the next section where the ACV is recorded for different concentrations of DDM.

The increase in the current by sweeping the voltage seems to suggest that more DDM molecules are adsorbed on the surface due to electrostatic forces. The currents in the capacitive region are measured again after the full scan (from -0.8 to 1.2 V vs. Ag/AgCl). The currents return to their original values (Figure 4-39-right sides), indicating that any additional DDM adsorbed at voltage extremes does so reversibly.

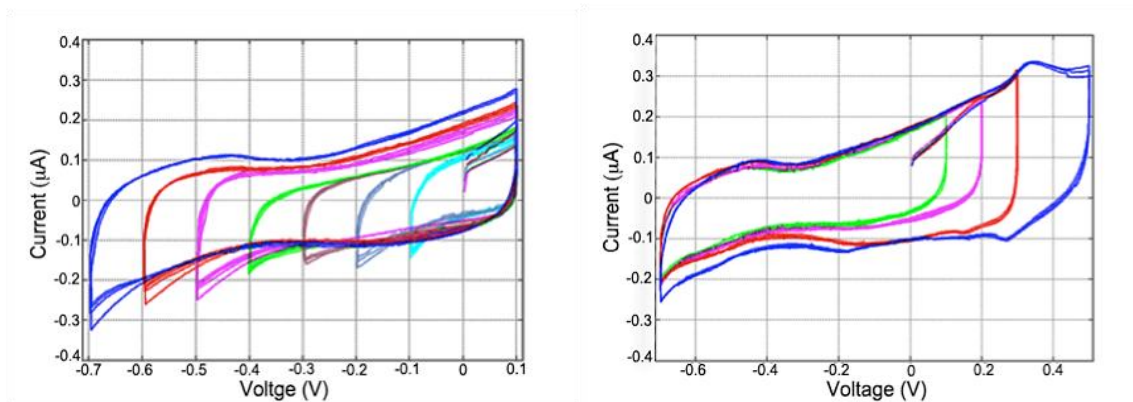


**Figure 4-41:** Cyclic voltammograms of bare gold electrode at 20 mV/s for 0.1% v/v DDM detergent in 100 mM potassium phosphate buffer pH 7 while increasing the voltage toward the left: negative values; right: positive values.

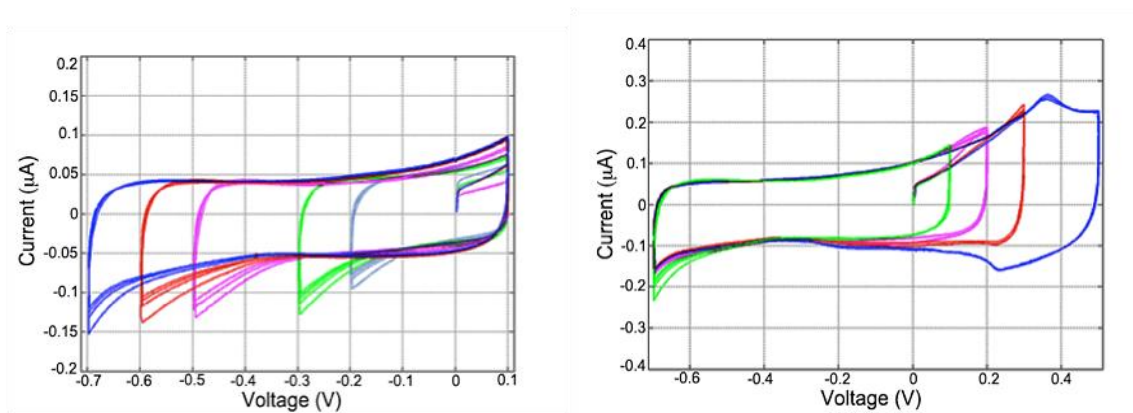


**Figure 4-42:** Cyclic voltammograms of bare gold electrode at 20 mV/s for 0.1% v/v  $\beta$ -OG detergent in 100 mM potassium phosphate buffer pH 7 while increasing the voltage toward the left: negative values; right: positive values.

Based on Figure 4-42, the anodic and cathodic currents remain fairly constant during both negative and positive scans for the solution of  $\beta$ -OG in the phosphate buffer. In addition, the currents in the capacitive regions are fairly close to the currents measured in pure phosphate buffer. These observations suggest that small amount of  $\beta$ -OG may adsorb on the gold surface compared to LDAO and DDM.

#### 4.8.6 Adsorption of DDM and $\beta$ -OG on Bare Gold Electrode

In order to measure the double layer capacitance and adsorption of detergents, ACV tests are performed on various concentrations of both DDM and  $\beta$ -OG diluted in 50 mM  $\text{KClO}_4$  and 100 mM potassium phosphate buffers both at pH 7. For both detergents, as can be seen in Figure 4-43 and Figure 4-44, the double layer capacitance when the detergent is dissolved in  $\text{KClO}_4$  is larger in

comparison with the double layer capacitance when DDM and  $\beta$ -OG are added to phosphate buffer. This may indicate that the detergent molecules replace the water molecules in the double layer in  $\text{KClO}_4$  solution, and result in significant double layer capacitance changes. However, in the presence of phosphate the detergent molecules should compete with the phosphate molecules adsorbed on the surface of the electrode. Hence, only a fraction of the double layer molecules may be exchanged with DDM or  $\beta$ -OG molecules. It is of significant importance to mention that, unlike what is detected for LDAO and DDM, the double layer capacitance in the presence of  $\beta$ -OG drops compared to the capacitance of the pure buffer.

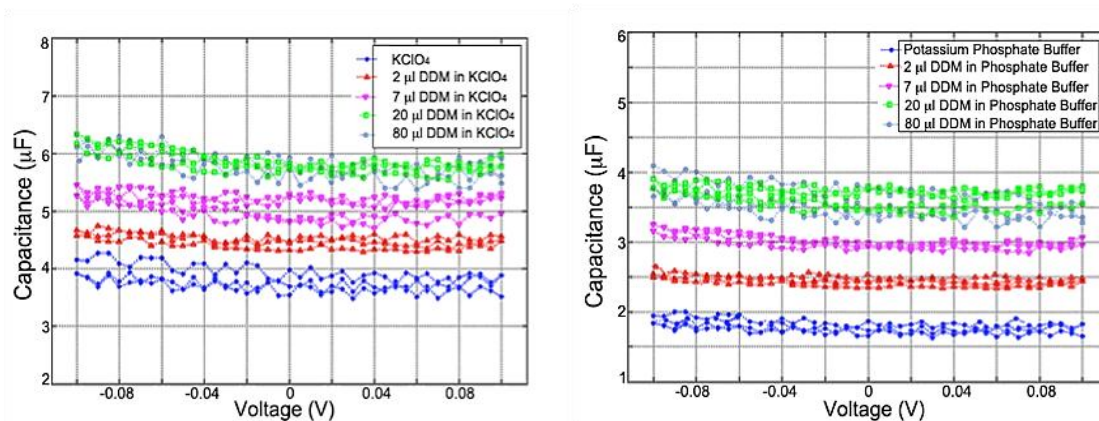


**Figure 4-43: Capacitance profile measurements for bare gold electrode exposed left: (50 mM  $\text{KClO}_4$ ) right : 100 mM Potassium phosphate buffer. blue: 2.5 ml buffer 2- red: 2  $\mu\text{l}$  3- magenta: 7  $\mu\text{l}$  4- green: 20  $\mu\text{l}$  5- purple: 80  $\mu\text{l}$  DDM detergent diluted in 2.5 ml buffer. The ACVs are recorded at scan rate: 5 mV/s, amplitude 5mV/s, and frequency: 25 Hz.**

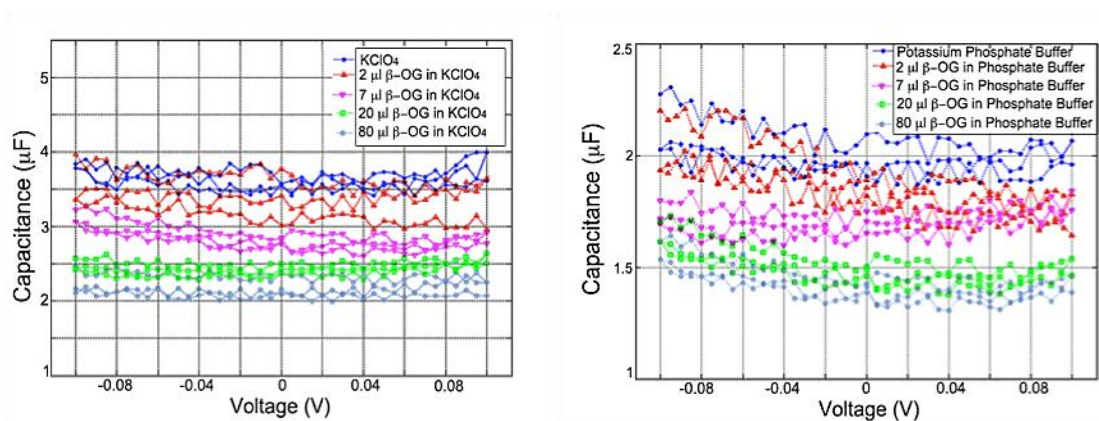


**Figure 4-44: Capacitance profile measurements for bare gold electrode exposed left: (50 mM  $\text{KClO}_4$ ) right : 100 mM Potassium phosphate buffer. blue: 2.5 ml buffer 2- red: 2  $\mu\text{l}$  3- magenta: 7  $\mu\text{l}$  4- green: 20  $\mu\text{l}$  5- purple: 80  $\mu\text{l}$   $\beta$ -OG detergent diluted in 2.5 ml buffer. The ACVs are recorded at scan rate: 5 mV/s, amplitude 5mV/s, and frequency: 25 Hz.**

Both detergents show some surface adsorption in the operational voltage range of the solar battery. Also the gold redox peaks are broadened in the presence of these detergents. However, the parasitic signals due to DDM and especially  $\beta$ -OG are significantly smaller than LDAO. In Addition, the capacitance changes due to the addition of  $\beta$ -OG and DDM are not as drastic as changes caused by the addition of LDAO into the buffer solutions. Therefore, to minimize the effect of the surfactant during the electrochemical measurements on the reaction centers, it may be beneficial to use DDM or  $\beta$ -OG in place of LDAO. To test this hypothesis in the presence of the RC, three separate reaction center batches each dissolved in LDAO, DDM, and  $\beta$ -OG are tested as described in the following section.

## 4.9 Reaction Center

The conversion of light into chemical potential in photosynthetic bacteria is enabled by reaction center (RC) protein complexes [37], [44], [45]. RCs are composed of 4 protein subunits called Heavy (H), Medium (M), Light (L), and cytochrome and 14 energy conversion cofactors. The reaction center from wild type Rhodobacter sphaeroides has a length of 13 nm from H subunit to cytochrome and has an elliptical cross section with axes sizes of 4 and 7 nm [46].

In this work we have tested reaction centers from Rhodobacter sphaeroides. The mentioned RCs have three H, M, and L subunits and lack the tightly bound cytochrome. The cofactors for the RC include a bacteriochlorophyll dimer which is the primary dimer donor (P),  $B_A$  and  $B_B$  which are two bacteriochlorophylls,  $H_A$  and  $H_B$  which are two bacteriopheophytins,  $Q_A$  and  $Q_B$  identified as quinone, and an iron atom ( $Fe^{2+}$ ) [43], [44]. The structural arrangement and energy- kinetic diagram of the Rhodobacter sphaeroides RC is shown in Figure 4-45.

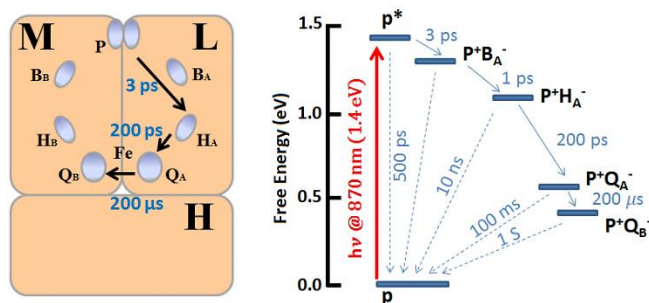


**Figure 4-45:** Left: schematic view of photosynthetic RC of Rhodobacter sphaeroides. L, M, and H represent the protein subunits. The photosynthetic electron transfer between the cofactors, indicated by arrows, is one sided along the L subunit. The corresponding time constants are shown for each electron transfer process. Right: photochemistry energy diagram for electron transfer process in reaction center. The potential is reported vs. NHE.

The redox potentials are indicated by the vertical position of the cofactors in the energy diagram at right which cover a range of approximately 1.5 V between the ground state to the excited state [47]. During illumination, the photo-excited primary electron donor (P) is transferred to an excited state (P\*). The electron is then transferred through the cofactors in the L subunit to Q<sub>B</sub> in three steps. The corresponding time for electron transfer from P\* to H<sub>A</sub>, from H<sub>A</sub> to Q<sub>A</sub>, and from Q<sub>A</sub> to Q<sub>B</sub> is 3 ps, 200 ps, and 200 μs respectively [48]. After the electron transfer to Q<sub>B</sub>, cytochrome, acting as the diffusible electron transfer mediator, reduces the P which results in the formation of P<sup>+</sup>Q<sub>A</sub>Q<sub>B</sub><sup>-</sup>. Similar photo-excitation and electron transfer process is repeated and hence Q<sub>A</sub> donates a second electron to Q<sub>B</sub><sup>-</sup>. Two protons are taken up by Q<sub>B</sub><sup>-2</sup>. Acting as an electron carrier mediator, the resulting hydroquinone (QH<sub>2</sub>) is released from the reaction centre after protonation and a quinone replaces the released QH<sub>2</sub> in the Q<sub>B</sub> binding site [47].

Cytochrome c and quinone, acting as electron donor and electron acceptor respectively, are used as mediators to complete the charge transport within bacteria.

#### 4.9.1 Electrochemistry of *Rhodobacter sphaeroides* RC

Cyclic voltammetry on a bare gold electrode exposed to RC solutions is done in a three electrode cell at room temperature in the dark and while illuminated by employing a 60 mW/cm<sup>2</sup> white light beam. The light beam is generated by a 150 W Newport solar simulator (www.newport.com, model: 67005). All the tests are done at 5 mV/s and in pH 7 100 mM Phosphate buffer.

To test the RCs dissolved in different detergents, LDAO is exchanged for 0.1% DDM and 0.1% OG. In order to dilute the RC in the new detergent and new buffer, a sample of readily mixed native RC sample dissolved in Tris-HCl using 0.1% v/v LDAO is spun down in a 500 μl Amicon Ultra Centrifugal concentrator to filter the detergent. A solution of 1 ml potassium phosphate buffer pH 7, 1 ml of 1% DDM, and 8 ml of DI water (0.1% v/v DDM-phosphate buffer) is added up to the original volume and the sample is centrifuged. The procedure is repeated two more times to ensure that the old detergent and Tris buffer are washed out. Ultra Violet-Visible light spectroscopy is performed to determine the concentration of the reaction center. The concentrations for the RCs in DDM and β-OG are calculated to be 0.48 mM and 0.52 mM respectively.

During electrochemical cycling of the RC/buffer/detergent solutions a quasi-reversible redox peak is detected when a clean gold electrode is exposed to 20 μM RC with different detergents in the dark (Figure 4-46). The experiments, in the potential working range of the bio-photovoltaic device, for the RCs with different detergents show a broad redox couple. Even though the same concentration of the

RC is used in all tests, the RCs in the DDM and  $\beta$ -OG show slightly larger redox peaks. It should be mentioned that the test results for samples dissolved in DDM and  $\beta$ -OG are reproducible; however, the redox peaks when the RCs are solvated using LDAO are not readily reproducible. The redox couple peak is probably the same peak observed due to the reaction between gold and buffer when the electrode is exposed to pure buffer. However, the potentials are shifted and reversibility of the reaction is, presumably affected due to surface adsorption of the proteins and the detergent. It is observed that the redox couple shifts more to the right when the potential is increased toward the positive limits.

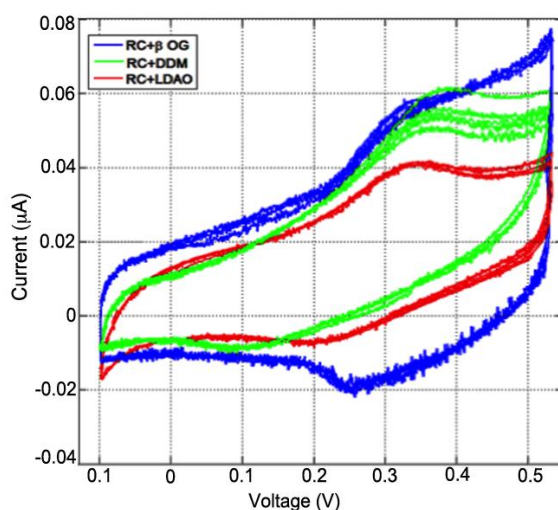


**Figure 4-46: CVs of 20  $\mu$ M Rhodospirillum rubrum RCs on bare gold electrode in potassium phosphate buffer (100 mM, pH 7) with 0.1% v/v red: LDAO, green: DDM, blue:  $\beta$ -OG.**

Full scan CVs from -0.8 V to 1.2 V vs. Ag/AgCl for 20  $\mu$ M RCs containing different detergents in phosphate buffer in the dark are shown in Figure 4-47. The largest peaks corresponding to gold redox behaviour are obtained for RC in phosphate buffer with  $\beta$ -OG. In addition, the experiments using RC in phosphate buffer with DDM and  $\beta$ -OG show a hardly observable, shallow, and broad reduction peak at around -0.6 V vs. Ag/AgCl. No reversibility is found for such peak.

A large background current is observed in the negative voltage limits when the gold is exposed to RC with LDAO. Thus, the effect of the protein and detergent combination on the surface of the electrode prevents us from observing the reduction peak, which should be in the same region. This chemically irreversible reduction peak at around -0.5 is also found in quinone CV tests (see Figure 4-26, page 44). This suggests that the irreversible peak is associated with the quinone that can be released upon illumination.

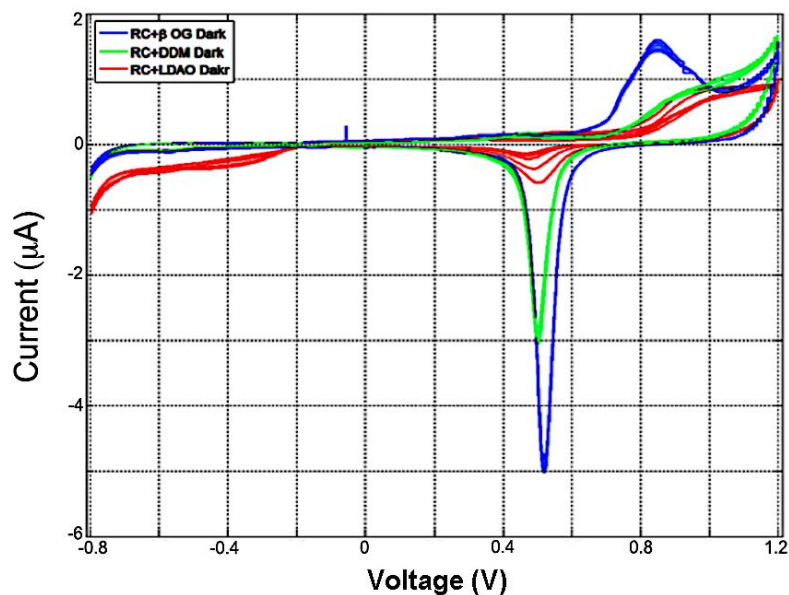


**Figure 4-47: Full scan CVs of 20  $\mu\text{M}$  Rhodobacter sphaeroides RCs on bare gold electrode in potassium phosphate buffer (100 mM, pH 7) with 0.1% v/v red: LDAO, green: DDM, blue:  $\beta$ -OG. The final sweep for each sample is recorded 1 hour after the last scan and its graph is superimposed on the plots.**

Similar cyclic voltammetry tests are recorded for 20  $\mu\text{M}$  RC in 100 mM phosphate buffer at pH 7 with LDAO, DDM and  $\beta$ -OG exposed to light. The results are shown in Figure 4-48 and Figure 4-49.

As can be seen the oxidation peak for the redox couple is shifted and the reduction peak is further shifted to the left, indicating that the reversibility of the reaction is affected by the change in the surface conditions. Moreover, the peak currents are considerably smaller than the peaks recorded while in dark.

Reduced gold redox peaks are also obtained during the illumination as illustrated in Figure 4-49. Illumination of the cell containing the native RCs, results in 30% decrease in the oxidation current at 0.85 V vs. Ag/AgCl at 5 mV/s in the first three cycles. However, the irreversible peak in the negative voltage limits is slightly more visible when the cell is illuminated.

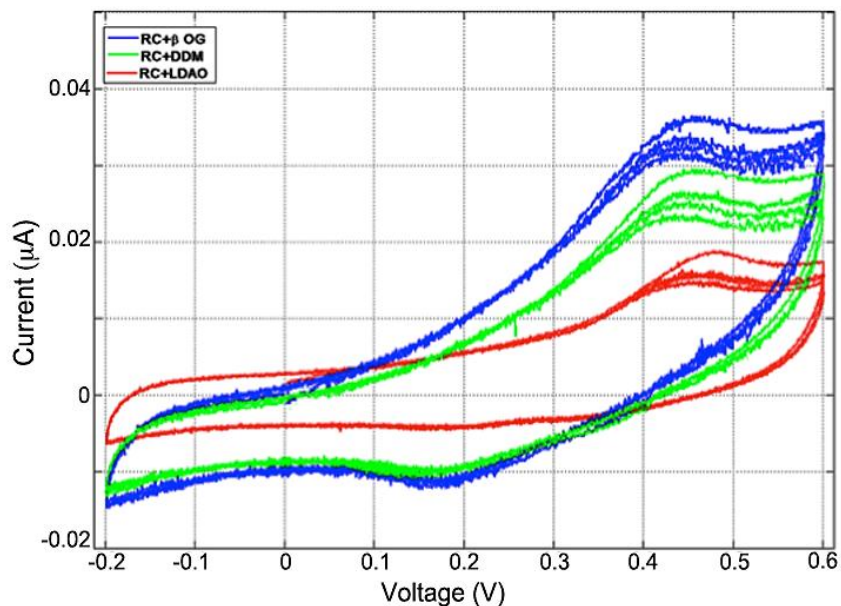


Figure 4-48: CVs of 20  $\mu\text{M}$  illuminated *Rhodobacter sphaeroides* RCs on bare gold electrode in potassium phosphate buffer (100 mM, pH 7) with 0.1% v/v red: LDAO, green: DDM, blue:  $\beta$ -OG.

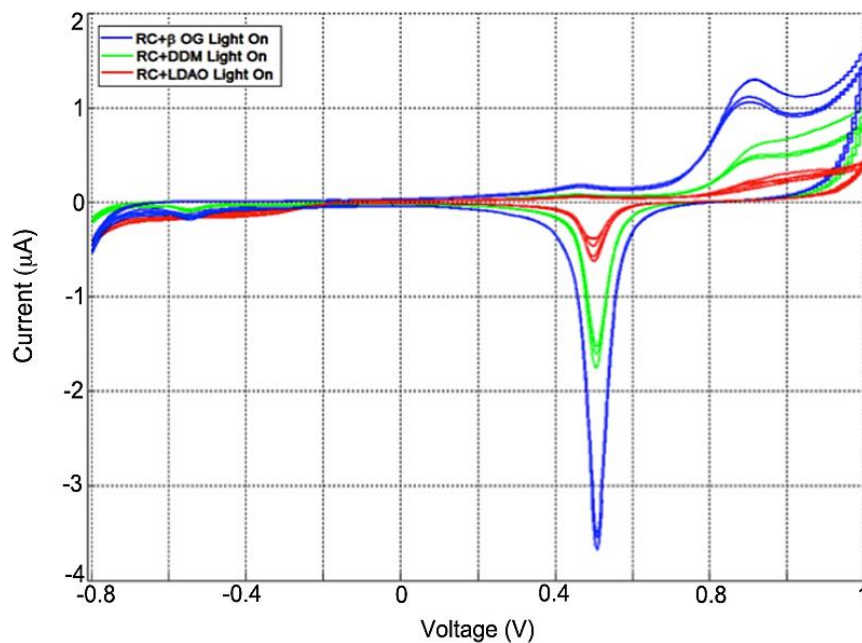
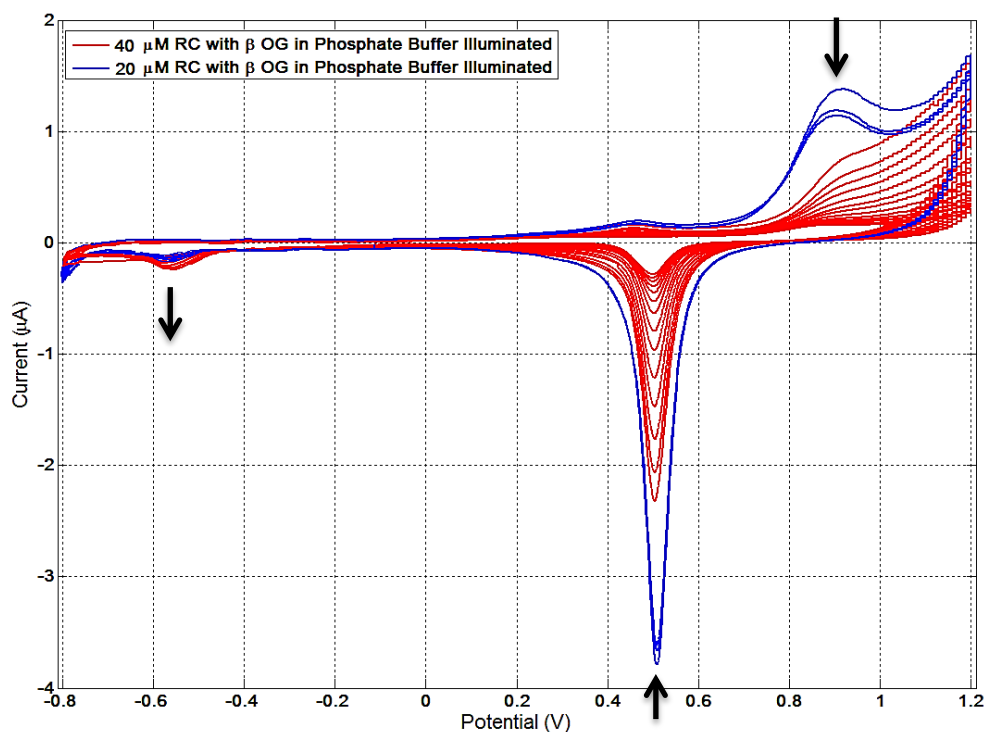


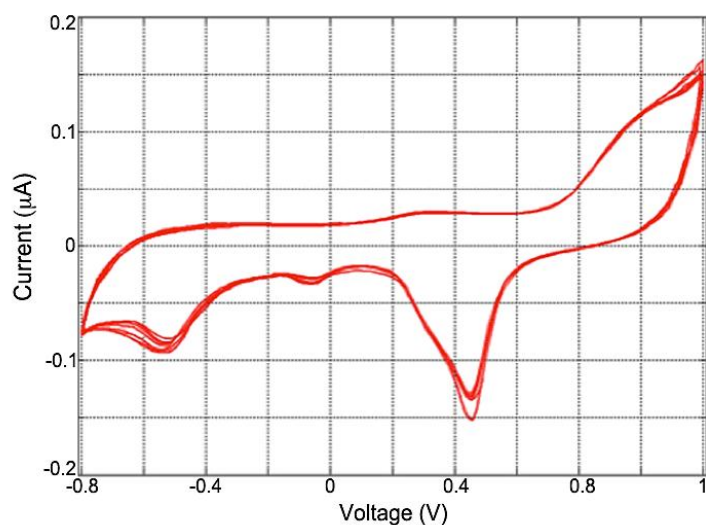
Figure 4-49: Full scan CVs of 20  $\mu\text{M}$  illuminated *Rhodobacter sphaeroides* RCs on bare gold electrode in potassium phosphate buffer (100 mM, pH 7) with 0.1% v/v red: LDAO, green: DDM, blue:  $\beta$ -OG.

To observe the influence of the visible light, several scans are recorded in the dark and light for 40  $\mu\text{M}$  RCs in Phosphate buffer with  $\beta$ -OG. It is observed that multiple scans in the light decreases the peak currents more drastically. The maximum current reduction from the first measured oxidation peak is about 20% in dark. The peak is not recovered nor is it decreased after 45 minutes. However, during the illumination, the peak currents are observed to reduce during each cycle. Figure 4-50 is a demonstration of how the gold redox couple is reduced due to illumination. Also as can be seen the irreversible peak belonging to quinone is increased visibly after each cycle as the concentration of RC is increased.



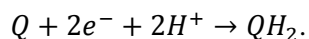
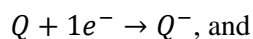
**Figure 4-50:** Cyclic voltammograms of blue: 20  $\mu\text{M}$ , red: 40  $\mu\text{M}$  RC with  $\beta$ -OG in potassium phosphate buffer (100 mM, pH7) when illuminated at 5 mV/s.

Figure 4-51 is a full scan (-0.8 to 1 V vs. Ag/AgCl) CV for illuminated 40  $\mu\text{M}$  RC with OG in phosphate buffer after the electrode has been exposed to the solution for 30 minutes. A reduction peak at -0.09 V vs. Ag/AgCl is found. This peak is probably due to the quinone reduction, since this peak is increased in size during illumination. This peak is not easily visible in Figure 4-50 due to large gold redox peaks that are gradually decreasing.



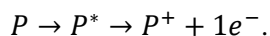
**Figure 4-51: Cyclic voltammogram of 40  $\mu\text{M}$  RC with  $\beta\text{-OG}$  in potassium phosphate buffer (100 mM, pH7) when illuminated at 5 mV/s.**

The two possible reactions for quinone are [36], [38]:



It is suspected that the observed peak may be associated with the second reaction since hydroquinone is released by the RCs when illuminated.

The oxidation peak at +0.85 V vs. Ag/ AgCl is shifted by 50 mV to right after shining light onto the cell. It is suspected that this peak consists of two overlapped peaks due to gold oxidation and RC light response. As shown in Figure 4-45, at around 1 V vs. NHE,  $P^+$  is generated by the photo-excited primary acceptor  $P^*$ . The possible reaction for RC is [43]:



It is possible that the positively charged  $p$  side of the RC reacts with the surface of the gold electrode or reacts with an unidentified reducing agent present in the system which terminates the reversibility of the process.

The approximate active surface areas of each electrode are evaluated from the integration of the gold oxidation peak and comparison with peak area when in buffer alone. The results are presented in Table 4-5.

**Table 4-5: Gold active surface area after RC adsorption in dark and light from a 20  $\mu\text{M}$  RC containing solution.**

RC + surfactant	LDAO	DDM	$\beta$ -OG
% active area-dark (After 1 hour)	25	35	70
% active area-illuminated (After 1 huor)	5	20	40

#### 4.9.2 Adsorption of Rhodobacter sphaeroides RC

Even though the sweeps in the dark for the RC solution show a high oxidation peak compared to the peaks that are measured in the light, the peaks recorded in the dark are much smaller than the pure buffer. Thus, ACV tests are performed to determine the adsorption of the RCs on the bare gold electrode. The ACVs are recorded for 3 different concentrations in both dark and light after an hour for three RC samples dissolved in LDAO, DDM, and  $\beta$ -OG shown in Figure 4-52, Figure 4-53, and Figure 4-54 respectively. The amounts, resultant average capacitances obtained from AC voltammetry tests, and  $\Delta\%$  capacitance are summarized in Table 4-6.

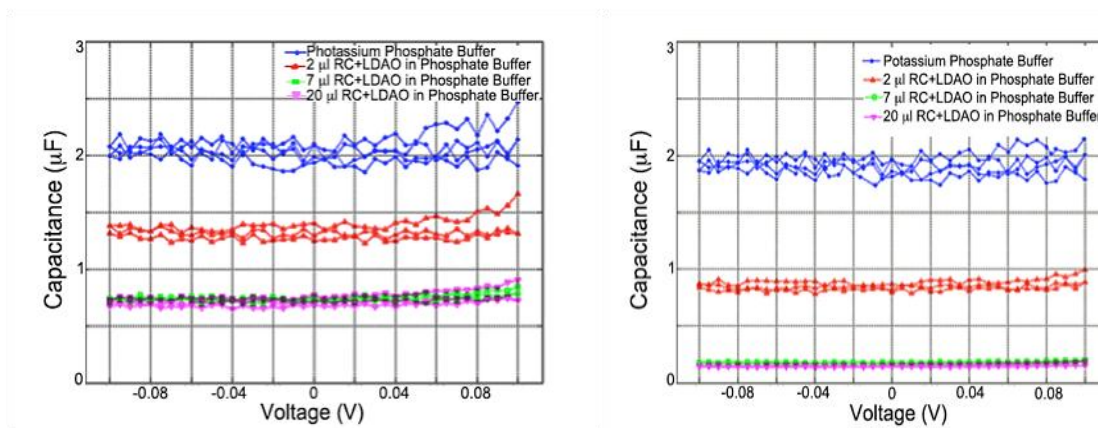


**Figure 4-52: Left: in dark; right: during illumination - Capacitance profile measurements for bare gold electrode exposed to blue: 2.5 ml 100 mM potassium phosphate buffer; red: 2  $\mu\text{l}$ ; green: 7  $\mu\text{l}$ ; magenta: 20  $\mu\text{l}$  RC with 0.1% v/v LDAO detergent diluted in 2.5 ml phosphate buffer. The ACVs are recorded at scan rate: 5 mV/s, amplitude: 5 mV, and frequency: 25 Hz.**

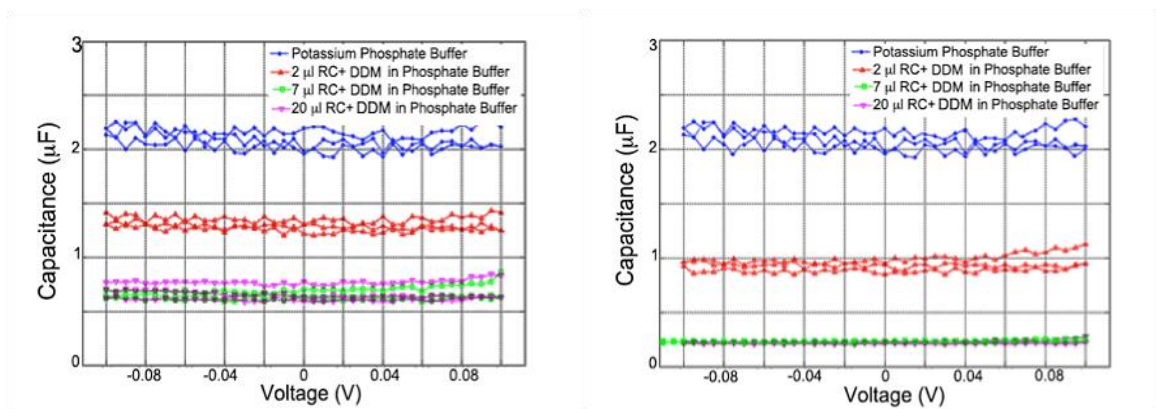


**Figure 4-53: Left: In dark; right: during illumination - Capacitance profile measurements for bare gold electrode exposed to blue: 2.5 ml 100 mM potassium phosphate buffer; red: 2  $\mu$ l; green: 7  $\mu$ l; magenta: 20  $\mu$ l RC in 0.1% v/v DDM detergent diluted in 2.5 ml phosphate buffer. The ACVs are recorded at scan rate: 5 mV/s, amplitude: 5 mV, and frequency: 25 Hz.**

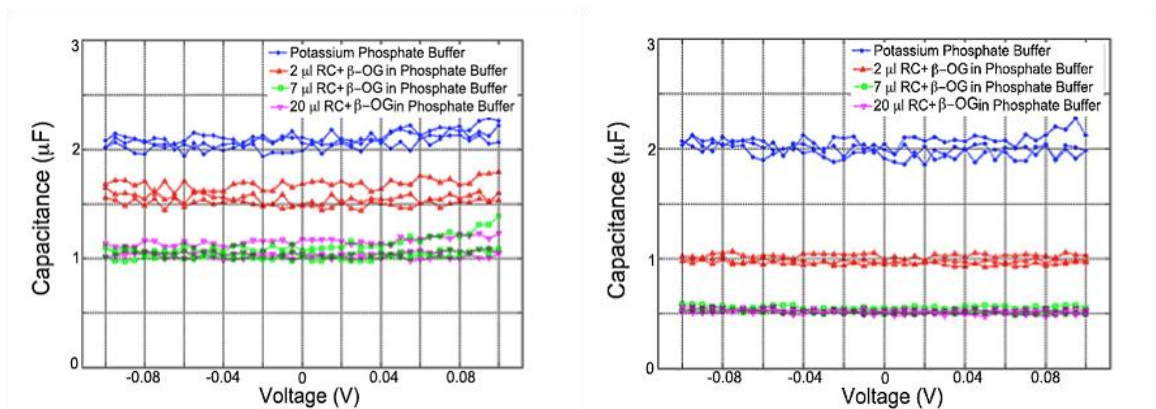


**Figure 4-54: Left: In dark-right: during illumination - Capacitance profile measurements for bare gold electrode exposed to blue: 2.5 ml 100 mM potassium phosphate buffer; red: 2  $\mu$ l; green: 7  $\mu$ l; magenta: 20  $\mu$ l RC in 0.1% v/v  $\beta$ -OG detergent diluted in 2.5 ml phosphate buffer. The ACVs are recorded at scan rate: 5 mV/s, amplitude: 5 mV, and frequency: 25 Hz.**

It is evident that upon exposure to the solution containing 2  $\mu$ l RC, the double layer capacitance reduces and it continues to decrease as the concentration of the protein is increased until the surface is saturated at 7  $\mu$ l of RC. The double layer capacitance in the dark declines more significantly when the gold electrode is exposed to the solution of RC compared to when the same surface area is exposed to cytochrome c or quinone. This may indicate that a thicker protein layer is formed on the surface of the electrode. It seems that upon protein adsorption on the surface of the gold, changes in thickness of the double layer dominate the changes in dielectric constant [39]. Therefore, the capacitance is reduced after the proteins replace the water molecules in the double layer. We conclude that the adsorption of

reaction center onto the high-energy gold surface causes the reduction of gold redox peaks since less gold surface is exposed to the electrolyte.

**Table 4-6: Double layer capacitance ( $\mu\text{F}$ ) and the capacitance changes when bare gold electrode is exposed to phosphate buffer containing RC at various amounts listed. Negative sign is an indication of capacitance reduction.**

Sample	RC with LDAO			RC with DDM			RC with $\beta$ -OG		
	2	7	20	2	7	20	2	7	20
Amount ( $\mu\text{l}$ )									
Capacitance in Light off	1.3	0.7	0.7	1.3	0.7	0.7	1.6	1.1	1.1
$\Delta\%$ capacitance Light off	-35	-65	-65	-35	-65	-65	-22	-45	-45
Capacitance Light on	0.8	0.2	0.2	0.9	0.2	0.2	1	0.5	0.5
$\Delta\%$ capacitance Light on	-60	-91	-93	-55	-90	-90	-50	-75	-75

Figure 4-52 - right, Figure 4-53 - right, and Figure 4-54 - right show double layer capacitance plots obtained using a gold surface exposed to 3 RC samples during illumination. In all cases it is observed that during illumination, the capacitance is further reduced. Moreover, according to the CVs (refer to previous section) recorded in the light, the redox peaks for the gold decline significantly and continue to drop in each cycle. It is detected that when illumination is removed, the double layer capacitance stays constant. This permanent reduction during the illumination can be due to photo-excitation of P. It seems that when illuminated, RCs start to release quinone into the system. It can be said that the nature, the size of the quinone-less RCs, and their conformational changes may be different from the native RCs. Due to the possible changes in the shape of the protein, the double layer thickness can be changed and thus the capacitance is changed. Also it is possible that photo-excited RCs could pump electrons into the gold while gold is donating electrons to reduce the photo oxidized reaction centers. Therefore, the oxidative current could be canceled out due to the photocurrent. However, potentiostatic tests showed that no significant change in the net current was observed when different potentials were applied to the electrode in the dark and during irradiation. The net current observed is the difference between the cathodic and anodic currents, and is thus very dependent on the average orientation of the RCs attached to the surface. Observing no change in the current may be an indication of native RC adsorption with no preferred orientation on the gold surface.

The cyclic voltammetry and AC voltammetry tests on RCs in the presence of different surfactants on gold shows that this protein adsorbs on the bare gold electrode irreversibly. Illuminating the cells containing reaction centers showed significant reduction of gold redox peaks and the double layer capacitance. Gold surface coverage during illumination especially when the cell contains LDAO is well above 90%. In addition, fairly high surface coverage is observed during illumination for high concentration the reaction centers in the presence of  $\beta$ -OG. Due to the non-specific nature of the RC adsorption, it is suggested that surface modification needs to be considered to prevent suppressing the electrode activities.

## 4.10 Cysteine-less Reaction Centers

Cysteine is an amino acid found in several proteins. Cysteine has a non-polar thiol group side chain which makes it a hydrophobic amino acid. One of the most common roles of cysteine is to attach the protein to a gold surface by employing multiple functional groups [49]. The Rhodobacter sphaeroides RC has 5 surface accessible cysteines. Two accessible surface cysteine residues (C156 and C234) of Rhodobacter sphaeroides RC protein which are located on the H subunit can bind to the gold surface covalently. However, the other cysteine residues, especially one that causes transmembrane helices of the RC to attach to an external surface, can result in non-specific adsorption of the RCs on the electrode surface [6], [29].

The objective of our tests in this section is to recognize whether the existence of cysteine is essential for binding and the electron transfer of the reaction centers and the surface of the gold electrode.

### 4.10.1 Electrochemistry of Cysteineless Rhodobacter sphaeroides RC

Cyclic voltammetry on a bare gold electrode placed in 20  $\mu$ M Cysteineless RCs dissolved in 0.1% LDAO solutions is performed in a three electrode cell at room temperature in the dark, while illuminated by the white light beam introduced in previous section. All the tests are done at 5 mV/s scan rate and in 100 mM Phosphate buffer at pH 7. The sample CVs for the Cysteineless RC tests are shown in Figure 4-55 and Figure 4-56.

As is evident, the currents in these tests are significantly larger than the currents measured for the native RCs dissolved in LDAO (refer to Figure 4-46 for native RC CV in the dark and Figure 4-48 for the illuminated native RC CV). From the capacitive plots, measured between -0.1 to 0.1 V vs. Ag/AgCl shown in blue in the mentioned figure, it can be seen that the generated current for the

illuminated RC is almost 50% less than the current for the same setup in dark, and thus the double layer capacitance is reduced considerably when the cell is exposed to light.

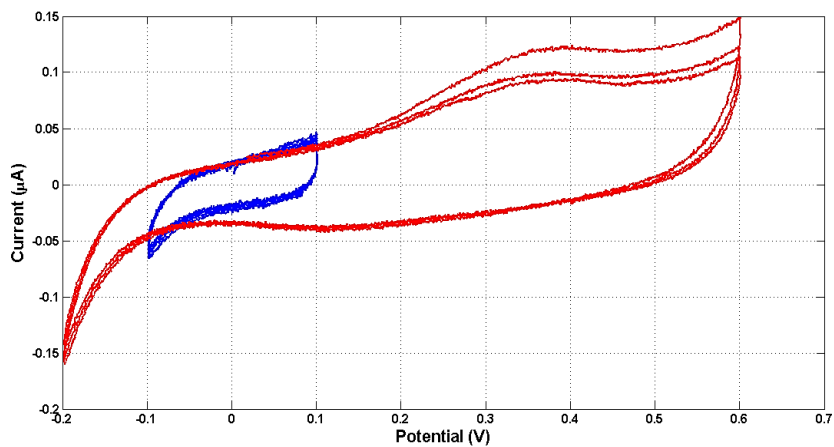


**Figure 4-55:** Two cyclic voltammograms (blue – small voltage range to probe the double layer, red – large voltage range) of 40  $\mu\text{M}$  cystineless *Rhodobacter sphaeroides* RCs on a bare gold electrode in potassium phosphate buffer (100 mM, pH 7) with 0.1% v/v LDAO in dark.

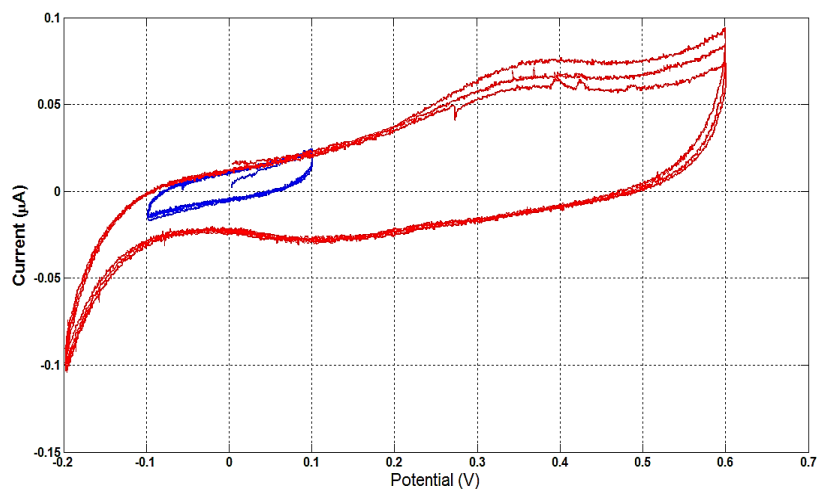


**Figure 4-56:** Two cyclic voltammograms of 40  $\mu\text{M}$  cysteineless *Rhodobacter sphaeroides* RCs on bare gold electrode under illumination in potassium phosphate buffer (100 mM, pH 7) with 0.1% v/v LDAO. The blue curve covers the capacitive region of the response.

The superimposed CVs for 40  $\mu\text{M}$  cysteineless reaction centers in 100 mM phosphate buffer when they are in the dark and illuminated are shown in Figure 4-57 and Figure 4-58. It is worth mentioning that for the tests shown in Figure 4-58 the same solution is used for both experiments, whereas, in Figure 4-57, the solution is changed and the electrodes and the container are cleaned before the

illumination. Comparing with the CVs obtained from gold electrode exposure to the pure phosphate buffer, both figures clearly demonstrate that the cysteineless RCs adsorb on the surface of electrode. It is also evident that the illumination causes more surface coverage - presumably due to the adsorption of the proteins. A very broad oxidation peak can be seen at -0.35 V vs. Ag/AgCl in the CVs which is significantly observable when the voltage is swept toward more negative values in the dark. This peak and the gold redox couple visibly get smaller when the cell is illuminated during the full scans. It is evident that the peak currents gradually decrease during each sweep when the cell is illuminated.

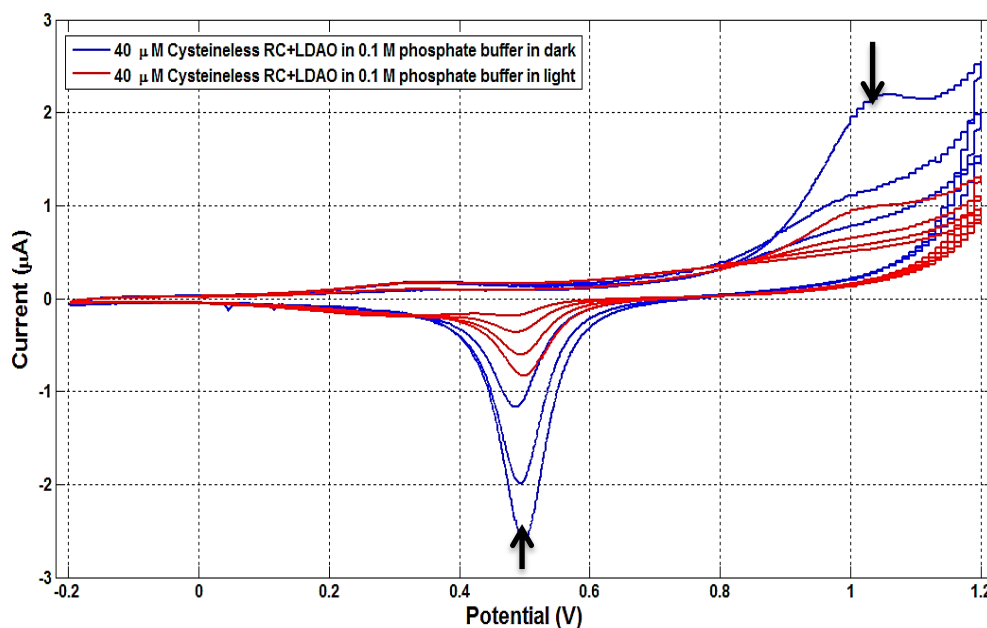


**Figure 4-57:** Cyclic voltammograms for 40 μM cysteineless RC in 0.1 M potassium phosphate buffer at pH 7 on gold electrode before (blue) and after (red) exposure to light. Scan rate: 5 mV/s.

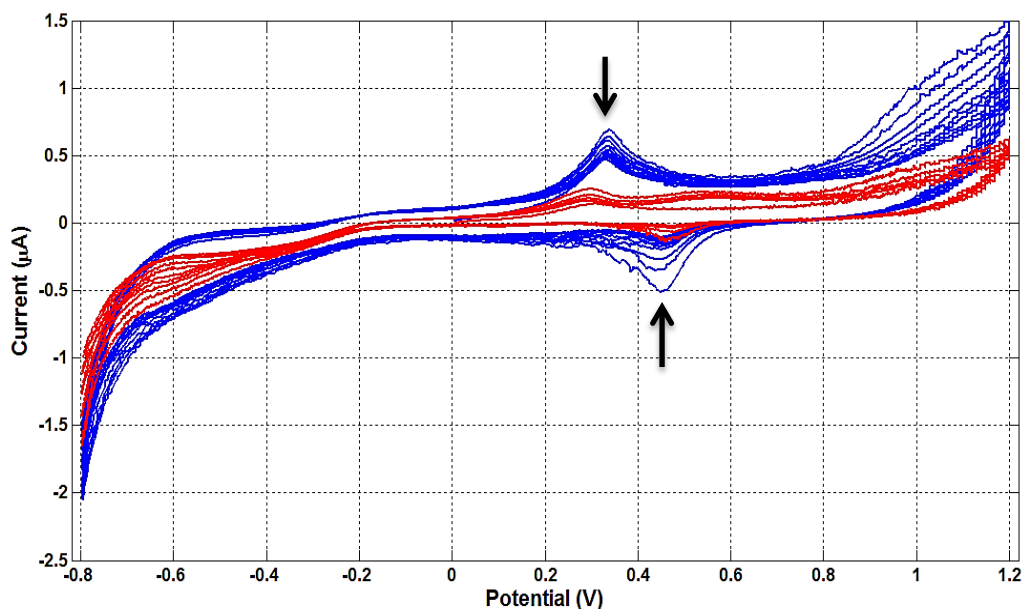


**Figure 4-58: Full cyclic voltammograms for 40  $\mu\text{M}$  cysteineless RC in 0.1 M potassium phosphate buffer at pH 7 on gold electrode before (blue) and after (red) exposure to light. Scan rate: 5mV/s.**

ACV tests are conducted and explained in the next subsection on cysteineless RCs. If the double layer capacitance changes where no faradaic reaction is taking place, it can be concluded that the coverage of the gold surface due to protein adsorption is resulting in reduced active gold site exposure to the solution and thus is resulting in less electron transfer and reduced peaks.

#### 4.10.2 Adsorption of Cysteineless Rhodobacter Sphaeroides RC

Since the CVs recorded for the gold peak redox couple when exposed to the solution containing cysteineless RC show reduced currents in comparison to the gold peaks when the electrode is exposed to the pure buffer, ACV tests are performed to detect the double layer capacitance changes for this group of reaction centers.

The ACVs are performed for 3 different concentrations in dark and light for the only available sample of modified reaction center dissolved in LDAO (See Figure 4-59 : in dark and Figure 4-60 : exposed to light). The amount of the dissolved proteins, measured double layer capacitance, and  $\Delta\%$  capacitance are indicated in Table 4-7.

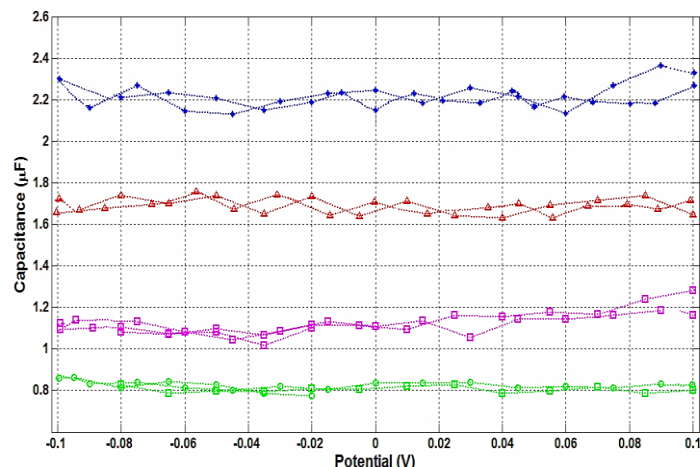


**Figure 4-59: In dark - Capacitance profile measurements for bare gold electrode exposed to: blue: 2.5 ml 100 mM potassium phosphate buffer; red: 2  $\mu$ l 3- magenta: 7  $\mu$ l, green: 20  $\mu$ l cysteineless RC with 0.1% v/v LDAO detergent diluted in 2.5 ml.**

As can be observed from the plot, the double layer capacitance reduces visibly as the cysteineless RC is added to the buffer solution. The capacitance further drops down by increasing the protein concentration which is an indication of protein adsorption on the surface of the electrode. However, unlike the case of native RCs in which the electrode surface became saturated after adding 7  $\mu$ l of protein in the dark, the electrode surface becomes saturated when 20  $\mu$ l of the modified RC is dissolved in the phosphate buffer when in the dark. Dissolving more reaction center in the solution does not affect the capacitance after this point.

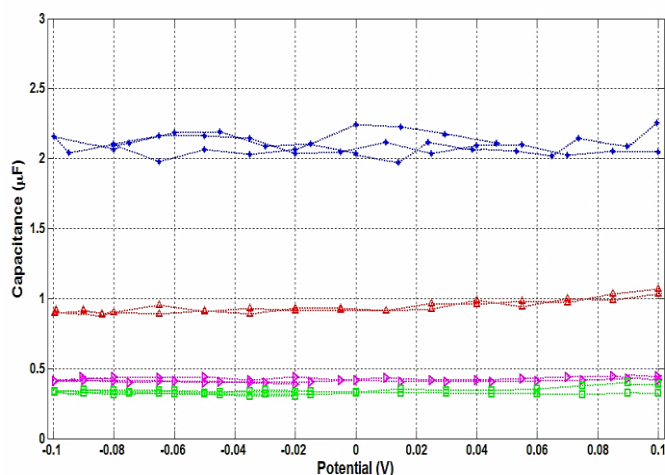


**Figure 4-60: During illumination - Capacitance profile measurements for bare gold electrode exposed to 1- Blue: 2.5 ml 100 mM Potassium Phosphate buffer 2- Red: 2  $\mu$ l 3- magenta: 7  $\mu$ l 4- green: 20  $\mu$ l cysteineless RC with 0.1% v/v LDAO detergent diluted.**

The ACV tests when the cysteineless RCs are illuminated show further capacitance reduction. In addition, similar to the case for native RCs, the CVs presented in previous subsection for cysteineless RCs show a significant decline in the gold redox peaks during each sweep until the entire surface is blocked.

**Table 4-7: Double layer capacitance ( $\mu\text{F}$ ) and the capacitance changes when bare gold is exposed to phosphate buffer containing cysteineless RC at various amounts listed. Negative sign is an indication of capacitance reduction.**

Sample	Cysteineless RC with 0.1% v/v LDAO		
	2	7	20
Amount of RC ( $\mu\text{l}$ )	2	7	20
Capacitance Light off ( $\mu\text{F}$ )	1.7	1.15	0.84
$\Delta\%$ capacitance Light off	-22	-48	-62
Capacitance Light on ( $\mu\text{F}$ )	0.95	0.45	0.35
$\Delta\%$ capacitance Light on	-57	-79	-84

The double layer capacitance and  $\Delta\%$  capacitance recorded for the cysteineless RCs is smaller than the data obtained for the native RC. Thus, it can be concluded that cysteine is not essential in attaching the reaction centers to the gold surface. The experiments performed with the cysteineless reaction centers show that cysteine is not the only possible amino acid that can provide a linkage between the protein and the electrode surface. According to the results, the cysteineless proteins still adsorb on the surface of the gold electrode irreversibly, hence, various forces other than the hydrophobic cysteine have a significant effect on the attachment between the protein and the metal surface.

Finally, according to Figure 4-58, the absence of the gold redox peaks indicates that the surface coverage due to proteins on the gold surface is close to 100%. The double layer then can be modeled by a parallel plate capacitor of an average thickness of  $d$ . If the dielectric constant of the protein layer is estimated to be a minimum of 3 (as is typical in organic materials) and a maximum of 18 (dielectric constant of water in a double layer – probably an exaggeration since each RC contains 200 water molecules [50]), and given the capacitance - measured to be around  $0.4 \mu\text{F}$  from the results presented in Figure 4-60 over a gold surface area of  $9.95 \text{ mm}^2$ , the thickness of the layer is then calculated to be between:

$$C = \epsilon_0 \epsilon_r \frac{A}{d} \rightarrow d = \frac{\epsilon_0 \epsilon_r A}{C} \rightarrow d_{min} = 0.66 \text{ nm} \text{ and } d_{max} = 4 \text{ nm}.$$

Based on this model and considering the original size of the reaction centers (4x7x11 nm), it is suggested that reaction centers spread themselves on the gold electrode surface, which is an effect commonly observed for a large number of proteins when they adsorb on the gold surface [51].

## 5 CONCLUSION

Many factors influence the efficiency of protein based solar cells, two of which are investigated in this work: Unintended Parasitic Reactions and adsorption at the electrode surface. In particular, adsorption of reaction centres, mediators, detergents are investigated, and all are for a gold electrode.

The importance of the system cleanliness and purity of the materials (in order to prevent electron back reactions via the electrode surface, and maximizing the electrode active area) has been neglected in the majority of our previous measurements of protein based solar cells. The results of the present work show that the removal of contamination (properly cleaning the electrodes), and deoxygenating the system become important in conditions when extremely low photo-currents (typical of protein based solar cells), are to be measured. Consequently, a new cell setup and a new electrode are proposed and used to perform the tests during this project. It is shown that for gold electrodes deoxygenation of the electrochemical cell and flaming of the electrodes are effective at reducing parasitic reactions and creating a clean electrode surface.

A methodology is presented for the analysis of electrochemical interactions and adsorption of buffer, mediators, surfactants, and the reaction centers with the gold surface (i.e. all the components of an electrochemical protein based- solar cell). Surface coverage is investigated using changes in double layer capacitance determined by cyclic voltammetry or AC voltammetry, as well as by determining the drop in gold oxidation by voltammetry. These methods are generalizable, and we suggest they should be employed in extended tests involving further electrode materials.

The electrochemistry of the gold electrode exposed to four potential buffers including Tris-HCl, MOPS, HEPES, and Potassium Phosphate is examined. It is observed that the first three buffers adsorb on the surface of the electrode and prevent us from observing the oxidation and reduction of gold at the expected applied potentials during cyclic voltammetry tests. As a result of using organic buffers, gold reactivity is suppressed, suggesting that these buffers may also prevent interactions between the mediators and the electrode.

Phosphate is observed to be adsorbed on the surface of the gold. However, the AC voltammetry shows that the double layer capacitance changes due to the exposure of gold to phosphate buffer are small, especially when compared to the changes observed after the exposure of other buffers.

Phosphate buffer is preferred over MOPS, Tris-HCl and HEPES, as it allows wanted reactions at the electrode.

LDAO, DDM, and  $\beta$ -OG surfactants are also tested in the presence of the gold electrode. Having a hydrophobic polar chain, LDAO showed high surface adsorption and high surface coverage. DDM is also observed to cover the electrode surface.  $\beta$ -OG shows minimal adsorption on the surface in comparison with the other two detergents, and is thus recommended for use in RC containing solar cells when gold electrodes are present.

The electrochemistry of gold in the presence of reduced cytochrome c is investigated. The results suggest that the electrochemical response of the reduced cytochrome c depends on the buffer concentration. In addition, the CVs that are obtained immediately after electrode immersion in the phosphate buffer solution containing reduced cytochrome c show no or sometimes broad and shoulder-like peaks associated with cytochrome c. After a few hours electrochemical activity due to cytochrome c oxidation and reduction becomes apparent.

As well as dependency on the ionic strength of the solution, reversible electrochemical behaviour of cytochrome seems to depend on the mechanical conditions of the cell (shaking the cell and stirring the solution) and probably the disaggregation of proteins. A gradual decline in the gold redox peak is observed in the presence of reduced cytochrome c. This peak reduction is associated with slow adsorption of the proteins on the gold surface.

The surface adsorption is confirmed by performing ACV and detecting the double layer drop which is an indication of increased surface coverage. The effect of the applied voltage on cytochrome c adsorption is examined. By increasing the voltage toward positive values faster adsorption is observed. Both cytochrome c and reduced cytochrome c are positively charged proteins. Therefore, it is hypothesized that the proteins orient and adsorb on the surface in an unexpected manner probably due to their conformational changes.

The electrochemistry and adsorption of quinone on the bare gold electrode is studied. Again, a gradual decline in the gold and quinone redox peaks, along with the drop in the double layer capacitance suggest quinone adsorption on the gold surface.

CV and ACV results for gold electrodes exposed to solutions containing RC and cysteineless RC prepared in phosphate buffer and in the dark show a decrease in double layer capacitance due to the presence of RC. The capacitance reduction is attributed to the formation of a protein layer on the

surface of the gold. Of the three samples of wild-type reaction centers (in either LDAO, DDM, or  $\beta$ -OG and phosphate buffer) the greatest capacitance changes are detected when RCs dissolved in LDAO and buffer adsorb at the gold surface. Further capacitance drop is observed when the cells containing the wild-type RCs are illuminated.

In the case of illuminated RC dissolved in LDAO, reactivity of the surface is reduced by approximately 90%. The same effect is observed when a solution containing cysteineless RC is illuminated. Upon illumination, a larger fraction of the gold surface is covered by proteins until surface coverage is essentially complete. Aggressive adsorption of cysteineless RCs is in contrast to the previous suggestion that cysteine is the dominant residue to cause RC adsorption on the surface.

Fairly strong adsorption between the genetically engineered RCs and the gold surface is observed since post-cyclic voltammetry tests on the washed electrode showed no signs of gold redox couple after a day. The accelerated and continuous protein adsorption on the surface upon illumination can be due to an induced conformational change and hence the spreading of the deformed proteins on the surface.

This work shows that there are complex interactions between gold and solvated components of the bio-photovoltaic solar cell. These interactions should be carefully considered in designing and understanding the response of electrochemical solar cells.

The methodology used may be broadly applicable to solar cells and other electrochemical devices. The adsorption of the protein and other components onto the electrode surface, which in turn reduces the accessibility of the surface, suggests that finding a means of minimizing such adsorption is essential to maximizing the performance of the cell. Final results and observations are summarized in Table 5-1.

**Table 5-1: Summary of the obtained results.**

<b>Cell Component</b>		<b>Adsorption</b>	<b>Observation</b>	<b>Capacitance changes compared to Potassium Phosphate buffer's capacitance</b>
<b>Buffers</b>	Tris-HCl HEPES MOPS	Irreversible	Unclear gold redox behaviour	N/A
	<b>Potassium Phosphate</b>	Weak	Clear electrochemical response of gold	Decrease Compared to KClO <sub>4</sub>
<b>Surfactants</b>	LDAO DDM	Irreversible	Unclear gold redox behaviour	Increase
	<b>β-OG</b>	Irreversible	Clear gold electrochemical response	Decrease
<b>Mediator (1)</b>	<b>Quinone</b>	Irreversible	Clear redox peaks of quinone	Decrease
<b>Mediator (2)</b>	<b>Cyt c<sup>2+</sup></b>	Irreversible	Time and ionic strength dependent electrochemical response. Voltage dependent adsorption	Decrease
<b>Reaction Center</b>	<b>Wild type</b>	Irreversible	Light dependent electrochemical and adsorption response	Decrease
	<b>Cysteineless</b>	Irreversible	Light dependent electrochemical and adsorption response/ Greater Adsorption when light on	Decrease/ Slightly higher than wild type RC dissolved in LDAO

## 5.1 Future Work

- A water based buffer is used during the tests in this work. Even though a buffer solution will resist the pH changes, a pH gradient formation near the surface of the gold electrode is possible, particularly away from the point of zero charge. The pH gradient can result in the migration of OH<sup>-</sup> or H<sup>+</sup> groups toward the surface of the electrode. Therefore, the real pH

near the surface of the electrode can be significantly greater than 7. Thus the proteins near the electrode surface can be more negatively charged or be placed at a pH at which they become unstable. Conducting the same experiments in a solution that minimizes or prevents the pH changes close to the electrode surface, will show whether some of the effects observed in the CVs are the impact of the pH gradient or not. However, choosing an adequate transparent solution in which the proteins can be stable and bio-active is a challenge and it might not be feasible.

- Methods such as AFM can be used to evaluate the morphology of the electrode surface before and after the protein adsorption to analyze the adsorbed layer. Valuable information regarding orientation and formation of the adsorbed layers and the number of the monolayers formed on the electrode might be gained using such technique.
- Examining reaction center adsorption under different intensities of illumination is another task that can help understand the reaction center adsorption behaviour. Questions regarding the aggressive adsorption and deformation of reactions centers during illumination may be answered after conducting further tests in several light intensities.
- The functionality of the adsorbed reaction centers should be examined in the absence and the presence of mediators. The adsorbed reaction centers can undergo major conformational changes which will result in having a non-functional blocking layer on the surface of the electrode regardless of the presence or the absence of the mediators. However, the adsorbed reaction centers could still be bioactive if a photocurrent is observed in the presence of mediators. The amount of photocurrent measured in the presence of mediators can provide valuable information about the orientation of the RCs adsorbed on the electrode surface, with the possibility of mediator diffusion and charge transfer through the adsorbed layer.

## 6 REFERENCES:

- [1] U. N. D. Programme, U. N. D. of E. and S. Affairs, and W. E. Council, *World energy assessment: overview : 2004 update*. United Nations Publications, 2004.
- [2] D. Y. Goswami, S. Vijayaraghavan, S. Lu, and G. Tamm, "New and emerging developments in solar energy," *Solar Energy*, vol. 76, no. 1-3, pp. 33-43, January.
- [3] A. A. Solov'ev, E. Y. Katz, V. A. Shuvalov, and Y. E. Erokhin, "Photoelectrochemical effects for chemically modified platinum electrodes with immobilized reaction centers from *Rhodobacter sphaeroides* R-26," *Bioelectrochemistry and Bioenergetics*, vol. 26, no. 1, pp. 29-41, Aug. 1991.
- [4] Personal communication with Ali Mahmoudzadeh, who estimated the fraction of light absorption based on the HOMO-LUMO level difference (as was done by Shockley and Queisser 1960 for silicon and other semiconductors), and given the energy drop needed to separate charge. Reaction centres from a number of species were used to find the best candidates, and it was assumed that electrons could be pulled off at any stage along the electron pathway (other than in the initial excited state).
- [5] O. Kievit and G. W. Brudvig, "Direct electrochemistry of photosystem I," *Journal of Electroanalytical Chemistry*, vol. 497, no. 1-2, pp. 139-149, Feb. 2001.
- [6] H. A. Heering, F. G. M. Wiertz, C. Dekker, and S. de Vries, "Direct Immobilization of Native Yeast Iso-1 Cytochrome c on Bare Gold: Fast Electron Relay to Redox Enzymes and Zeptomole Protein-Film Voltammetry," *J. Am. Chem. Soc.*, vol. 126, no. 35, pp. 11103-11112, 2004.
- [7] K. Matsumoto, K. Nomura, Y. Tohnai, S. Fujioka, M. Wada, and T. Erabi, "Immobilization of Photosynthetic Reaction Center Complexes onto a Hydroquinonethiol-Modified Gold Electrode," *Bulletin of the Chemical Society of Japan*, vol. 72, no. 10, pp. 2169-2175, 1999.
- [8] S. A. Trammell, L. Wang, J. M. Zullo, R. Shashidhar, and N. Lebedev, "Orientated binding of photosynthetic reaction centers on gold using Ni-NTA self-assembled monolayers," *Biosensors and Bioelectronics*, vol. 19, no. 12, pp. 1649-1655, Jul. 2004.
- [9] John Albery, W., and Andrew W. Foulds. "Photogalvanic Cells." *Journal of Photochemistry* 10, no. 1 (1979): 41-57.
- [10] A. Takshi, J. D. Madden, and J. T. Beatty, "Diffusion model for charge transfer from a photosynthetic reaction center to an electrode in a photovoltaic device," *Electrochimica Acta*, vol. 54, no. 14, pp. 3806-3811, May 2009.
- [11] A. Takshi, J. D. W. Madden, A. Mahmoudzadeh, R. Saer, and J. T. Beatty, "A Photovoltaic Device Using an Electrolyte Containing Photosynthetic Reaction Centers," *Energies*, vol. 3, no. 11, pp. 1721-1727, Oct. 2010.
- [12] N. Lebedev et al., "Bio-inspired photo-electronic material based on photosynthetic proteins," *Proceedings of SPIE*, vol. 7403, no. 1, pp. 740304-740304-12, Aug. 2009.

- [13] M. MALMSTEN, "Formation of adsorbed protein layers," *Journal of colloid and interface science*, vol. 207, no. 2, pp. 186-199.
- [14] Nakanishi, T. Sakiyama, and K. Imamura, "On the adsorption of proteins on solid surfaces, a common but very complicated phenomenon.," *Journal of Bioscience and Bioengineering*, vol. 91, no. 3, pp. 233-44, 2001.
- [15] Norde, F. Macritchie, G. Nowicka, and J. Lyklema, "Protein adsorption at solid liquid interfaces: Reversibility and conformation aspects," *Journal of Colloid and Interface Science*, vol. 112, no. 2, pp. 447-456, 1986.
- [16] G. Jeffrey J, "The interaction of proteins with solid surfaces," *Current Opinion in Structural Biology*, vol. 14, no. 1, pp. 110-115, Feb. 2004.
- [17] J.-Y. Yoon, H.-Y. Park, J.-H. Kim, and W.-S. Kim, "Adsorption of BSA on Highly Carboxylated Microspheres—Quantitative Effects of Surface Functional Groups and Interaction Forces," *Journal of Colloid and Interface Science*, vol. 177, no. 2, pp. 613-620, Feb. 1996.
- [18] F. Höök, M. Rodahl, B. Kasemo, and P. Brzezinski, "Structural changes in hemoglobin during adsorption to solid surfaces: Effects of pH, ionic strength, and ligand binding," *Proceedings of the National Academy of Sciences*, vol. 95, no. 21, pp. 12271 -12276, Oct. 1998.
- [19] M. M. Stevens et al., "pH-Dependent Behavior of Surface-immobilized Artificial Leucine Zipper Proteins," *Langmuir*, vol. 20, no. 18, pp. 7747-7752, 2004.
- [20] A. J. Bard and L. R. Faulkner, *Electrochemical methods: fundamentals and applications*. Wiley, 1980.
- [21] J. O'M. Bockris, M. A. V. Devanathan, and K. Muller, "On the Structure of Charged Interfaces," *Royal Society of London Proceedings Series A*, vol. 274, pp. 55-79, Jun. 1963.
- [22] B. . Young, W. . Pitt, and S. . Cooper, "Protein adsorption on polymeric biomaterials: II. Adsorption kinetics," *Journal of Colloid and Interface Science*, vol. 125, no. 1, pp. 246-260, Sep. 1988.
- [23] Hajra and D. K. Chattoraj, "Protein Adsorption at Solid-Liquid Interfaces .2. Adsorption from Binary Protein Mixture," *Indian Journal of Biochemistry Biophysics*, vol. 28, pp. 184-192, 1991.
- [24] P. W. Atkins, *Physical Chemistry: Science of Biology*, 6th ed. W.H. Freeman & Company, 1997.
- [25] P. R. V. Tassel, P. Viot, and G. Tarjus, "A kinetic model of partially reversible protein adsorption," *Journal of Chemical Physics*, vol. 106, no. 2, pp. 761-770, 1997.
- [26] Z. Adamczyk and P. Weroński, "Random sequential adsorption on partially covered surfaces," *The Journal of Chemical Physics*, vol. 108, no. 23, pp. 9851-9858, Jun. 1998.
- [27] J. L. Lebowitz, E. Helfand, and E. Praestgaard, "Scaled Particle Theory of Fluid Mixtures," *The Journal of Chemical Physics*, vol. 43, no. 3, pp. 774-779, Aug. 1965.

- [28] L. Guemouri, J. Ogier, and J. J. Ramsden, "Optical properties of protein monolayers during assembly," *The Journal of Chemical Physics*, vol. 109, no. 8, pp. 3265-3268, Aug. 1998.
- [29] B. D. Reiss, D. K. Hanson, and M. A. Firestone, "Evaluation of the Photosynthetic Reaction Center Protein for Potential Use as a Bioelectronic Circuit Element," *Biotechnology Progress*, vol. 23, no. 4, pp. 985-989, Jan. 2007.
- [30] J. Wang, *Analytical electrochemistry*. John Wiley and Sons, 2006.
- [31] L. M. Fischer et al., "Gold cleaning methods for electrochemical detection applications," *Microelectronic Engineering*, vol. 86, no. 4-6, pp. 1282-1285, April.
- [32] Personal Communications with Dr. Dan bizzotto, .
- [33] P. Baglioni, E. Fratini, B. Lonetti, and S. H. Chen, "Gelation in cytochrome C concentrated solutions near the isoelectric point: the anion role," *Current Opinion in Colloid & Interface Science*, vol. 9, no. 1-2, pp. 38-42, Aug. 2004.
- [34] S. Papadopoulos, K. D. Jürgens, and G. Gros, "Protein diffusion in living skeletal muscle fibers: dependence on protein size, fiber type, and contraction," *Biophysical Journal*, vol. 79, no. 4, pp. 2084-2094, Oct. 2000.
- [35] J. L. Cape, M. K. Bowman, and D. M. Kramer, "Computation of the redox and protonation properties of quinones: Towards the prediction of redox cycling natural products," *Phytochemistry*, vol. 67, no. 16, pp. 1781-1788, Aug. 2006.
- [36] M. R. Gunner, J. Madeo, and Z. Zhu, "Modification of quinone electrochemistry by the proteins in the biological electron transfer chains: examples from photosynthetic reaction centers," *Journal of Bioenergetics and Biomembranes*, vol. 40, no. 5, pp. 509-519, Nov. 2008.
- [37] B. Munge, Z. Pendon, H. A. Frank, and J. F. Rusling, "Electrochemical reactions of redox cofactors in *Rhodobacter sphaeroides* reaction center proteins in lipid films," *Bioelectrochemistry*, vol. 54, no. 2, pp. 145-150, Nov. 2001.
- [38] P. S. Guin, S. Das, and P. C. Mandal, "Electrochemical Reduction of Quinones in Different Media: A Review," *International Journal of Electrochemistry*, vol. 2011, pp. 1-22, 2011.
- [39] S. I. Bailey and I. M. Ritchie, "A cyclic voltammetric study of the aqueous electrochemistry of some quinones," *Electrochimica Acta*, vol. 30, no. 1, pp. 3-12, Jan. 1985.
- [40] G. B. Sigal, M. Mrksich, and G. M. Whitesides, "Using Surface Plasmon Resonance Spectroscopy To Measure the Association of Detergents with Self-Assembled Monolayers of Hexadecanethiolate on Gold," *Langmuir*, vol. 13, no. 10, pp. 2749-2755, 1997.
- [41] N. I. Zakharova, M. Fabian, N. I. Uspenskaia, A. A. Kononenko, and A. B. Rubin, "[Structural-functional characteristics of photosynthetic reaction centers extracted by treatment with lauryldimethylamine oxide from *Rhodospseudomonas sphaeroides* (wild type)]," *Biokhimiia (Moscow, Russia)*, vol. 46, no. 9, pp. 1703-1711, Sep. 1981.

- [42] A. Bonincontro, G. Briganti, A. D'Aprano, C. La Mesa, and B. Sesta, "Dielectric Behavior of Octyl  $\beta$ -D-Glucopyranoside Micelles in Water and in Water-Glycine Solutions," *Langmuir*, vol. 12, no. 13, pp. 3206-3210, 1996.
- [43] B. Huang, H. Wu, S. Kim, and R. N. Zare, "Coating of poly(dimethylsiloxane) with n-dodecyl- $\beta$ -D-maltoside to minimize nonspecific protein adsorption," *Lab Chip*, vol. 5, no. 10, pp. 1005-1007, Sep. 2005.
- [44] J. Deisenhofer and H. Michel, "The photosynthetic reaction centre from the purple bacterium *Rhodospseudomonas viridis*," *Bioscience Reports*, vol. 24, no. 4-5, pp. 323-361, Oct. 2004.
- [45] G. Feher, J. P. Allen, M. Y. Okamura, and D. C. Rees, "Structure and function of bacterial photosynthetic reaction centres," *Nature*, vol. 339, no. 6220, pp. 111-116, May 1989.
- [46] J. Kong et al., "Fast reversible electron transfer for photosynthetic reaction center from wild type *Rhodobacter sphaeroides* re-constituted in polycation sandwiched monolayer film," *Bioelectrochemistry and Bioenergetics*, vol. 48, no. 1, pp. 101-107, Feb. 1999.
- [47] H. Levanon and K. Möbius, "ADVANCED EPR SPECTROSCOPY ON ELECTRON TRANSFER PROCESSES IN PHOTOSYNTHESIS AND BIOMIMETIC MODEL SYSTEMS," *Annual Review of Biophysics and Biomolecular Structure*, vol. 26, no. 1, pp. 495-540, Jun. 1997.
- [48] G. F. Moore and G. W. Brudvig, "Energy Conversion in Photosynthesis: A Paradigm for Solar Fuel Production," *Annual Review of Condensed Matter Physics*, vol. 2, no. 1, pp. 303-327, Mar. 2011.
- [49] R. Di Felice and A. Selloni, "Adsorption modes of cysteine on Au(111): Thiolate, amino-thiolate, disulfide," *The Journal of Chemical Physics*, vol. 120, no. 10, pp. 4906-4914, Mar. 2004.
- [50] E. C. Abresch et al., "Identification of proton transfer pathways in the X-ray crystal structure of the bacterial reaction center from *Rhodobacter sphaeroides*," *Biophysical Journal*, vol. 55, pp. 119-125, 1998.
- [51] P. Roach, D. Farrar, and C. C. Perry, "Interpretation of Protein Adsorption: Surface-Induced Conformational Changes," *J. Am. Chem. Soc.*, vol. 127, no. 22, pp. 8168-8173, 2005.